Effective Notch Stress Concept Investigations for Mode-III Loading & Response Conditions

Koen van Essen

Technische Universiteit Delft

TU Delft

AMPELMANN

Effective Notch Stress Concept Investigations for Mode-III Loading & Response Conditions

by

Koen van Essen

to obtain the degree of Master of Science
at the Delft University of Technology,
to be defended publicly on Wednesday October 20, 2021 at 16:00 AM.

Student number:	4384199	
Project duration:	November 16, 2020 – October 20, 2021	
Thesis committee:	Dr. ir. J.H. Den Besten	TU Delft, Supervisor and Chair
	Dr. ir. J.F.J. Pruyn	TU Delft
	Ir. G. Bufalari	TU Delft, Daily Supervisor
	Ir. R. Hoogendoorn	Ampelmann Operations BV, Daily Supervisor

This report is the master thesis performed marking the end of the master Marine Technology.

An electronic version of this thesis is available at `http://repository.tudelft.nl/`.

TU Delft

AMPELMANN

Abstract

Fatigue is typically a governing limit state for maritime structures that encounter stochastic sea loading conditions. Predicting accurate fatigue strength and lifetime is important for structures like offshore wind turbines that are supposed to be out at sea for decades and can be used to optimise the design so that fatigue failure is predicted for, or material is saved in preventing for conservative estimates. This research contributes to the investigation of multiaxial fatigue concepts by getting insight in the mode-III loading & response conditions as input for an effective notch stress concept fatigue assessment. The considered structural detail is a tubular welded joint exposed to torsion; a typical fatigue sensitive one in offshore wind turbine monopile flange connection.

A semi-analytical formulation has been developed to describe the weld notch shear stress distribution analytically. This formulation can be used as input for the effective notch stress concept. The formulation is based on three components, the notch stress, weld load carrying stress and far field stress component. Furthermore, the static force and moment equilibrium is satisfied. The weld load carrying stress component is based on a weld load carrying stress estimate. This coefficient is used because the weld geometry causes a local change in stiffness, a shift in neutral axis, meaning the weld becomes load carrying up to some extent. The stress distribution must include this component since this one is unique for each welded joint configuration.

Applying torsion to the tubular joint cause mode-III shear in the through thickness direction at the weld notch level. The weld load carrying stress estimate is based on non-dimensional geometry parameters of the assessed welded joints. It is individually fitted for 6,300 geometries by comparing the results to stress distributions obtained with 2D finite element analysis. The results of the individual fitted load carrying stress estimates are used as input of a multi variable polynomial regression analysis. The regression analysis led to a polynomial function that describes the load carrying stress estimate as function of the non-dimensional geometry parameters.

The far field information and geometry dimensions are the input for the semi-analytical formulation to obtain the weld notch shear stress distributions analytically. Accurate results are obtained and therefore the formulation can be used as input for the effective notch stress concept.

The effective notch stress concept requires a material characteristic length, ρ^*, over which the stress distribution can be integrated to obtain the effective notch stress. This parameter is obtained using a maximum likelihood regression analysis and provided a most likely value of 1 [mm]. Although this is a good result, the confidence regarding the value is low due to low variety in the experimental fatigue test data set and the limited amount of data in general.

The findings of this study will be used in further research regarding the 4D fatigue project and the effective notch stress concept in general at the Delft University of Technology.

Preface

This master thesis is initiated by Ampelmann in cooperation with the Delft University of Technology. The topic multiaxial fatigue is of both interested to obtain better lifetime estimates for marine structures. Furthermore, this graduation project will mark the end of my period in Delft and the final hurdle to obtain my Master's degree Marine Technology. To achieve my diploma, I will present my results to the department Ship and Offshore Structures of the Faculty 3mE, Delft University of Technology.

March 26th, 2014, I have breakfast with my dad as we had every morning around 6.15 AM before jumping in our cars to the office. This time is different, I tell him I want to quit my study at Nyenrode University and my job at EY as junior auditor. I was 20 years old by then and some weeks later I decided to start a bachelor Marine Technology in Delft. At that moment, I would not have thought that I would write once in the future a thesis about fatigue strength in marine structures and would become a structural engineer.

It was a long journey, but fortunately every journey comes to an end. I want to thank Henk, Gabriele and René for their guidance during my project. Henk, your knowledge about fatigue is impressive. You pushed me to the limit which in the end led to a thesis on a level I would never have expected of myself. Gabriele, your patience helping me almost every day with all my struggles is "eccezionale". It is still strange that you almost felt like a friend before we even had met in real life. René, it is laudable that although your already an engineer for quite some years, your interest and knowledge of the scientific part of the job is still so high. I hope I can follow your example on this, learn a lot from you, and of course I am proud I can finally call you a real colleague on the 1st of December.

Next to all the professional help, I want to thank my friends from marine technology for all their help during our endless coffee breaks the past years and cooperation during projects. Special thanks to the structures boys, which were very helpful during my graduation period with all kinds of support. My friends from Mortier who were always there for non-study distractions. And last but no least, my family and girlfriend, I am very grateful they were always there to help me, listen to my moaning and still were able to keep giving this really stubborn guy advise, thank you very much!

Koen van Essen
Delft, October 6, 2021

Table of Contents

Abstract ii

Preface iii

List of Figures viii

List of Tables x

Nomenclature xi

1 Introduction 1
- 1.1 General Background . . . 1
- 1.2 Problem Statement . . . 1

2 Literature Review 3
- 2.1 Fatigue in Maritime Structures . . . 3
- 2.2 Fatigue Assessment Concepts Overview. . . . 4
  - 2.2.1 Fatigue Damage Criteria . . . 4
  - 2.2.2 Nominal Stress Concept . . . 5
  - 2.2.3 Structural Hot Spot Stress Concept. . . . 6
- 2.3 Effective Notch Stress Concept . . . 6
  - 2.3.1 Critical Distance Theory . . . 6
  - 2.3.2 Fictitious Notch Radius Based Effective Notch Stress. . . . 7
  - 2.3.3 Averaged Effective Notch Stress . . . 7
  - 2.3.4 Weld Notch Stress Distribution. . . . 8
  - 2.3.5 Material Characteristic Length ρ^* . . . 10
- 2.4 Multiaxial fatigue . . . 11
  - 2.4.1 Interaction Equations . . . 11
  - 2.4.2 Critical Plane Criteria . . . 13
  - 2.4.3 Invariant Plane Criteria . . . 13
  - 2.4.4 Integral Plane Criteria . . . 14
  - 2.4.5 Damage Plane Criteria . . . 14
  - 2.4.6 Strength and Mechanism Contributions . . . 15
- 2.5 Conclusion and Research Method. . . . 15
  - 2.5.1 Conclusion. . . . 15
  - 2.5.2 Road map . . . 16
  - 2.5.3 Deliverables . . . 16

3 Mode-III Weld Notch Shear Stress Distributions 17
- 3.1 Welded Joint Geometry . . . 17
- 3.2 Finite Element Solutions . . . 18
  - 3.2.1 The Modelling . . . 18
  - 3.2.2 Solutions. . . . 18
- 3.3 Semi-Analytical Solutions. . . . 20
  - 3.3.1 Notch Stress Component. . . . 20
  - 3.3.2 Weld Load Carrying Stress Component . . . 21
  - 3.3.3 Far Field Stress Component . . . 21
  - 3.3.4 Weld Notch Stress Formulation . . . 23
  - 3.3.5 Weld Notch Load Carrying Stress Estimate . . . 24

3.4 Evaluation and Conclusion . . . 25
3.4.1 Stress Distributions . . . 25
3.4.2 Solid and Shell FE Model Based Far Field Stress . . . 29
3.4.3 Weld Load Carrying Stress Coefficient . . . 29
3.4.4 Weld Load Carrying Stress Fitting Functions . . . 32
3.4.5 Road map Semi-Analytical Formulation . . . 35
3.4.6 Conclusion. . . . 36

4 Material Characteristic Length ρ^* 37
4.1 Experimental Fatigue Test Data . . . 37
4.1.1 The Experimental Data Sets . . . 37
4.1.2 Walker Mean Stress Correction. . . . 39
4.2 Regression Analysis . . . 39
4.2.1 Maximum Likelihood Regression . . . 39
4.2.2 Maximum Likelihood Regression Using Profile Likelihood Plots . . . 40
4.2.3 Maximum Likelihood Regression Using Monte Carlo . . . 40
4.2.4 Akaike Information Criterion . . . 40
4.3 Evaluation and Conclusion . . . 41

5 Conclusion and Discussion 45
5.1 Research Questions . . . 45
5.1.1 Sub-Questions . . . 45
5.1.2 Main Research Question . . . 45
5.2 Recommendations . . . 46

A Polynomial Functions for the Weld Load Carrying Stress Estimate, C_{bw} 47

B Trends C_{bw} for the Simplified Function. 51

C Detailed Figures of Specimens 55

List of Figures

2.1 The crack surface displacement of the modes [22] . . . 4
2.2 Fatigue damage criterion overview [8] . . . 5
2.3 Nominal stress in a beam with a welded attachment [18] . . . 5
2.4 Structural hot spot stress [18] . . . 6
2.5 Weld Notch Stress Distribution [9] . . . 9
2.6 The effective notch stress concept with micro-structural support length (a. left) and fictitious notch radius (b. right). [7] . . . 10
2.7 The range of principal stress is smaller for non-proportional loading than for proportional loading. [31] . . . 12
2.8 Visualition of the critical plane in a weld notch.[31] . . . 13

3.1 The 2D geometry of the tubular joint with dimensions. . . . 17
3.2 3D Ansys model used for verification of the 2D model with a radius of 50 mm. . . . 19
3.3 2D Ansys model used for verification and obtaining of C_{bw} with a radius of 50 mm. . . . 19
3.4 Stress distribution obtained with the 2D and 3D model. . . . 20
3.5 Stress distribution for a large and small value of r_{τ_s} with corresponding distributions for τ_f and τ_m. . . . 22
3.6 Stress distributions for specimens with realistic dimensions. . . . 25
3.7 Stress distributions for extreme dimensions . . . 26
3.8 Global error estimates for the stress distribution using no C_{bw}, the complete and the simplified function. . . . 26
3.9 Mean error plotted over the through thickness direction with the standard deviation. . . . 27
3.10 Stress distributions with different method of calculating τ_s and r_{τ_s}. . . . 28
3.11 Global error estimate, η_2 for the analytical method and η_3 for the numerical method including all 6300 geometries. . . . 28
3.12 The shell model of the tubular welded joint . . . 30
3.13 The virtual weld seam in the shell model used to obtain nodal forces. . . . 30
3.14 Stress distributions of the compared parameters shown in Table 3.3 . . . 31
3.15 Global error estimate for complete and simplified C_{bw} function compared to the linear fitted one, Equation (3.38). . . . 32
3.16 All fitted, $C_{bw,fit}$, and complete function $C_{bw,function}$ values for all geometry configurations regarding W and T. . . . 33
3.17 All fitted, $C_{bw,fit}$, and simplified function $C_{bw,function}$ values for all geometry configurations regarding W and T. . . . 33
3.18 Trends of C_{bw} for varying dimensions. . . . 34
3.19 Goodness of fit plot and fitting parameters of Equation (A.1) . . . 35

4.1 The geometries of the experimental data [31]. . . . 38
4.2 Results of a Monte Carlo simulation to obtain ρ^*. . . . 40
4.3 Akaike information criterion for varying ρ^*. . . . 41
4.4 SN-curve showing the research project and load ratio in one. . . . 42
4.5 Profile log likelihood plots of the parameters to obtain a fatigue resistance curve for the effective notch stress concept SN-curve. . . . 43
4.6 SN-curves showing the trends of differences between the specimens. . . . 44

A.1 Goodness of fit plot and fitting parameters of Equation (A.1) . . . 47
A.2 Goodness of fit plot and fitting parameters of Equation (A.2) . . . 48
A.3 Goodness of fit plot and fitting parameters of Equation (A.3) . . . 49

B.1 All fitted and simplified function C_{bw} values for all geometry configurations regarding W and S. 51
B.2 All fitted and simplified function C_{bw} values for all geometry configurations regarding W and R. 52
B.3 All fitted and simplified function C_{bw} values for all geometry configurations regarding R and T. . 52
B.4 All fitted and simplified function C_{bw} values for all geometry configurations regarding R and S. . 53
B.5 All fitted and simplified function C_{bw} values for all geometry configurations regarding S and T. . 53

C.1 Tube–flange connection investigated by Sonsino et al. [48]. 55
C.2 Tube–flange connection investigated and seam geometry by Amstutz et al. [3]. 55
C.3 Geometry of specimen investigated by Siljander et al. [43] 56
C.4 Geometry of the specimen of Yousefi et al. [59]. (a) Detail of the seam preparation. (b) Detail of the seam. 56
C.5 Geometric data for calculating the nominal stress [59] 57
C.6 Geometry of the specimen of Seeger et al. [42]. This research is using option B. 57
C.7 Geometry of the specimen of Yung et al. [61] 58

List of Tables

3.1 The dimensions of the Ansys models. 18
3.2 Properties of the material of the specimen. 18
3.3 Difference between τ_s and r_{τ_s} obtained analytically and via a shell model. 29
3.4 Road map: How to use the semi analytical formulation, Equation (3.39) in different situations. . 36

4.1 Dimensions of the used experimental fatigue test data. 37

Nomenclature

Abbreviations

AIC	Akaike information criterion
CA	Constant amplitude
CV	Critical value
CVMAE	MAE of LOOCV
CVMAESTD	MAESTD of LOOCV
EESH	Effective equivalent stress hypothesis
EM	Energy method
FE	Finite element
FEA	Finite element analysis
FEM	Finite element method
IIW	International Institute of Welding
LOOCV	Leave One Out Cross Validation
MAE	Normalized Mean of Absolute Error
MAESTD	Standard Deviation of Absolute Error
MLE	Maximum log likelihood estimate
PbP	Projection-by-projection method
PDMR	Path dependent maximum range method
VA	Variable amplitude

Greek symbols

α	Notch angle	[rad]
β	Stress angle	[rad]
χ_a, χ_s	First eigenvalue coefficient of anti-symmetry part	[-]
$\Delta\sigma_R$	Normal stress fatigue strength	[N/mm^2]
$\Delta\sigma_{EC3}$	Eurocode 3 equivalent stress range	[N/mm^2]
$\Delta\sigma_{IIW}$	IIW equivalent stress range	[N/mm^2]
$\Delta\tau_R$	Shear stress fatigue strength	[N/mm^2]
δ	Data type {complete = 1, censored = 0}	[-]
$\Delta\sigma$	Stress range	[N/mm^2]
γ	Load ratio coefficient	[-]

λ	Eigen value	[-]
μ_a, μ_s	Force and bending moment equilibruim coefficient	[-]
ρ	Density	[kg/m^3]
ρ	Notch radius	[mm]
ρ^*	Micro-structural support length	[mm]
ρ_{real}	Real notch radius	[mm]
σ	Standard deviation	[-]
σ	Stress	[N/mm^2]
σ_n	Weld Notch Stress Distribution for a T-Joint (Mode I)	[N/mm^2]
σ_u	Tensile strength	[N/mm^2]
σ_1	Principal stress	[N/mm^2]
σ_e	Effective notch stress	[N/mm^2]
σ_{max}	Maximal stress	[N/mm^2]
σ_{min}	Minimum stress	[N/mm^2]
σ_{vM}	Von Mises stress	[N/mm^2]
σ_x	Normal stress perpendicular to weld	[N/mm^2]
σ_y	Normal stress parallel to weld	[N/mm^2]
τ_f	Far field stress	[N/mm^2]
τ_n	Weld notch shear stress	[N/mm^2]
τ_b	Bending stress component	[N/mm^2]
τ_m	Membrane stress component	[N/mm^2]
τ_s	Structural shear stress	[N/mm^2]
τ_{xy}	Shear stress parallel to weld	[N/mm^2]
φ	Airy stress function	

Latin symbols

ΔK	Stress intensity range	[-]
a	Critical distance	[mm]
as	Singularity length	[mm]
C	Fatigue resistance constant	[N/mm^2]
C_{bw}	Weld load carrying stress coefficient	[-]
C_b	Bending coefficient (Moment Equilibrium)	[-]
C_m	Membrane coefficient (Force Equilibrium)	[-]
D	Palmgren-Miner damage sum	[-]
E	Young's Modulus	[N/mm^3]

F	Cumulative distribution function	[-]
f	Probability density function	[-]
F_n	Force at node n	[N]
f_n	Line fore at finite element n	[N/mm]
$F_{x,n}$	Force at node n in x-direction	[N]
$f_{x,n}$	Line force at node n in x-direction	[N/mm]
$F_{y,n}$	Force at node n in y-direction	[N]
$f_{y,n}$	Line force at node n in y-direction	[N/mm]
h_w	Weld height	[mm]
K	Stress intensity factor	[-]
k	Constant related to normal/shear stress relation	[-]
K_c	Fracture toughness of the material	[N/mm$^{1.5}$]
L	Critical length	[mm]
l_w	Weld length	[mm]
m	Fatigue resistance slope	[-]
M_t	Torsion moment	[Nm]
N	Total number of cycles until failure	[-]
N_i	Allowable cycles per stress level	[-]
n_i	Cycles of certain stress level (stress block)	[-]
r	Radial coordinate	[mm]
R^2	Coefficient of Estimation	[-]
r_{τ_s}	Structural linear stress ratio (mode-III)	[-]
R_f	Flange radius	[mm]
r_{lr}	Load ratio	[-]
r_s	Structural bending stress ratio (mode-I)	[-]
R_t	Tube radius	[mm]
S	Stress range	[N/mm^2]
s	Support factor	[-]
S_n	Nominal stress range	[N/mm^2]
t_b	Thickness base plate, tube (Mode III)	[mm]
t_c	Thickness cross plate, flange	[mm]
t_p	Thickness base plate (Mode I)	[mm]
CVR^2	Mean squared error of LOOCV	[-]

1 Introduction

1.1. General Background

In the offshore industry, transferring people from on- to offshore locations is a daily necessity. Helicopters were typically regarded as the best option, since conventional ship methods like rope swinging and basket transfers do not comply with current safety standards for most modern companies [27]. The former is quite expensive and safety regulations have become stricter over the years. New ways of transferring people had to be invented, which led to offshore gangway systems as the most feasible way of getting people safely offshore.

The last two decades, gangway systems have been introduced by several companies. These are placed on the deck of ships or integrated into the design. The advantages of transfers via ships are safer crossings, more capacity as well as safer access to offshore wind turbines [20]. While transporting people by boat is more cost-effective compared to helicopters, Ampelmann is investigating whether it is more environmental friendly as well. Gangway systems and other mission equipment are welded to the deck of a ship. Therefore, the equipment encounters forces that can be related to the response of the ship resulting from highly stochastic sea loads generated by wind and swell. The response is cyclic by nature, which can lead to fatigue damage. This occurs when cyclic loading above a certain threshold induces damage to the material with fracture as the end state. When the ship is in transit, this loading can exceed a certain threshold, making fatigue a governing limit state for ships and therefore, possibly for mission equipment [8].

This research investigates the Ampelmann system, a gangway that can compensate motions induced by sea loads in six degrees of freedom. The system enables a safe transfer from ship to offshore locations by reducing the movements such that the gangway is horizontally stable. In the end, it turned out to be more towards investigating a new innovative method to assess the fatigue lifetime which could be used for all type of marine structures.

1.2. Problem Statement

As described in Section 1.1, the Ampelmann system, and marine structures in general, are subjected to various loads that may generate a local multiaxial (mixed Mode I and Mode III) stress state, especially in the intersection region between two or more parts of the structural assembly, i.e. at welded joints. The cyclic nature of the load source due to wind, wave, swell and eventually operational loads may induce multiaxial fatigue damage in the welds. Accurate stress calculations are necessary to ensure the structure is strong enough to prevent failure during its lifetime. Methods to assess multiaxial fatigue lifetime are not sufficiently accurate, leading to over-prediction due to conservative estimations.

This research aims to establish a more accurate way of predicting the lifetime of structures. The research topic is: Effective notch stress concept investigations for mode-III loading & response conditions." The main research question regarding this topic reads: "How can the effective notch stress concept be used to investigate welded joints subjected to mode-III loading & response conditions and contribute to multiaxial fatigue assessment of welded joints in marine structures?" This assessment can be obtained by establishing a way to use the effective notch stress concept for mode III, using the through-thickness weld notch shear stress distribution. In future research, the methods for both modes can be combined to a multiaxial fatigue criterion in future research, which can be used to determine a more accurate fatigue lifetime.

2

Literature Review

In this literature review, the state-of-the-art fatigue research will be presented. First, a brief introduction will be given about fatigue in ship and offshore structures in general and about the different fatigue assessment concepts in particular. Next, the effective notch stress concept is discussed more extensively, and the related stress distributions will be set out. Finally, the current multiaxial fatigue assessments are reviewed.

2.1. Fatigue in Maritime Structures

In 1994, Schütz [41] presented a overview of what type of research has been done between 1837 and 1994 with respect to fatigue in steel structures. In 1860, Wöhler [60] already presented a study which suggested design for finite fatigue life time and linear damage accumulation, while a four parameter equation for the SN-curve was introduced by Palmgren in 1924 [29]. Many investigations have been carried out in the course of the 20th century, however, many parameters have not yet been proved nor accepted. This holds even more for predictions related to fatigue under variable amplitude and multiaxial loading.

Stress ranges or stress intensity factors lie at the basis of fatigue assessment. The cumulative effect of all stress range occurrences determines the fatigue life time. These ranges are calculated by taking the superposition of all non permanent fluctuating loads [19]. In Equation (2.1) and (2.2), the ranges are stated that are used to determine the stress or stress intensity range used for fatigue assessment.

$$\Delta\sigma = \sigma_{max} - \sigma_{min} \tag{2.1}$$

$$\Delta K = K_{max} - K_{min} \tag{2.2}$$

Where:

$\Delta\sigma$ = Stress range [N/mm^2]
σ = Stress [N/mm^2]
ΔK = Stress intensity range [-]
K = Stress intensity factor [-]

Three modes are defined for the type of loading that can cause fatigue. In Figure 2.1, they are shown where the arrows define the direction of the loading that is initiating the potential crack. Mode I is mostly governing for marine structures due to thin walled approximation. Mode I is caused by normal and bending stress and is also referred to as the mode that opens the structure. Furthermore, mode I is the governing mode for fatigue in thin-walled structures. Mode II is induced by in-plane shear and does not occur often in thin walled structures. The contribution of Mode III loading, caused by out-of-plane shear, to the fatigue life time is less known in an individually, but also in a multiaxial way. It is interesting to investigate which influence is related to this type of loading. [12]

Due to the cyclic and random nature of wind, waves and swell, the structural response of a marine structure will be consequently dominated by a cyclic and variable amplitude type of loading. When this type of loading is encountered by marine structures it can cause serious damage since fatigue is a damage accumulating process. Therefore, it is necessary to sum up the damage in a way the lifetime can be predicted. The Palmgren-Miners rule is a linear damage accumulation model, stated in Equation (2.3). This is one of the most common and mostly used damage accumulation model for constant and variable amplitude loading.

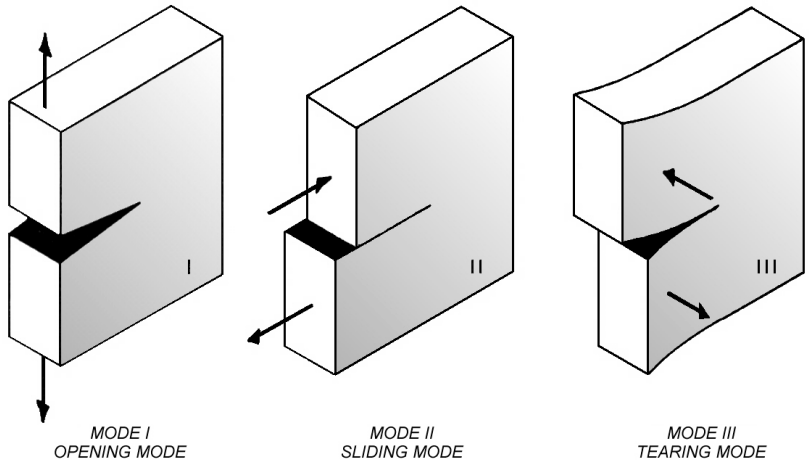

Figure 2.1: The crack surface displacement of the modes [22]

$$D = \sum_{i=1}^{k} \frac{n_i}{N_i} \tag{2.3}$$

Where:

D = Palmgren-Miner damage sum [-]
n_i = Cycles of certain stress level (stress block) [-]
N_i = Allowable cycles per stress level [-]

The different stress levels and in which frequency they occur need to be determined so that stress blocks can be established for the damage accumulation. All types of loading that can affect the fatigue lifetime of a structure should be considered e.g. construction, transportation, installation and in-service [19]. The design load spectrum should be on the upper bound estimate of what is expected during the design lifetime of the structure. Accurate fatigue assessment concepts may prevent the estimate from being too conservative, and help the process in that respect.

2.2. Fatigue Assessment Concepts Overview

Several fatigue assessment concepts have been developed in the past. In general, the more accurate they are, the higher the complexity of the applied concept. They determine the fatigue damage criterion and with that the corresponding resistance curve [12]. In this section, the nominal stress and structural hot spot stress are discussed. In the next section, the effective notch stress will be discussed, since this will be the method this research will focus on. First, several distinctions will be made based on Figure 2.2.

2.2.1. Fatigue Damage Criteria

The criteria related to fatigue assessment concepts are stated in Figure 2.2. Den Besten [8] set it out as follows:

- Global or local information criteria
- Intact or cracked geometry criteria
- Stress, strain or energy parameter criteria.
- Point, line, or area/volume- and defect size or crack increasing process zone criteria

The structural detail level can be global or local. The global fatigue damage criterion is relatively large compared to the hot spot, while the local one takes weld notch information into account up to some extent. Furthermore, distinction is made between intact and cracked geometries. The intact geometry criteria depend on stress, strain or energy related to work hardening, elastoplasticity and multiaxiality considerations

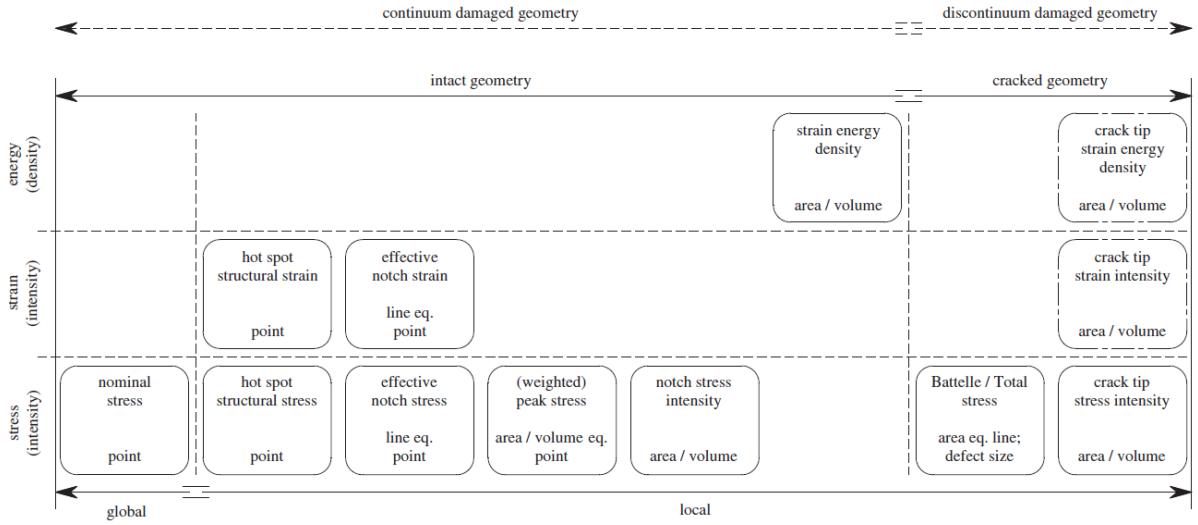

Figure 2.2: Fatigue damage criterion overview [8]

influence the stress or strain concentration factor which is the governing crack initiation parameter. The cracked geometry criteria depend on stress intensity, strain intensity or energy density. The crack growth is controlled by the stress or strain intensity factor which involves the earlier mentioned criteria. The last point will be discussed in section 2.3.1.

2.2.2. Nominal Stress Concept

The nominal stress concept is the most direct method to assess the fatigue strength of welded joints and uses the parameter S_n as the stress range as stated in Equation 2.4 [21]. The global structural response is linear elastic and the concept is based on an intact geometry. Local information near the weld is not taken into account but it includes effects of the macro-geometric shape of the component in the vicinity of the joint [18].

$$S_n = \Delta\sigma_n = 2\sigma_n \tag{2.4}$$

Where:

S_n = Nominal stress range [N/mm^2]
$\Delta\sigma_n$ = Nominal stress range [N/mm^2]
σ_n = Nominal stress [N/mm^2]

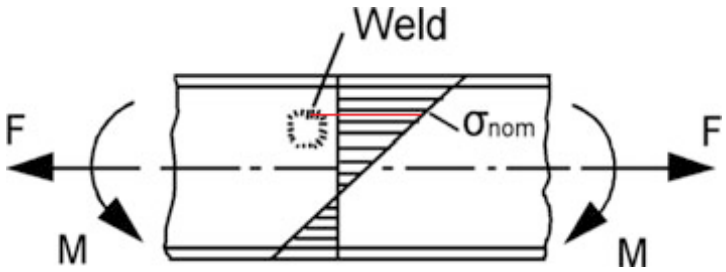

Figure 2.3: Nominal stress in a beam with a welded attachment [18]

The stress can vary over the width of the component as shown in Figure 2.3. The nominal stress can be calculated using structural mechanics theories based on elastic behaviour for simple components. If the nominal stress at the weld needs to be determined, the stress level corresponding to the red line has to be used for this concept. When components get more complex, finite element methods (FEM) can be used with a relatively simple and coarse mesh to obtain the nominal stress [18].

2.2.3. Structural Hot Spot Stress Concept

The structural hot spot stress concept uses the hot spot stress which is an intact geometry local stress point criterion [12]. Local information is taken into account when compared to the nominal stress concept and can be used for more complex structures where the nominal stress cannot be clearly defined. The hot spot stress can be found by extrapolation using reference points as shown in Figure 2.4. It excludes the non-linear peak stress caused by the local notch. The location of reference points and extrapolation equations differ for different hot spots [18].

The major advantage of the structural hot spot stress concept is its possible application at most locations using FEM. Besides, this method is more accurate compared to the nominal stress concept and therefore, the fatigue assessment criterion that is obtained gives a better estimate of the fatigue lifetime. Its disadvantage lies in the limitation to weld toe failure. Furthermore, more accurate results could be obtained with the effective notch or total stress concept.

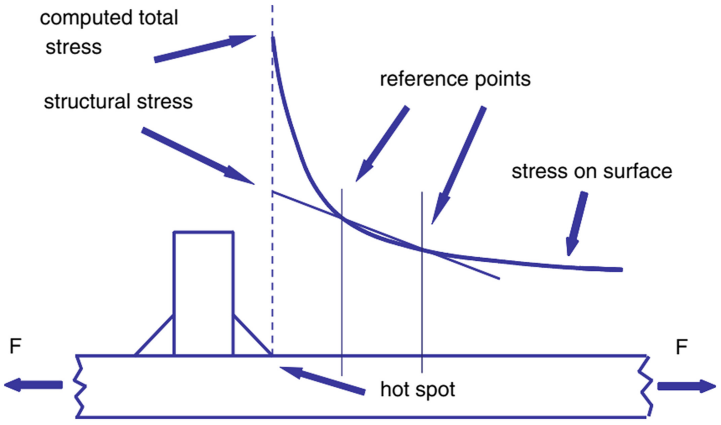

Figure 2.4: Structural hot spot stress [18]

2.3. Effective Notch Stress Concept

The effective notch stress concept uses a local information intact geometry parameter. As concluded by Qin et al. [35], this method is the most promising for the application this research is aiming for. It is supposed to be the most accurate method to obtain the input for the fatigue lifetime calculations. Therefore, the literature review will focus on this method. First of all, the method itself will be explained. Subsequently, the weld notch stress distribution for mode I and mode III will be discussed.

2.3.1. Critical Distance Theory

The theory of critical distances is a name given to a group of theories by Taylor [53]. These theories are used for the prediction of the effect of notches and other stress concentration factors. They make use of material-characteristic microstructural length, area or volume that is defined from the notch tip or notch root [36]. A commonly used length conform Taylor is stated in Equation (2.5). A visualisations of the critical length, in this indicated as ρ^*, is shown in Figure 2.6.

$$L = \frac{1}{\pi}\left(\frac{K_c}{\sigma_u}\right)^2 \tag{2.5}$$

Where:

L = Critical length [mm]
K_c = Fracture toughness of the material [N/mm$^{1.5}$]
σ_u = Tensile strength [N/mm^2]

The critical distance theory distinguishes three main criteria, the point, line and area/volume criteria. The point method uses an elastic stress analysis. Failure is assumed to occur when stress is equal to the fatigue strength measured at a certain distance from the notch, a [32]. Several studies have shown that the

critical distance for the point method is L/2 [52, 54, 57]. Sometimes the point method is referred to as the critical distance method [5]. The line method can be compared to the point method but instead of one point, a line from the notch is defined. Over the length of this line the stress is averaged to obtain the stress value. The length of the line is related to L as well and has a value of 2L [53]. The line method is also the method that Neuber came up with [28]. In a similar way, an area or volume can be used to define the stress intensity around the notch. In this case, the critical distance is a radius around the notch [8]. In Figure 2.2, several fatigue damage criterion and there related critical distance are mentioned.

2.3.2. Fictitious Notch Radius Based Effective Notch Stress

The International Institute of Welding (IIW) advises to use a fictitious notch radius of 1 mm to avoid the singularity effects, this method is called the fictitious notch radius based effective notch stress and has predominantly developed for mode-I [18]. The radius has to be modelled into FEA which leads to a maximum stress value smaller than infinity and usable as effective notch stress. This assumption requires a plate thickness of $t_p > 5$ [mm] because of artificial cross-sectional weakening or strengthening at the weld toe and root notches which would lead to necessary structural stress corrections [8]. More recent research proposes also values of 0.3 and 0.05 [38] for various plate thicknesses to obtain more realistic results for the effective notch stress. If the fictitious notch radius is used, the effective notch stress can be calculated with Equation (2.6). One of the main problems of the theories/concepts discussed in the literature on this subject is that most of them use a fictitious notch radii in one way or another. Since this research will focus on notches with $\rho = 0$ these studies are not applicable.

$$\sigma_e = \sigma_{max}(\rho = \rho_f) \tag{2.6}$$

Where:

σ_e = Effective notch stress [N/mm^2]
ρ = Notch radius [mm]
ρ_f = Fictitious notch radius [mm]

2.3.3. Averaged Effective Notch Stress

The averaged effective notch stress can be obtained by averaging the stress over the critical distance. This includes the contribution of the notch stress gradient [8]. In Equation (2.7), the stress distribution is integrated over the microstructural length ρ^* which can also be seen as the line method. In Equation (2.8), it is shown that the effective stress can be obtained by using the location of the point. Both methods use the weld notch stress distribution to obtain the effective notch stress.

$$\sigma_e = \frac{1}{\rho^*}\int_0^{\rho^*} \sigma_n\left(\frac{r}{t_b}\right) \mathrm{d}\left(\frac{r}{t_b}\right) \tag{2.7}$$

$$\sigma_e = \sigma_n\left(\frac{r}{t_b} = a\right) \tag{2.8}$$

Where:

ρ^* = Micro-structural support length [mm]
$\sigma_n\left(\frac{r}{t_b}\right)$ = Weld notch stress distribution [N/mm^2]
a = Critical distance [mm]
r = radial coordinate [mm]
t_b = Thickness base plate [mm]

In contrast to the nominal and hot spot stress concept, this concept incorporates local notch information. The theoretical stress concentration at the weld notch is not fully effective and, therefore, using this value would give too conservative results. The effective notch stress concept has two methods to obtain the effective stress concentration, the fatigue damage criterion, affecting the fatigue lifetime. The first option is using the weld notch stress distribution, σ_n. σ_n is integrated over the micro-structural support length or taken at the critical distance which gives σ_e. The second is enlarge the actual weld contour by replacing it by an effective

one and implement a fictitious notch radius. This lowers the maximum stress at the notch to the effective stress value. Both methods are given in Figure 2.6.

The advantage of this method is that it gives more accurate results compared to the hot spot structural stress concept. More notch information is taken into account which makes it more complex as well. The disadvantages are that the method is not applicable when significant stress is present in the component parallel to the weld and even more complex to apply than the structural hot spot method [18].

2.3.4. Weld Notch Stress Distribution

The weld notch stress distribution describes the variation of the stress over the through thickness direction of a plate in the vicinity of a weld or notch. This can be seen in Figure 2.5. It is a linear superposition of the equilibrium equivalent stress part and the self-equilibrating part. The former is related to the linear stress field. The latter is a combination of the weld load carrying stress and the V-shaped notch stress component. The weld load carrying part can be determined with FEM which makes it possible to calculate the V-shaped notch part as the difference between the self-equilibrating part and the weld load carrying stress. The idea of formulations of the weld notch stress distribution are that they only require σ_s and r_s as far field information, obtained using a relative coarse meshed plate/shell FE model which does not include any weld geometry information [12].

Williams' Asymptotic The singularity at the notch follows from the V-shaped weld toe. The linear elastic stress distribution near the notch has been introduced by Williams who developed the Airy Stress function in polar coordinates [58]. This function describes the behaviour of the stress near the sharp notch. Williams showed that the degree of the stress singularity depends on the notch angle, α. In this case the notch angle is taken as shown in figure 2.5, which leads to Equation (2.9) for the eigen value.

$$\lambda = \frac{\pi}{2\alpha} \tag{2.9}$$

The Airy stress function is stated in Equation (2.10). This formulation makes it possible to describe a stress distribution of a sharp notch for which the shear formulation is given in Equation (2.11) [58]. The formulation of the eigen value together with the distance from the notch, $r^{\lambda-1}$, shows the incorporation of a singularity in the formulation. This presence can be used to define whether or not a formulation is capable of representing a singularity, i.e. sharp notches.

$$\varphi = r^{\lambda+1} F(\theta;\lambda) \tag{2.10}$$

$$\tau_{r\theta} = r^{\lambda-1}\left[-\lambda F'(\theta)\right] \tag{2.11}$$

$$\begin{aligned} F(\theta;\lambda) = [&C_1\cos\{(\lambda+1)\theta\} + C_2\cos\{(\lambda-1)\theta\} + \\ &C_3\sin\{(\lambda+1)\theta\} + C_4\sin\{(\lambda-1)\theta\}] \end{aligned} \tag{2.12}$$

φ = Airy stress function
$\tau_{r\theta}$ = Shear stress [N/mm^2]
θ = Angular coordinate [rad]
F = Constant
C = Constant

Mode I Filippi et al. [15] proposed some explicit formulations to describe the stress distribution in a more accurate way than Neuber did in 1958 [28]. In this case the notches have a fictitious radius and are not sharp, which make them less suitable for welded joints since they have a singularity at the notch. Therefore, Den Besten [9] established an analytical formulation for the weld notch stress distribution which is stated in Equation (2.13). This formulation is especially valid for a T-joint, anti-symmetric geometry, and is related to mode I fatigue. It takes into account the singularity at the weld notch and uses force equilibrium to obtain the constants μ_s and μ_a. The eigen values are based on Williams' solution. The weld load carrying stress coefficient, C_{bw}, can be estimated with a function. This function is obtained by using a parametric function, fitted with input from FE notch stress distributions for a range of geometry dimensions and loading parameter values

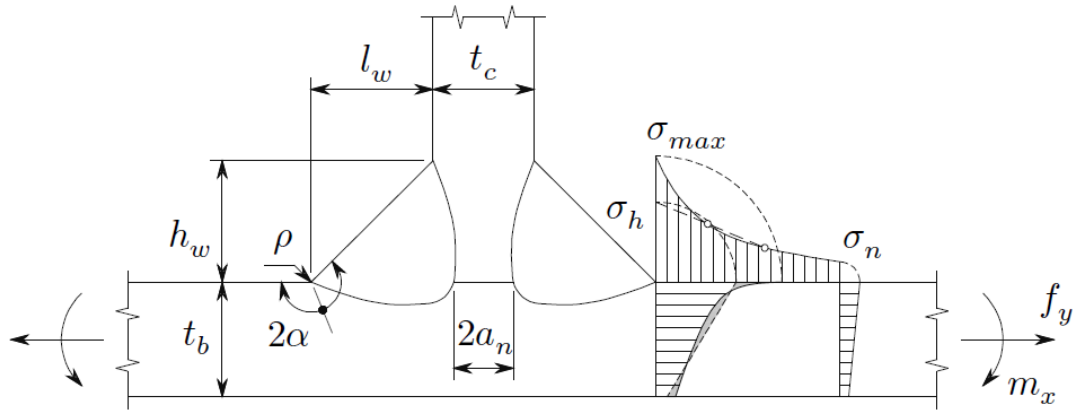

Figure 2.5: Weld Notch Stress Distribution [9]

[34]. Qin et al. [35] concluded that this formulation of the weld notch stress distribution seems to give the best results and could therefore be used as the multiaxial fatigue criterion as state-of-the-art Mode I component.

$$\begin{aligned}\sigma_n\left(\frac{r}{t_p}\right) = \sigma_s \Bigg\{ &\left(\frac{r}{t_p}\right)^{\lambda_s - 1} \mu_s \lambda_s (\lambda_s + 1) \left[\cos\{(\lambda_s + 1)\beta\} - \chi_s \cos\{(\lambda_s - 1)\beta\}\right] \\ &+ \left(\frac{r}{t_p}\right)^{\lambda_a - 1} \mu_a \lambda_a (\lambda_a + 1) \left[\sin\{(\lambda_a + 1)\beta\} - \chi_a \sin\{(\lambda_a - 1)\beta\}\right] \\ &+ C_{bw} \cdot \left\{2\left(\frac{r}{t_p}\right) - 1\right\} - 2 \cdot r_s \cdot \left(\frac{r}{t_p}\right)\Bigg\}\end{aligned} \tag{2.13}$$

Where:

β = Stress angle [rad]
λ_a, λ_s = Eigen value
μ_a, μ_s = Force and bending moment equilibruim coefficient [-]
χ_a, χ_s = First eigenvalue coefficient of anti-symmetry part [-]
C_{bw} = Weld load carrying stress coefficient
r_s = Structural bending stress ratio (mode-I) [-]
t_p = Thickness base plate (Mode I) [mm]

Mode III Literature related to the weld notch shear stress distribution, mode III induced stress, is scarce. A formulation, which could be coupled with the formulation of Den Besten [9] might provide a way to establish a multiaxial fatigue criterion. In order to obtain a distribution that approaches this method studies about the notch shear stress distribution for tubular joints and notches in plates will be investigated. These theories might be useful for establishing a weld notch shear stress distribution for thin-walled structures, which can then be coupled to the study carried out by Qin et al. [35].

$$\begin{Bmatrix} \tau_{zr} \\ \tau_{z\varphi} \end{Bmatrix} = -\lambda_3 r^{\lambda_3 - 1} A_2 \begin{Bmatrix} \sin\lambda_3\varphi \\ \cos\lambda_3\varphi \end{Bmatrix} \tag{2.14}$$

$$A_2 = -\frac{K_{3\rho}}{\sqrt{2\pi}\lambda_3} \tag{2.15}$$

$$K_{3\rho} = \sqrt{2\pi} \lim_{r \to r_o^+} \left[r^{1-\lambda_3} \tau_{z\varphi}(r, \varphi = 0)\right] \tag{2.16}$$

$$A_2 = \frac{-\tau_{\max}}{\lambda_3 r_0^{\lambda_3 - 1}} \tag{2.17}$$

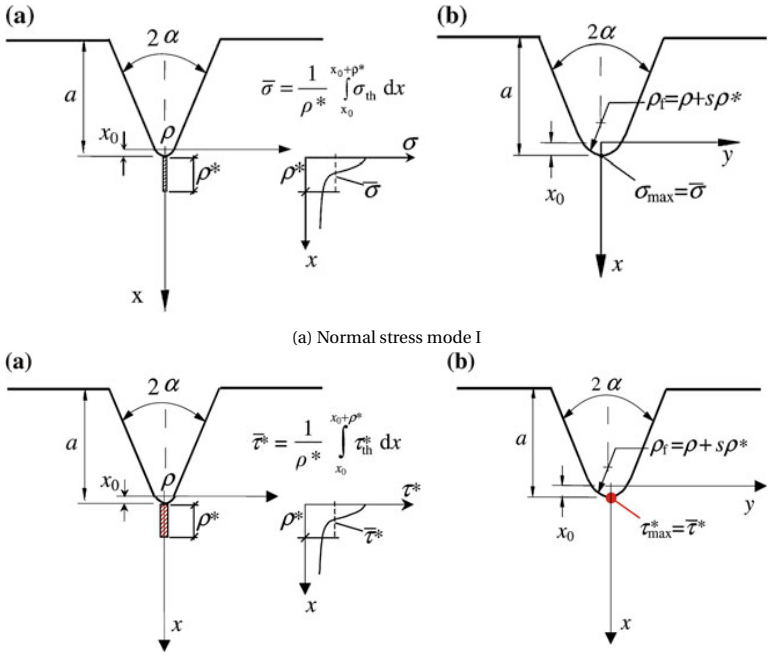

(a) Normal stress mode I

(b) Shear stress mode III

Figure 2.6: The effective notch stress concept with micro-structural support length (a. left) and fictitious notch radius (b. right). [7]

Where:

$\tau_{max}, \tau_{zr}, \tau_{z,\varphi}$ = Shear stress [N/mm^2]
A_2 = Constant
K_3 = Notch stress intensity factor [-]

The stress distribution established by Qin et al. [33] uses the notch stress intensity factor for sharp notches or the maximum shear stress in case of a blunt notch to obtain the stress distribution. The stress intensity factor is a function of $\tau_{z\phi}$. The aim of this research is to obtain the stress distribution directly from the structural shear stress and the bending ratio as can be seen for Mode-I. The τ_{max} method cannot be applied as it assumes a blunt notch or a fictitious notch radii.

The formulation by Qin et al. contains the $r^{\lambda-1}$ which can be related to the same construction as the Mode-I formulation of Equation (2.13) and can therefore be used as the basis for a shear stress formulation with a sharp notch ($\rho = 0$).

Hu et al. [21] proposed the singularity length method. This theory uses $'as'$ as the geometry dependent parameter, which is determined by using FEA. The parameter can be obtained by means of approximation formulas. The way in which Hu et al. [21] determine the values might be of use to this study, even though they apply a minimum of two values, depending on the macro-geometric information, it would be better to present a unique solution for every geometry possibility.

$$\tau_{z\theta} = \frac{\tau_s}{\sqrt{2}} \left(\frac{as}{r} \right)^{1-\lambda_3} \tag{2.18}$$

Where:

as = Singularity length [mm]
τ_s = Structural shear stress [N/mm^2]

2.3.5. Material Characteristic Length ρ^*

The micro-structural support length was introduced by Neuber in 1958. Neuber assumed that using the peak stress at a notch as fatigue strength parameter would be too conservative as fatigue damage criterion and introduced ρ^*. It is a material characteristic parameter which is used for averaging the stress over a certain length. In this way, several values for ρ^* are obtained. Baumgartner et al. [5] found $\rho^* = 0.4$, using a reference

radius of 0.05 [mm] in his research while using the principal stress. When applying Von Mises they found $\rho^* = 0.2$ which gives where both values give a sufficient result for the assessment. Furthermore, they investigated the influence of ρ^*. The assessment quality is almost the same for any value in the range of $0.3 \leq \rho^* \leq 0.7$ [mm] for the principal stress method. A critical distance of respectively $a = 0.1$ [mm] and $a = 0.05$ [mm] are recommended, which is in line with $\rho^* = 4a$ [53].

Neuber [28] used Equation (2.19) with a reference radius of 1 [mm], as used by the IIW. For steel under tension or bending loads a factor $s = 2.5$ would be used with a $\rho^* = 0.4$ [mm]. For shear, $s = 1$ is proposed. This leads to a lower value for the fictitious or reference radius implying a higher effective notch stress [5].

$$\rho_{\mathrm{f}} = \rho_{\mathrm{real}} + s \cdot \rho^* \tag{2.19}$$

Where:

ρ_{real} = Real notch radius [mm]

All the information in this section is related to mode-I except for the $s = 1$ for shear from Baumgartner. It could be used to determine ρ^* with reversed engineering when a fictitious notch radius is already defined for mode-I. The available literature does not provide information about the material characteristic length for mode III loading with regard to sharp notches.

2.4. Multiaxial fatigue

The criteria for the assessment of multiaxial fatigue of welded joints, provided in literature, are typically based on interaction equations or critical plane approach. There is no consensus in literature about which method is the most accurate. Pedersen [31] published a review paper that evaluates the commonly applied multiaxial fatigue criteria with regard to the effective notch stress approach. The criteria for multiaxial fatigue loading can be divided into three concepts: equivalent stresses, interaction equations and critical plane approaches. All three concepts will be discussed in this section.

In order to assess fatigue life time, stress ranges need to be defined as discussed in Section 2.1. IIW has specific guidelines regarding the use of principal- and Von Mises stresses [17]. IIW uses the methods only for proportional loading, whereas Petersen also applies them for non-proportional loading, which is a better representation of engineering load cases.

2.4.1. Interaction Equations

Equivalent stress ranges were used from the beginning of multiaxial fatigue life time assessments in design codes and were evaluated against uniaxial SN-curves. [26]. Later on, design codes like IIW and EC3 started to apply interaction equations that made use of the individually design curves to evaluate the corresponding normal and shear stress component. Most criteria are not allocated to one particular stress system but can be used for all three fatigue assessment concepts, nominal-, structural hot spot- and effective notch stress concept.

Principal Stress The principal stress range is recommended for proportional loading when the minimum and maximum principal stress are both positive or negative [17]. Furthermore, a less significant influence of shear stress is assumed. The stress range is calculated from the maximum and minimum value of the principal stress during the load cycle.

$$\sigma_1 = \left(\sigma_x + \sigma_y + \sqrt{\left(\sigma_x - \sigma_y\right)^2 + 4\tau_{xy}^2}\right)/2 \tag{2.20}$$

A study by Bäckström [4] showed that for the hot spot stress method the principal stress range is a quite poor damage parameter. Furthermore, Figure 2.7 makes clear that the principal stress range does not always lead to the maximum damage when the loading is non-proportional. This leads to a non-conservative life time prediction for non-proportional loading. However, as observed by Siljander et al. [44], the opposite is generally the case.

Von Mises In cases were the multiaxial fatigue loading includes significant shear IIW recommends using Von Mises [17]. The notch stress components are used to calculate the Von Mises equivalent stress range, which is shown in Equation (2.21). The Von Mises stress could also be used as function over time and in that

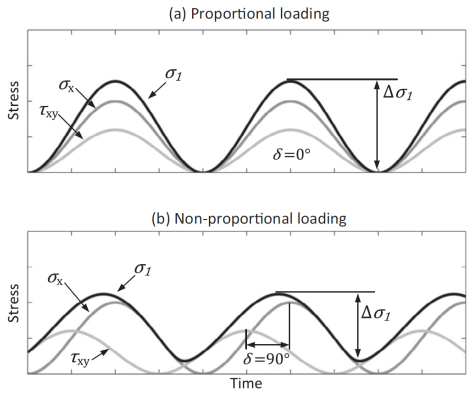

Figure 2.7: The range of principal stress is smaller for non-proportional loading than for proportional loading. [31]

way obtaining the stress range. The Von Mises method neglects compressive stress. It is not integrated in the method due to the positive nature of the Von Mises stress [31].

$$\Delta\sigma_{vM} = \sqrt{\Delta\sigma_x^2 + \Delta\sigma_y^2 - \Delta\sigma_x\Delta\sigma_y^2 + 3\Delta\tau_{xy}^2} \tag{2.21}$$

Both equivalent stress methods do not incorporate a change of direction for the critical stress. Therefore, the most unfavourable direction has to be chosen for the whole calculation.

Interaction Equation, Eurocode 3 The interaction equations proposed by Eurocode 3 use uniaxial fatigue strength of normal and shear. The damage parameter D_{EC3} should stay below 1 for all cases. For this interaction, the possibility of non-proportional loading is not taken into account, the fatigue strength criterion is compared with their respective fatigue strengths. The effective stress range as stated in Equation (2.23) is evaluated against the uniaxial SN curve given by $\Delta\sigma_R$.

$$\left(\frac{\Delta\sigma_x}{\Delta\sigma_R}\right)^3 + \left(\frac{\Delta\tau_{xy}}{\Delta\tau_R}\right)^5 \leqslant D_{EC3} \tag{2.22}$$

$$\Delta\sigma_{EC3} = \sqrt[3]{\Delta\sigma_x^3 + k\cdot\Delta\tau_x^5} \tag{2.23}$$

$$k = \frac{\Delta\sigma_R^3}{\Delta\tau_R^5} \tag{2.24}$$

Interaction Equation, IIW The interaction equations proposed by IIW apply the uniaxial fatigue strength of normal and shear as well, but uses the Gough-Pollard equation as shown in Equation (2.25).

$$\left(\frac{\Delta\sigma_x}{\Delta\sigma_R}\right)^2 + \left(\frac{\Delta\tau_{xy}}{\Delta\tau_R}\right)^2 \leqslant CV \tag{2.25}$$

The stress range can then be obtained with Equation (2.26).

$$\Delta\sigma_{IIW} = \frac{1}{\sqrt{CV}}\sqrt{\Delta\sigma_x^2 + k\cdot\Delta\tau_{xy}^2} \tag{2.26}$$

$$k = \frac{\Delta\sigma_R^2}{\Delta\tau_R^2} \tag{2.27}$$

If the load is proportional a critical value (CV) of 1 is recommended, for non-proportional loading CV = 0.5, and for a fluctuating mean stress a CV of 0.2 [1].

2.4.2. Critical Plane Criteria

The options described above only take one stress direction into account. Findley presented the first type of critical plane method [16]. This method is initially developed for non-welded components, but there are several publications that extended the method to welded joints. The critical plane includes the maximum damage parameter in all possible directions for every time step, which gives a more complete overview.

$$\boldsymbol{\sigma}(t) = \begin{bmatrix} \sigma_x(t) & \tau_{xy}(t) & \tau_{xz}(t) \\ \tau_{xy}(t) & \sigma_y(t) & \tau_{yz}(t) \\ \tau_{xz}(t) & \tau_{yz}(t) & \sigma_z(t) \end{bmatrix} \tag{2.28}$$

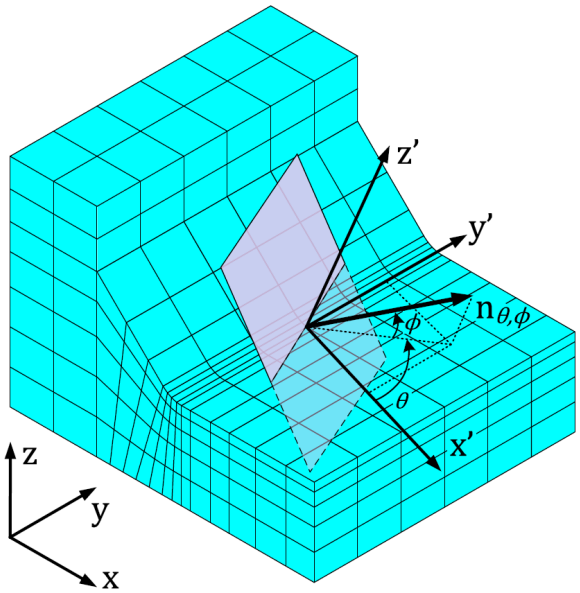

Figure 2.8: Visualition of the critical plane in a weld notch.[31]

Susmel [51] came up with the Modified Wöhler Curve method, which is based on a shear stress approach. This method assumes that the critical plane reaches the largest shear stress range during the load cycle. It tries to find a load curve that is based on both the normal and the shear stress. Susmel combines this method with the effective notch stress method and obtained good, though conservative, results [50].

Carpinteri et al. [11] proposed a method in which the critical plane orientation is determined a priori, based on the direction of the first maximum principal stress. The damage parameter is equal to Equation (2.26) with $\sigma_x = \sigma_{eq}$ and CV = 1. It could be seen as the Gough-Pollard equation applied in a critical manner. Carpinteri et al. tested the criterion and got moderately good and mainly conservative results when comparing the used experimental data with the predictions.

Other available methods are the structural stress critical plane and stress-strain. These seem to be less suitable since more research has to be carried out to test their application to welded joints or (non-proportional) variable amplitude loading [56].

2.4.3. Invariant Plane Criteria

Based on a different physical ground with respect to the critical plane method, the invariant plane method has been developed. Computational efforts and model complexity are significantly reduced by using stress invariants. Different formulations exist, but invariant based multiaxial fatigue models typically use one term that accounts for the dilation (i.e. volume change) and another one for the distortion (i.e. yielding). The hydrostatic stress σ_H or the first stress invariant I_1 are related to dilation while the second invariant of the deviatoric stress J_2 is related to the distortion, see Equations (2.29)–(2.30). An earlier invariant based approach for multiaxial fatigue assessment was the one proposed by Crossland and Sines [10, 45]. The fatigue criterion they suggested can be described by the generic equation provided in Equation (2.31). Material parameter k represents a function of the uniaxial fatigue strength and is used to obtain the equivalent fatigue strength [97]. Mode I and Mode III fatigue resistance data are needed for multiaxial cases. The infinite fatigue life is consid-

ered in the equation, which is represented by a fatigue limit criterion. The left-hand-side can be represented by a Basquinlike equation (2.31) for a finite fatigue lifetime [56].

$$I_1 = \sigma_x + \sigma_y + \sigma_z \tag{2.29}$$

$$J_2 = \frac{1}{6}\left(\left(\sigma_x - \sigma_y\right)^2 + \left(\sigma_y - \sigma_z\right)^2 + \left(\sigma_z - \sigma_x\right)^2\right) + \tau_{xy}^2 + \tau_{yz}^2 + \tau_{zx}^2 \tag{2.30}$$

$$\tau_{a,f} = \sqrt{J_2} + k\sigma_H \tag{2.31}$$

The most promising invariant plane criteria method in literature seems to be the projection-by-projection method (PbP) by Benasciutti et al. [6]. Accurate results were found with reduced computational efforts. However, in time domain, the method has not yet been validated for non-proportional variable amplitude (VA) loadings. The results that have been generated so far are promising and, therefore, the PbP method is included in this study. However, further research is required to validate the method for non-proportional VA loads and its application to welded joints [56].

2.4.4. Integral Plane Criteria

In order to compensate the shortcomings of the critical plane based methods in dealing with non-proportionality induced lifetime reduction in ductile materials, integral plane criteria have been developed. Interaction effects induced by non-proportionality are taken into account by integrating a particular fatigue parameter, for a specified (elementary) material volume. Significant computational effort is needed to optimise such calculations. The integration has to be executed over all material planes within an acceptable level of accuracy [30]. Integral methods are generally considered to be more computational intensive, and therefore, less beneficial than the critical plane or invariant based methods [56].

The literature on the different integral plane criteria mentions two methods, the effective equivalent stress hypothesis (EESH) and the Energy method (EM). The EESH is based on the Von Mises equivalent stress method. However, it has been modified, based on local stress, to overcome its deficiency in case of non-proportional loadings. The results, as compared to the experimental data of welded joints under multiaxial constant amplitude loading, are promising [47, 48]. Several studies [48, 49, 46] have been carried out to investigate whether EESH can also be applied for more complex VA loadings. However, these studies encounter problems in time varying phase differences and, moreover, the hypothesis requires a realistic damage sum. Representative multiaxial fatigue data are needed in order to carry out further investigations and validations [56].

Saintier et al. proposed an integral based approach, which is formulated using an energy based fatigue parameter, hence called EM. It is assumed that material behaves elastically in the high cycle fatigue range, which makes it possible to consider the elastic strain density as fatigue parameter for EM. The stresses and strains are evaluated with FEA and used as input for describing a incremental damage parameter. The advantage of this method is that it circumvents the cycle counting [56]. The method is validated with experimental data sets of plane geometries and also cover multiaxial fatigue load cases [39]. Good results have been obtained so far, however, more research needs to be done to apply the method to notched geometries and welded joints encountering complex loads [56].

2.4.5. Damage Plane Criteria

Multiaxial fatigue behaviour can also be described by means of damage mechanics. The thermomechanical behaviour of solids describes the fundamentals of damage mechanics. Crack initiation occurs as result of local plasticity, so damage models can relate damage to local stress/strain. The constitutive equations follow from the laws of thermodynamics for irreversible processes. Observable and (not directly measurable) internal state variables at a certain time instant are used to describe the thermodynamic state of a material at the same instant. This so-called state potential is described by state laws and associated variables. The dissipation potential $F(\sigma, X, R, Y)$ for dissipative processes is considered and described by evolution laws. The evolution of the damage is governed by a so-called yield function. It describes the relationship between local plasticity and damage [25, 24]. The use of damage mechanics also circumvents cycle counting by applying a continuous damage variable. Furthermore, the model can be specified for different material characteristics and load conditions (e.g. brittle/ductile materials, isotropic/anisotropic behaviour, crack closure/opening) [56].

Several studies have investigated damage mechanics specifically in relation to marine structures[14, 23, 55]. Erny et al. [14] showed promising results for a method which was developed and validated to assess fatigue in a butt-welded plates for S355 steel. It makes use of very extensive FE models that incorporate weld toe geometry, residual stresses, material zone dependent yield stresses and elastic-plastic material behaviour. By post processing the results in a damage model, the crack initiation could be studied. However, the research was only conducted for uniaxial fatigue problems. Erny et al. [14] and Thevenet et al. [55] used the same approach with different geometries, a structural detail of a stiffened panel and a cruciform joint. Experimental data were collected. Although the numerical and experimental results showed agreement, conclusions could not yet be drawn [14] [56].

2.4.6. Strength and Mechanism Contributions

Fatigue damage is often indicated by a single damage parameter, which accumulates cycles related to strength from 0 to failure, like the Miner rule. However, all changes in the material, occurring as a result of the cyclic load should be defined and taken into account. For example: local decohesion (cracking), fatigue damage including crack tip plasticity, local strain hardening in the crack tip zone, residual stresses around the crack tip, and, for notched elements, also macroplasticity at the root of the notch. These phenomena all change the conditions of the assessed structural element, or material and influence the fatigue lifetime. It can also be expected to not fully interact with the magnitude of the cyclic load [40]. Existing fatigue cycle counting methods do not incorporate the fatigue strength, for example the path dependent maximum range method (PDMR) by Dong et al. [13]. In Equation (2.32), the term β is introduced, which is typically based on the Von Mises concept, and is, therefore, taken as 3. The proposition would be to vary β, which give varying fatigue resistance curves as well.

$$\Delta S_e = \int \sqrt{(d\sigma)^2 + \beta\,(d\tau)^2} \tag{2.32}$$

2.5. Conclusion and Research Method

In this section, the conclusion regarding the literature review is given. The hypotheses and research questions are presented, and subsequently, a road map and corresponding deliverables of this thesis are presented.

2.5.1. Conclusion

The state-of-the-art literature provides a starting point for a through thickness weld notch shear stress distribution formulation. However, it cannot yet be used for the effective notch stress concept since necessary information is still missing. To obtain the averaged effective notch stresses a material-characteristic microstructural length for mode-III is needed. This length has not yet been found for mode-III and should be established. Furthermore, multiaxial fatigue criteria incorporating strength and damage mechanisms that could be used for fatigue assessment are present, but are not yet considered for multiaxial effective notch stress purposes.

Hypotheses The hypothesis of this research is that a mode-III specific strength and damage mechanism contributes to better fatigue damage criteria for the effective notch stress multiaxial application. In general, this should provide better fatigue strength and life time estimates. The effective notch stress could be determined with a weld notch shear stress distribution. The effective notch stress concept for mode I and mode III could then be combined to a multiaxial criterion.

Main Research Question: How can the effective notch stress concept be used to investigate welded joints subjected to mode-III loading & response conditions and contribute to multiaxial fatigue assessment of welded joints in marine structures?

Sub-question 1 In which way is it possible to find a semi-analytical formulation for the through thickness weld notch shear stress distribution that can be used for the effective notch stress concept?

Sub-question 2: Can the obtained semi-analytical formulation be used for practical engineering applications? In other words, is it possible to obtain information about the through thickens weld notch shear stress distribution from a coarse FE shell model without including local details (i.e. welds)?

Sub-question 3: What is the effective notch stress related material-characteristic microstructural length parameter for mode-III loading?

2.5.2. Road map

In order to obtain the required knowledge and parameters to find a solution for the research problem described in the problem analysis, the next steps have to be taken:

- Establish the weld notch shear stress distribution formulation
  - Make a 3D solid FE model to obtain through thickness shear stress distributions at the weld notch
  - Obtain the structural- and bending stress distributions from nodal forces
  - Generate an analytical formulation for the through thickness shear stress distribution and compare the obtained stress distributions with numerical FE results
  - Establish a parametric function for the weld load carrying stress coefficient by fitting the analytical formulation through the FE stress distribution.
  - Validate the model for several cases by varying local weld geometry dimensions.
- Test the obtained formulation for practical engineering applications
  - Create a simplified FE shell model for a particular structural assembly (tube to plate joint) and obtain far field stress information.
  - Use the obtained information as input for the semi-analytical formulation and validate if it matches the results obtained with FE solid model.
- Establish a material-characteristic microstructural length for mode-III
  - Collect experimental fatigue resistance data under mode III loading
  - Check the type of failure.
  - Use the semi-analytical stress distribution and experimental data to establish material-characteristic microstructural length.

2.5.3. Deliverables

The deliverables for this research are as follows:

- A semi-analytical weld notch shear stress distribution formulation.
- How to use the weld notch shear stress distribution formulation in engineering (with FE shell model).
- Material-characteristic microstructural length for mode-III.

3

Mode-III Weld Notch Shear Stress Distributions

In this chapter, the process is described how to obtain a semi-analytical formulation to describe mode-III shear stress distributions. The considered structural detail is a tubular welded joint exposed to torsion. The torsion moment causes mode-III shear in the through thickness direction at the notch. This stress distribution can be grasped by using FEA. The found stress distributions are used to develop the semi-analytical formulation for mode-III. The formulation will exist of several components which describe the behaviour of the stress near the notch. Furthermore, an empirical function for the weld load carrying stress estimate will be outlined. A fitting function is made to obtain the estimate. After all, an evaluation is made, and conclusions are drawn regarding the semi-analytical formulation.

3.1. Welded Joint Geometry

The assessed structural detail is a tubular welded joint as related studies [21, 48, 61, 59, 3, 42, 37] uses this type. Also, it is the most used geometry to obtain mode-III shear stress in a structure and these types face mode-III fatigue in engineering practices. A typical example is the flange connection in offshore wind turbine monopiles. The schematic overview of the tubular welded joint in 2D is given in Figure 3.1. The dotted red line represents the through thickness direction at the weld notch level for which the shear stress distributions will be calculated in this research, hereafter called the through thickness direction. Geometry parameters have been varied which has lead to 6,300 different geometries which are used for the analysis of the stress distributions. These parameters are the outer radius of the tube (R_t), the thickness of the base (t_b)- and cross (t_c) plate, and the weld length (l_w) and height (h_w). The complete overview of the dimensions can be found in Table 3.1.

The chosen parameters for the thickness and the weld dimensions are based on what is used in industry.

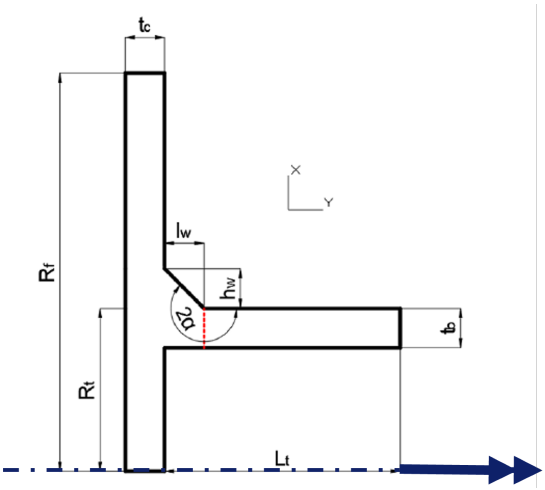

Figure 3.1: The 2D geometry of the tubular joint with dimensions.

Dimension	Size in mm
R_t	[50, 100, 200, 500, 1000, 2000, 4000]
t_b	[4, 8, 16, 20, 24]
t_c	[4, 8, 16, 20, 24]
l_w	[4, 6, 8, 10, 12]
h_w	[4, 6, 8, 10, 12]
R_f	$R_t + 21 \times l_w$

Table 3.1: The dimensions of the Ansys models.

It is also chosen so that the formulation of the weld load carrying stress estimate is comprehensive so that a good fit can be obtained. The outer tube radius dimensions are chosen so that planar loading & response conditions are approached, $R_t = 4000 >> t_b = 4$. This is done so that the formulation will also hold for planar geometries.

The material of the specimens is specified in Table 3.2. The used material is steel with nominal values for the Young's modulus, Poisson's ratio and density of the material.

Property	Magnitude	Unit
E	210	[GPa]
ν	0.3	[-]
ρ	7850	$\left[\frac{kg}{m^3}\right]$

Table 3.2: Properties of the material of the specimen.

3.2. Finite Element Solutions

In this section, the work performed regarding finite element models is discussed. FEA is used to obtain stress distribution in the through thickness direction. These stress distributions are used to fit the weld load carrying stress estimate for all particular non-dimensional geometry parameters.

3.2.1. The Modelling

Linear elastic finite element analysis is used to construct a 2D and 3D model of the geometry mentioned in the previous section. In this research, the used software is Ansys. These models are used to obtain FE through thickness weld notch shear stress distribution. This distribution is used to validate the semi-analytical formulation and to establish the weld load carrying stress coefficient.

3D model

The 3D solid model is constructed to obtain the stress distribution over the through thickness at the weld notch level. The element type that is used is solid185. This model is used to obtain the first results for a stress distribution under mode-III loading & response conditions, in this case torsion. Thereafter, the model is used to verify if the 2D model provides accurate results. If the results of the 2D and 3D model correspond, the 2D model can be used to save modelling time. The 3D solid model is shown in Figure 3.2.

2D model

Hu et al. [21] constructed a 2D model in Ansys with the Ansys plane25 elements. These elements are suitable for the modelling of axisymmetric structures with non-axisymmetric loading such as torsion. The element is defined by four nodes. The model is axisymmetric around the y-axis, which is the reason the axis system is defined as in Figure 3.3. The nodes on the x-axis are all fully constrained which models how the specimen would be constrained in a fatigue test.

3.2.2. Solutions

The 2D model is used to obtain the stress distributions at the weld notch level. The 2D model has the advantage that it saves computation time compared to the 3D model while it also has a higher mesh density near the notch, 100 elements vs 60 elements (20 elements for the student version of Ansys) over the thickness. Furthermore, the meshing of the 2D model near the notch can be kept constant instead. This was not possible

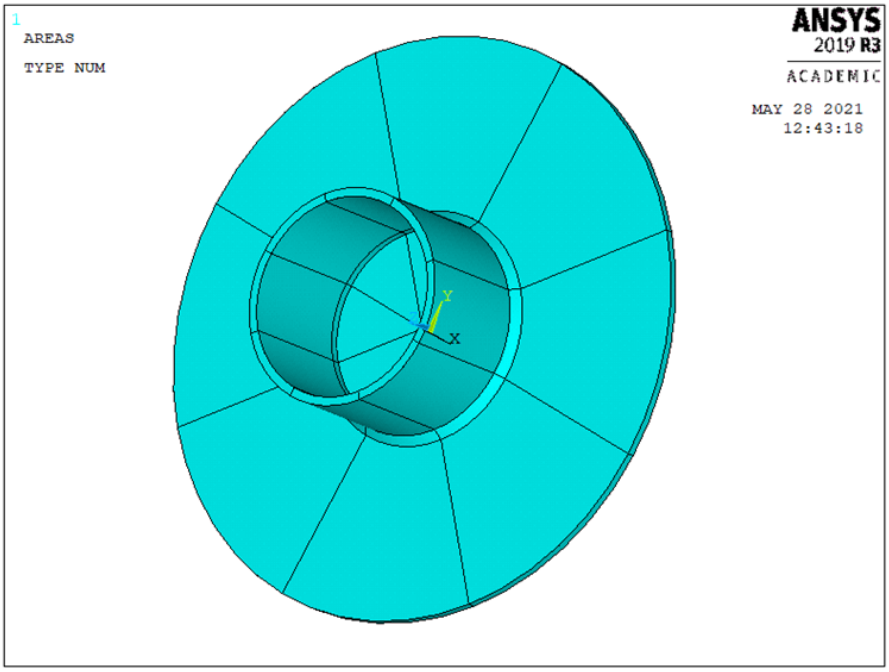

Figure 3.2: 3D Ansys model used for verification of the 2D model with a radius of 50 mm.

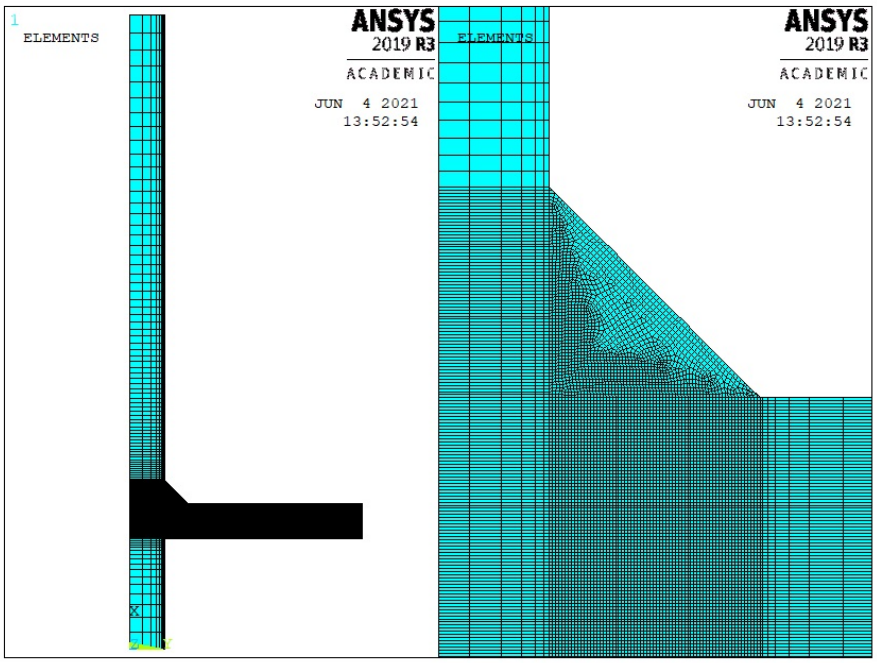

Figure 3.3: 2D Ansys model used for verification and obtaining of C_{bw} with a radius of 50 mm.

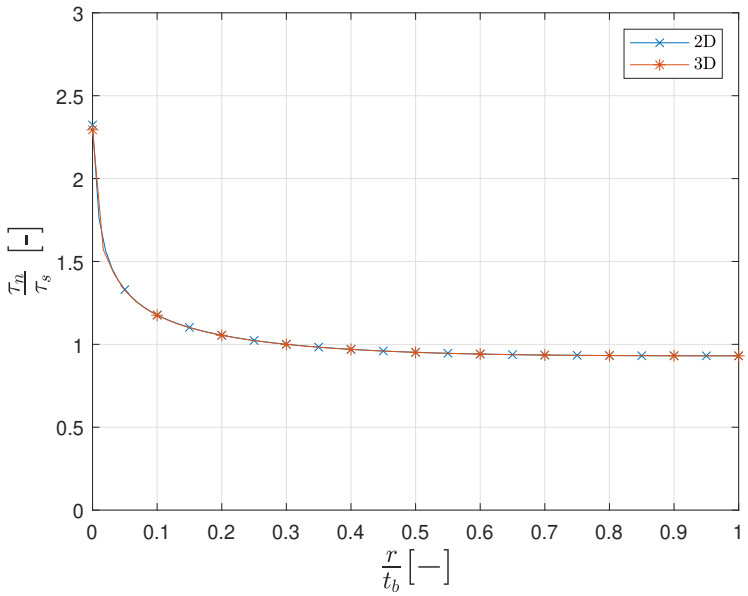

Figure 3.4: Stress distribution obtained with the 2D and 3D model.

for the 3D model due to changing weld dimensions. Matlab is used for post-processing the results. In Figure 3.4, the difference between the distributions obtained with a 2D and 3D model can be noted. It can be seen that there are minor differences in the notch zone but this is negligible. Therefore, it can be concluded that working with the 2D model gives accurate results.

3.3. Semi-Analytical Solutions

In this section the process of developing the semi-analytical formula that will be used in the effective notch stress concept is described. The subsections are divided into the different parts which are included in the formula, respectively, the notch stress component, the weld load carrying stress component and the far field stress component. Combined they form the weld notch stress formulation. The weld load carrying stress estimate is elaborated on in since it this one is unique for each welded joint configuration. Last but not least, the application of the formulation with a shell model is assessed.

3.3.1. Notch Stress Component

In this section, the notch stress component, also called the V-shaped notch term, used to obtain the semi-analytical formulation is discussed. The related parts are highlighted with a box in Equation (3.1).

$$\tau_n\left(\frac{r}{t_b}\right) = \boxed{\tau_s}\left[C_m\boxed{\left(\frac{r}{t_b}\right)^{\lambda-1}} - (C_b + C_{bw})\left\{2\cdot\left(\frac{r}{t_b}\right) - 1\right\} - 2\cdot r_{\tau_s}\cdot\left(\frac{r}{t_b}\right)\right] \tag{3.1}$$

Where:

$\tau_n\left(\frac{r}{t_b}\right)$ = Weld notch shear stress distribution [N/mm^2]
τ_s = Structural shear stress [N/mm^2]
C_m, C_b = Force and moment equilibruim coefficient [-]
r_{τ_s} = Structural linear stress ratio (mode-III) [-]

As described in Section 2.3.4, a formulation is found which describes the shear stress distribution for sharp notches and mainly the notch stress component, Equation (3.2). In Section 2.3.4, the basics of the description of stresses at singularities is explained with the Williams' asymptotic solution [58] and Neuber's work [28]. The V-shaped notch term is used to describe the stress distribution in the notch affected zone taking into account the singularity and the theoretical infinite stress level at the notch. The equation is rewritten to a function that depends on the notch through thickness ratio, $\frac{r}{t_b}$.

$$\tau_n(r) = -\lambda r^{\lambda-1} A_2 cos(\lambda\beta) \tag{3.2}$$

$$\tau_n\left(\frac{r}{t_b}\right) = \boxed{-\lambda t_b^{\lambda-1} A_2 cos(\lambda\beta)} \left(\frac{r}{t_b}\right)^{\lambda-1} \tag{3.3}$$

$$\lambda = \frac{\pi}{2\alpha} \tag{3.4}$$

In Equation (3.3), the box indicates the part that needs to be established in this study. Hu et al. [21] also came up with a formulation which they verified with FEA, Equation (3.5). Their equation gave inside in how others did a similar research and gave insides how to start building the formulation. They also used the V-shaped notch term, boxed in Equation (3.5), but did not use extra terms to describe the far field stress and the weld load carrying stress coefficient.

$$\tau_{z\theta} = \frac{\tau_s}{\sqrt{2\pi}} \boxed{\left(\frac{t_b}{r}^{1-\lambda}\right)} cos(\lambda\beta) A_2 \tag{3.5}$$

3.3.2. Weld Load Carrying Stress Component

In this section the weld load carrying stress component is discussed. The related parts are highlighted with a box in Equation (3.6).

$$\tau_n\left(\frac{r}{t_b}\right) = \boxed{\tau_s} \left[C_m \left(\frac{r}{t_b}\right)^{\lambda-1} - \left(C_b + \boxed{C_{bw}}\right) \boxed{\left\{2 \cdot \left(\frac{r}{t_b}\right) - 1\right\}} - 2 \cdot r_{\tau_s} \cdot \left(\frac{r}{t_b}\right) \right] \tag{3.6}$$

The semi-analytical formulation will make use of the weld load carrying stress coefficient, C_{bw}, as will be discussed in Section 3.3.5. This coefficient is used because the weld geometry causes a local change in stiffness, a shift in neutral axis, meaning the weld becomes load carrying up to some extent. The weld gives a discontinuity in the structure which distorts the stress flow and lets stress flow through the weld. This causes a higher stress concentration at the weld toe. Furthermore, C_{bw} makes the semi-analytical τ_n formulation dependent on the geometry of the assessed piece of structure. The other terms only rely on the tube radius, R_t and the notch angle, α. The C_{bw} value is used to correct the distribution with a linear term around the equilibrium point $\left(\frac{r}{t_b} = 0.5\right)$ which can also be distinguish from the part of the equation that is related to C_{bw}:

$$\left(2\left(\frac{r}{t_b}\right) - 1\right) \tag{3.7}$$

3.3.3. Far Field Stress Component

In this section the far field stress component is discussed. The related parts are highlighted with a box in Equation (3.8).

$$\tau_n\left(\frac{r}{t_b}\right) = \boxed{\tau_s} \left[C_m \left(\frac{r}{t_b}\right)^{\lambda-1} - (C_b + C_{bw}) \left\{2 \cdot \left(\frac{r}{t_b}\right) - 1\right\} - \boxed{2 \cdot r_{\tau_s} \cdot \left(\frac{r}{t_b}\right)} \right] \tag{3.8}$$

In the semi-analytical formula, the structural shear stress τ_s and the linear shear stress ratio r_{τ_s} have a large impact on the shape of the stress distribution and are known as the far field information. The far field projection is $\tau_s \left\{1 - 2r_{\tau_s}\left(\frac{r}{t_b}\right)\right\}$ which is also used for the mode-I formulation. This formulation is rotating around the equilibrium point $\left(\frac{r}{t_b} = 0.5\right)$.

In Figure 3.5, the different stress components are plotted for a large and small value of the linear stress coefficient, r_{τ_s}. The shape of the far field stress is used to determine how to incorporate the linear terms. Figure 3.5a is related to a tubular welded joint with a radius of 50 [mm]. This means a relative large linear term is presented as can be noted in the far field stress distribution. Figure 3.5b is related to a geometry with a radius of 4000 [mm]. This approaches a planar geometry which can be noted by the almost identical constant stress term, τ_m, and far field stress term, τ_f.

The far field information can be obtained in two ways for the 2D model, analytically and numerically. The analytical way uses the initial loading parameters to calculate the parameters without local notch information

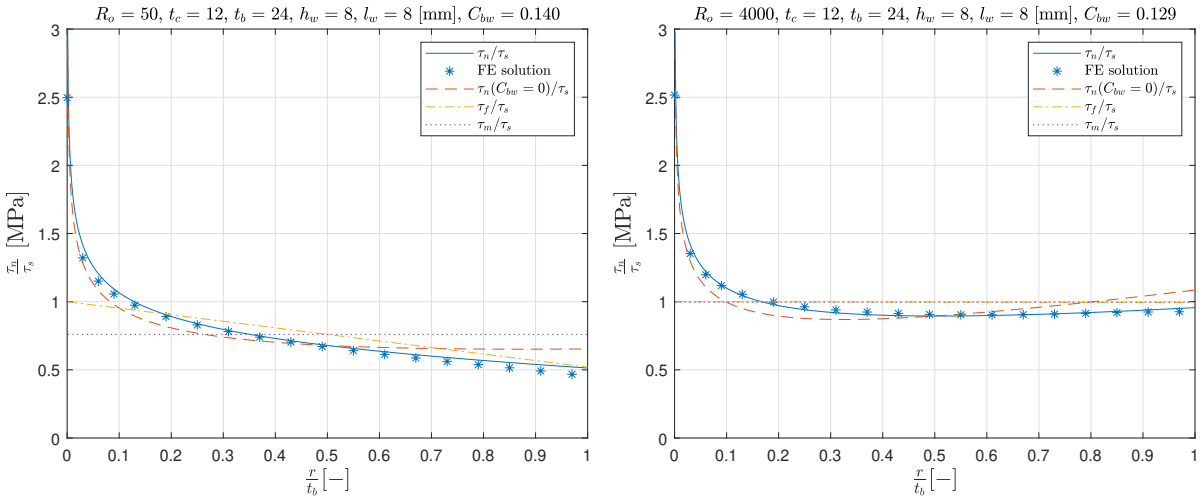

(a) $r_{\tau_s} = 0.24$ (b) $r_{\tau_s} = 0.003$

Figure 3.5: Stress distribution for a large and small value of r_{τ_s} with corresponding distributions for τ_f and τ_m.

incorporated. The numerical method uses the values calculated through obtaining the nodal forces from FEA, in this case Ansys. These numerical obtained values from the solid model already include the local notch information.

Analytical Method The analytical method, in this case excluding local notch information in the far field information, uses the initial loading to calculate τ_s and r_{τ_s}. In the case of this research, it is the torsion moment, M_t, which is applied at the end of the tube. The structural shear stress can be obtained with Equation (3.9). The constant and linear stress can be obtained from τ_s with respectively Equation (3.12) and (3.13), and are dependent on the geometry of the structure. The linear stress ratio is used as far field input for the semi-analytical formula and can be obtained using Equation (3.14). For a planar geometry or tubular geometry where $R_t >> t_b$, τ_b goes to zero and therefore r_{τ_s} as well.

$$M_t = \frac{J_t \tau_s}{R_t} \tag{3.9}$$

$$J_t = \frac{\pi}{2}\left(R_t^4 - (R_t - t_b)^4\right) \tag{3.10}$$

$$\tau_s = \frac{M_t R_t}{J_t} \tag{3.11}$$

$$\tau_m = \tau_s \frac{R_t - \frac{t_b}{2}}{R_t} \tag{3.12}$$

$$\tau_b = \tau_s - \tau_m \tag{3.13}$$

$$r_{\tau_s} = \frac{\tau_b}{\tau_s} \tag{3.14}$$

Numerical Method The numerical method, in this case including local notch information in the far field information, uses the τ_s and r_{τ_s} calculated from the node information in through thickness direction. Every node has a force in both the x and y direction. These forces can be rewritten to a force related to the mode-I and mode-III component, see Equation (3.18) where F'_x and F'_y are the mode components. In the tubular joint case, only the mode-III component has a value since a pure torsion load is applied. The nodal forces related to mode-III are transformed into line forces, Equation (3.19). The line forces are the input for the formulations to obtain τ_m (Equation (3.15)) and τ_b (Equation (3.16)) by nodal forces obtained from FEA. These can be used to calculated r_{τ_s} which are then input for the semi-analytical formula.

$$\tau_m = \frac{\sum f_{x,n}}{t_b} \tag{3.15}$$

$$\tau_b = \frac{6\left(\sum f_{x,n} \cdot y_i - \tau_m \cdot \frac{t_b^2}{2}\right)}{t_b^2} \tag{3.16}$$

$$r_{\tau_s} = \frac{\tau_b}{\tau_m + \tau_b} \tag{3.17}$$

$$\begin{Bmatrix} F'_{x,n} \\ F'_{y,n} \end{Bmatrix} = \begin{bmatrix} \cos(\alpha) & -\sin(\alpha) \\ \sin(\alpha) & \cos(\alpha) \end{bmatrix} \begin{Bmatrix} F_{x,n} \\ F_{y,n} \end{Bmatrix} \tag{3.18}$$

$$\begin{Bmatrix} F_1 \\ F_2 \\ F_n \\ \vdots \\ F_{n-1} \\ F_n \end{Bmatrix} = \begin{bmatrix} \frac{l_1}{3} & \frac{l_1}{6} & 0 & \cdots & \cdots & 0 \\ \frac{l_1}{6} & \frac{l_1+l_2}{3} & \frac{l_2}{6} & 0 & \ddots & \vdots \\ 0 & \frac{l_2}{6} & \frac{l_2+l_3}{3} & \frac{l_3}{6} & \ddots & \vdots \\ \vdots & \ddots & \ddots & \ddots & \ddots & 0 \\ \vdots & \ddots & \ddots & \ddots & \frac{l_{n-2}+l_{n-1}}{3} & \frac{l_{n-1}}{6} \\ 0 & \cdots & \cdots & 0 & \frac{l_{n-1}}{6} & \frac{l_{n-1}}{3} \end{bmatrix} \begin{Bmatrix} f_1 \\ f_2 \\ f_n \\ \vdots \\ f_{n-1} \\ f_n \end{Bmatrix} \tag{3.19}$$

3.3.4. Weld Notch Stress Formulation

Several combinations for the weld notch stress formulation are established and have been tried as semi-analytical formulation for the application in the effective notch stress concept. The semi-analytical formulation that is most comparable to the mode-I version and gives good results is stated in Equation (3.20). It gives the best shape and besides that the equation has the most logical structure. The notch stress component is considered as the part covering the constant part and with that the sharp notch. The far field stress component is correcting the distributions for the linear term that is related to the torsion loading. The far field part will be zero for a planar geometry since $r_{\tau_s} = 0$. The weld load carrying stress component is the geometry dependent part where C_{bw} is obtained by a parametric fit which will be discussed in Section 3.3.5. The constants regarding the static force, C_m, and moment equilibrium, C_b, are defined later in this section.

$$\tau_n\left(\frac{r}{t_b}\right) = \tau_s\left[C_m\left(\frac{r}{t_b}\right)^{\lambda-1} - (C_b + C_{bw})\left\{2\cdot\left(\frac{r}{t_b}\right) - 1\right\} - 2\cdot r_{\tau_s}\cdot\left(\frac{r}{t_b}\right)\right] \tag{3.20}$$

$$C_m = \lambda \tag{3.21}$$

$$C_b = \frac{3(\lambda-1)}{\lambda+1} \tag{3.22}$$

$$\lambda = \frac{\pi}{2\alpha} \tag{3.23}$$

Force and Moment Equilibrium

In this paragraph, the force and moment equilibrium will be discussed. The constants that will satisfy this are highlighted with a box in Equation (3.24).

$$\tau_n\left(\frac{r}{t_b}\right) = \tau_s\left[\boxed{C_m}\left(\frac{r}{t_b}\right)^{\lambda-1} - \left(\boxed{C_b} + C_{bw}\right)\left\{2\cdot\left(\frac{r}{t_b}\right) - 1\right\} - 2\cdot r_{\tau_s}\cdot\left(\frac{r}{t_b}\right)\right] \tag{3.24}$$

Static force and moment equilibrium should be satisfied at the through thickness level, see respectively Equation (3.25) and (3.26). This equilibrium is used to obtain two constants, C_m and C_b. These assure that the equilibrium is always settled since the C_{bw} term "rotates" the distribution around the equilibrium point $\left(\frac{r}{t_b} = 0.5\right)$. These two constants are an important part to conserve all the energy in the system. The force and moment equilibrium are also used by Den Besten to obtain formulations for Mode-I [9].

$$\int_0^1 \tau_n \, d\left(\frac{r}{t_b}\right) = \int_0^1 \tau_f \, d\left(\frac{r}{t_b}\right) \tag{3.25}$$

$$\int_0^1 \tau_n \cdot \left(\frac{r}{t_b}\right) d\left(\frac{r}{t_b}\right) = \int_0^1 \tau_f \cdot \left(\frac{r}{t_b}\right) d\left(\frac{r}{t_b}\right) \tag{3.26}$$

$$\tau_f = \tau_s \left(1 - 2r_{\tau_s}\left(\frac{r}{t_b}\right)\right) \tag{3.27}$$

3.3.5. Weld Notch Load Carrying Stress Estimate

The weld load carrying stress estimate, C_{bw}, is fitted for 6,300 individual stress distributions by varying all the dimension which are stated in Table 3.1. This is done by the curve fitting toolbox of Matlab, where the custom fitting function $\left\{C_{bw,fit}\left(2\left(\frac{r}{t_b}\right)-1\right)\right\}$ is used to obtain the $C_{bw,fit}$ values. It uses the difference between the FEA results and the semi-analytical formula without a C_{bw} to obtain a fitting value for C_{bw}, $C_{bw,fit}$. These values are used as input to determine an empirical function which is obtained using a multi polynomial regression analysis function in Matlab.

Four non-dimensional geometry parameters are chosen as the independent variables which are stated in Equation (3.29) to (3.31) distinguishing the difference in load carrying level. All geometry ratios are individually incorporated as well as in the correlations terms in the formula that is obtained with the parametric fitting function. Furthermore, the order to which the parameters are fitted can be manually set which can make the function more precise, though more complex.

The geometry parameters are chosen based on the Mode I equations [34] and the nature of the mode-III shear stress in the geometry. Qin et al. used T, thickness related, and W, weld related, in the same way as is done in this research. The log parameter in T is chosen since the parameter is following a more linear trend on log-scale which realises a better fit. R, radius ratio related, and S, weld size plate thickness related, are added to gain precision to the fit. If $R_t = 0$, which implies a full planar geometry, R is zero and this follows the trend for C_{bw}. S is based on the relation between the thickness of the plate and the weld length. A relatively large weld length simulates a thicker end of the plate. A small weld length creates a sharper angle which influences the stress flows. Therefore, this factor has an important influence as well. Other non-dimensional geometry parameter combinations were also tested but did not add valuable changes to the fit.

Functions for the weld load carrying coefficient are determined. The function in Equation (3.28) is simplified by not using all parameters to the 4th order $\left(T^1, W^2, S^2 \, and \, R^4\right)$ and is related to the analytical approach of obtaining τ_s and r_{τ_s}. Furthermore, small terms which do not influence the distributions significantly are removed. The function is simplified to make it more amenable which improves the easiness of using it in engineering practices. In Appendix A, the higher order formulations can be found.

$$\begin{aligned} C_{bw} = {} & 0.04918T - 0.06191W + 0.3476S + 0.3817R - 0.01052W^2S^2 - 0.05106T^2R^2 + 0.1372S^2R^2 \\ & - 0.1022TS + 0.1981TR - 0.1503WS - 0.101WR - 0.5244SR - 0.004839TW^2 + 0.05057TS^2 \\ & - 0.07678TR^2 + 0.07238WS^2 + 0.01302T^2S - 0.2183TR^3 + 0.2089WR^2 + 0.01449WR^3 - 0.966SR^2 \\ & + 0.1021S^2R + 0.8919SR^3 + 0.017T^2 - 0.1256S^2 + 0.257R^2 - 1204R^3 + 0.5704R^4 - 0.01868TWS^2 \\ & + 0.0135TW^2S + 0.04942TWR^2 + 0.04197TSR^2 - 0.01334TS^2R + 0.1069WSR^2 \\ & - 0.01327TWR + 0.02516TSR + 0.1468WSR - 0.03644TWSR + 0.1172 \end{aligned} \tag{3.28}$$

with:

$$T = log\left(\frac{t_c/2 + l_w}{t_b}\right) \tag{3.29}$$

$$W = \frac{l_w}{h_w} \tag{3.30}$$

$$R = \frac{t_b}{R_t} \tag{3.31}$$

$$S = \frac{l_w}{t_b} \tag{3.32}$$

3.4. Evaluation and Conclusion

In this section, the findings regarding the mode-III weld notch shear stress distribution are evaluated. The stress distributions for different geometries are discussed. The engineering application is evaluated based on the far field information obtained from a shell and a solid model. The goodness of the fit for the weld load carrying stress estimate is presented. Ultimately, a road map for how to create the semi analytical formulation is given.

3.4.1. Stress Distributions

The obtained semi-analytical formulation for the weld notch stress distribution is used to plot the distribution in Figure 3.6. The distributions follow the same trends as the FE distributions. The values in the notch affected region are important since this part of distributions is needed to calculate the effective notch stress. That part is also in line with the FE solution. In the error bar plots in Figure 3.8, η_2 is related to the distributions and shows that the distribution is meeting the requirements.

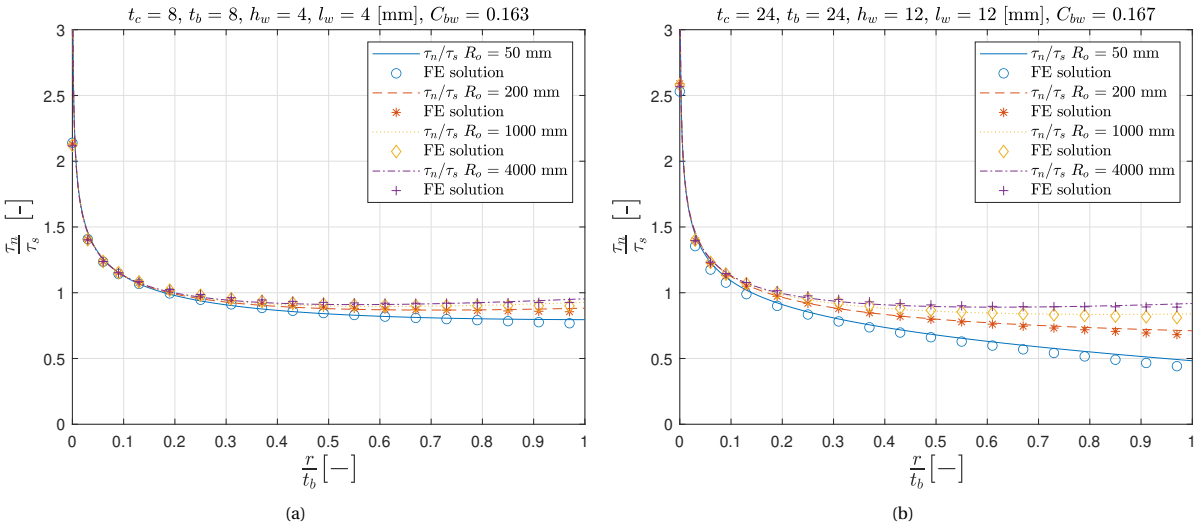

Figure 3.6: Stress distributions for specimens with realistic dimensions.

The weld notch shear stress distributions that are obtained with the semi-analytical formulation follow the trends of the FE solution. The errors are small and the largest errors are close to the notch or related to geometries that are not realistic or even not allowed due to regulations. Therefore, it can be concluded that the formulation can be used for the effective notch stress concept.

For the analytical distribution, the stress at the notch goes to the theoretical value of infinity where the value obtained with FEA varies between 1 and 3 MPa. The discrepancy is due to the modelling and both values are probably unrealistic. The expectation is that the stress distribution in reality will be somewhere in the middle between the FEA and the semi-analytical formulation. This will not lead to problems since the analytical formulation is more conservative in that respect.

The formulations can be used to calculate the effective notch stress although the micro-structural support length, $\rho*$, needs to be determined for Mode-III. An effort to do this is presented in Chapter 4 of this thesis. If this can be realised it will be a more accurate assessment of the fatigue lifetime of structures.

The geometries used in this research are all tubular welded joints with varying dimensions. Ideal geometries like the specimens in this research behave differently compared to as-built structures where more deviation can be found. This should be taken into account when assessing structures and might be something to assess in future studies. Although the geometries for which the radius is large ($R_t = 4000$ [mm]) are approaching planar geometry behaviour, in a parallel study next to this thesis, a pure planar geometry will be assessed.

The relative errors for all the 6,300 geometries are visualised in the bar plots in Figure 3.8. The way the errors are calculated is stated in Equation (3.33) to (3.35). η_1 is related to the function without taking into account the stress that is carried by the weld ($C_{bw} = 0$). η_2 is showing the errors for which C_{bw} is taken into account with the complete function and obtained by using Equation (3.20). η_3 is showing the errors for which C_{bw} is taken into account with the simplified function. 98.75 % of the stress distribution has an relative error

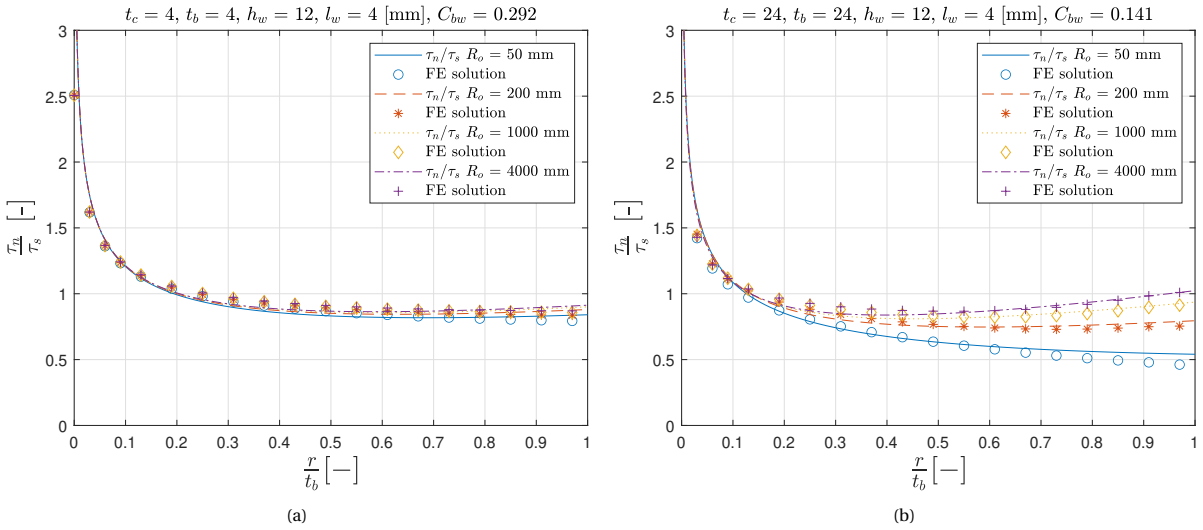

Figure 3.7: Stress distributions for extreme dimensions

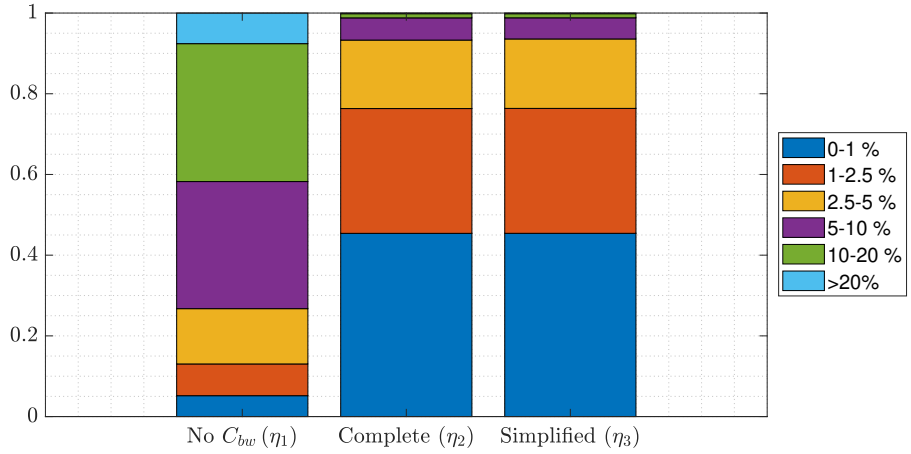

Figure 3.8: Global error estimates for the stress distribution using no C_{bw}, the complete and the simplified function.

which is lower than 10 % and are therefore acceptable.

$$\eta_1 = \frac{\tau_{FEA} - \tau_n\left(C_{bw} = 0\right)}{\tau_{FEA}} \tag{3.33}$$

$$\eta_2 = \frac{\tau_{FEA} - \tau_n\left(C_{bw,complete}\right)}{\tau_{FEA}} \tag{3.34}$$

$$\eta_3 = \frac{\tau_{FEA} - \tau_n\left(C_{bw,simplified}\right)}{\tau_{FEA}} \tag{3.35}$$

In Figure 3.9a, the mean error and corresponding standard deviation for all geometries are plotted. In Figure 3.9b, this is done for all geometries with a weld angle between 40° and 50°, i.e. weld dimensions which are as supposed to be in as-built structures. In this case Equation 3.28 is used to obtain the C_{bw} values. Both figures show that the relative error in the far field zone is small. The error in the notch affected zone is significant, but can be explained. The theoretical weld notch shear stress distribution obtained with the semi-analytical formulation approaches a maximum notch stress of infinity. The stress distributions obtained with FEA have a finite maximum notch stress value, which makes that a flatter trend in the notch affected zone is observed.

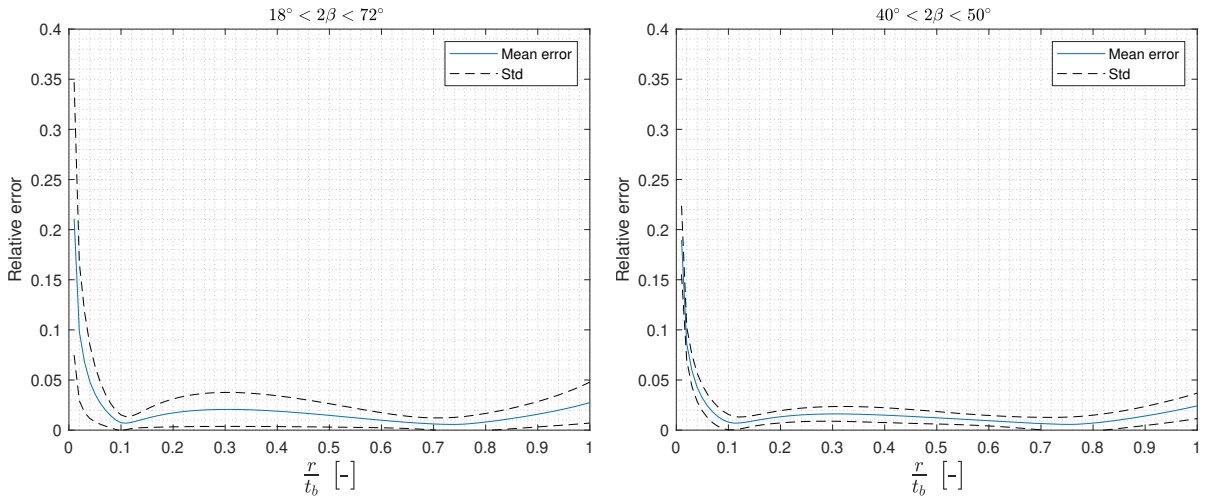

(a) For all weld dimensions incorporated in this study.

(b) Realistic weld dimensions with a weld angle between 40°and 50°.

Figure 3.9: Mean error plotted over the through thickness direction with the standard deviation.

Unusual dimensions

The obtained stress distributions for common weld dimensions are shown in Figure 3.6. The distributions are as one would expect and they follow the same trend as the FE solution. Unusual dimension combinations are also taken into account to get a complete function for C_{bw} and the fit in general. Some of them are more off compared to the ones in Figure 3.6 and are shown in Figure 3.7. Although these dimensions are not common in practice, a weld angle of 45 degrees is standard, the distributions still follow the trends of the FE solution. This means that even for the extreme cases, good results can be obtained using the developed formulation for C_{bw} and τ_n.

The Structural Shear Stress, τ_s and the Linear Stress Ratio, r_{τ_s}

In Section 3.3.3, it is shown that an analytical and numerical method can be used to obtain the values for τ_s and r_{τ_s}. The analytical values give a slightly better estimation for the through thickness stress distribution regarding the solid models. Furthermore, the values are easier to obtain since no FEA including weld modelling is necessary. The loading and geometry parameters are sufficient to calculate the analytical values and with that for establishing a stress distribution. The advantage of the numerical values is that more local information near the notch is included by τ_s and r_{τ_s} instead that this information is included in C_{bw} which makes it less dependent of that parameter. The shape with a $C_{bw} = 0$ for the numerical case is naturally already quite good due to the incorporated local information in τ_s and r_{τ_s}, compared to the one with the analytical values. This phenomenon can be seen in Figure 3.10b.There the two are almost identical where the two distributions obtained with the analytical method are more off as can be seen in Figure 3.10a. Though the error using the relatively large C_{bw} is smaller.

In Figure 3.10a, the trend of the weld notch shear stress distribution obtained with the analytical method is more in line with the FE solution than the numerical method. The latter starts above the FE solution then goes down a bit where after it reaches infinity. The analytical one follows the distributions of the FE solution over the complete through thickness distribution. But an even more important aspect are the results from the shell model analysis in Section 3.4.2. The numerical obtained values for τ_s and r_{τ_s} are comparable to the analytical values obtained for the solid model. Since no local information regarding the weld and notch is present in the shell model it is logical that these values are in line with the analytical calculated far field information. If one wants to use the numerical far field information obtained with shell models, the C_{bw} value obtained with the analytical values is the one to use. This is one of the goals of this research since these methods should in the end be implemented in engineering practices where shell models are the standard. Therefore, it can be said that this method is the one to use.

The different errors for both methods are stated in Figure 3.11. It is clear that the distribution obtained with the analytical method is more accurate. Since it is also easier to obtain and less FEA is necessary the analytical method is the best to use in practice. However, once the structure becomes more complex, it is no longer possible to obtain τ_s and $r_{\tau s}$ by simply considering its geometric dimensions as in Equations (3.9)-(3.14). Therefore, for complex structures it is suggested to numerically obtain τ_s and $r_{\tau s}$ from a FE shell model

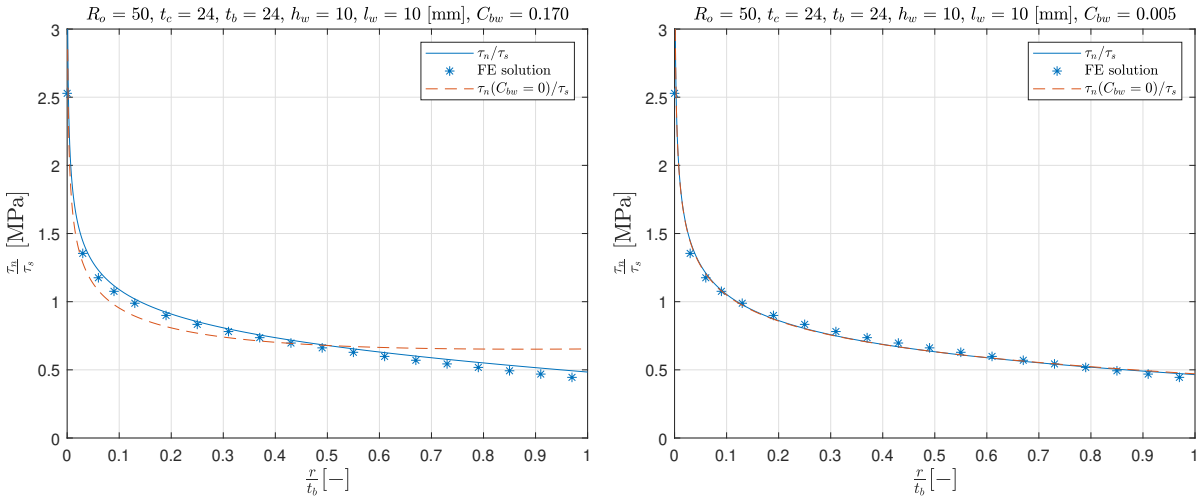

(a) Analytical method

(b) Numerical method

Figure 3.10: Stress distributions with different method of calculating τ_s and r_{τ_s}.

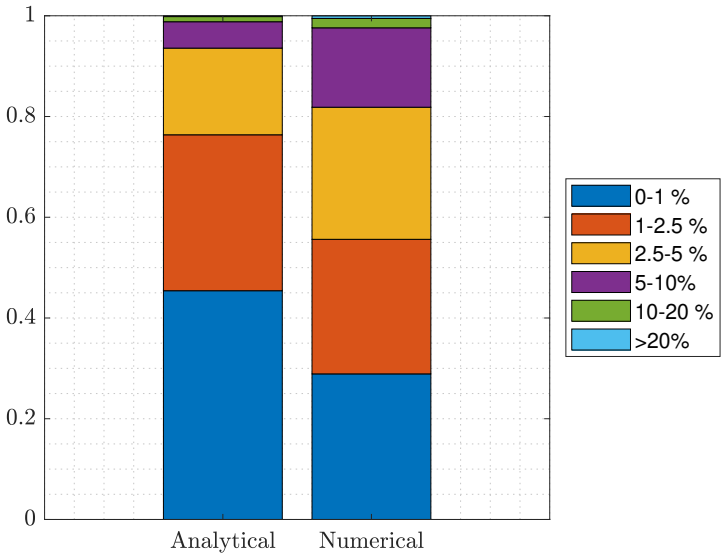

Figure 3.11: Global error estimate, η_2 for the analytical method and η_3 for the numerical method including all 6300 geometries.

and then proceed with the so called "analytical method". The "numerical method" could be used when using a FE solid model since the local information is then obtained from FE and should not already be included in the weld load carrying stress estimate, C_{bw}. A method to obtain this could be introduced in future research.

Another way to evaluate the analytical and numerical results is the outcome of the effective notch stress calculated with the two separate methods. This could be done when the procedures in Chapter 4 are successfully executed. It is recommended to do future research on the topic of the relation between the numerical and analytical obtained effective notch stress.

Comparison with Mode-I Distribution

In the literature review, the formulation for mode-I is mentioned. Since the mode-III formulation has followed from the development of the formulation for mode-I an evaluation has been made regarding the differences. The mode-III formulation contains an extra bending term, C_b, which depends on the notch angle. This term has followed from the moment equilibrium that is satisfied. Also the first term is different, the sine and cosine terms are dissipated in the force equilibrium term, C_m, since static force equilibrium is satisfied as well.

	$R_t = 50$ $t_b = 24$		$R_t = 100$ $t_b = 24$		$R_t = 500$ $t_b = 24$		$R_t = 4000$ $t_b = 24$	
	τ_s	r_{τ_s}	τ_s	r_{τ_s}	τ_s	r_{τ_s}	τ_s	r_{τ_s}
FEA	0.93	0.12	0.98	0.04	0.99	0.02	1	0.003
Analytical	1	0.24	1	0.12	1	0.02	1	0.003

Table 3.3: Difference between τ_s and r_{τ_s} obtained analytically and via a shell model.

$$\begin{aligned}\sigma_n\left(\frac{r}{t_p}\right) = \sigma_s \Bigg\{ & \left(\frac{r}{t_p}\right)^{\lambda_s - 1} \mu_s \lambda_s (\lambda_s + 1) \left[\cos\left\{(\lambda_s + 1)\beta\right\} - \chi_s \cos\left\{(\lambda_s - 1)\beta\right\}\right] \\ & + \left(\frac{r}{t_p}\right)^{\lambda_a - 1} \mu_a \lambda_a (\lambda_a + 1) \left[\sin\left\{(\lambda_a + 1)\beta\right\} - \chi_a \sin\left\{(\lambda_a - 1)\beta\right\}\right] \\ & + C_{bw} \cdot \left\{2\left(\frac{r}{t_p}\right) - 1\right\} - 2 \cdot r_s \cdot \left(\frac{r}{t_p}\right)\Bigg\}\end{aligned} \tag{3.36}$$

$$\tau_n\left(\frac{r}{t_b}\right) = \tau_s \left[C_m \left(\frac{r}{t_b}\right)^{\lambda - 1} - (C_b + C_{bw}) \left\{2 \cdot \left(\frac{r}{t_b}\right) - 1\right\} - 2 \cdot r_{\tau_s} \cdot \left(\frac{r}{t_b}\right)\right] \tag{3.37}$$

3.4.2. Solid and Shell FE Model Based Far Field Stress

In engineering practices, reduced computation time can be important for the application of fatigue assessment concepts. In structural analysis problems, FE shell models are preferred over solid models for their ease of creation and reduced computation time. However, shell models are inherently missing structural details which, as described Section 3.3, have a fundamental importance for the through thickness stress distribution near weld notches. Therefore, in order to combine engineering practices and accuracy, it is of importance that the information necessary to obtain the stress distribution with the semi-analytical formulation can be grasped from a shell model. In this section, this is done and documented.

In Ansys, a shell model is constructed of a tubular welded joint as can be seen in Figure 3.12. The nodal forces at the nodes along the weld seam, visualised in Figure 3.13, can be grasped and used to obtain the parameters as input for the semi-analytical formulation. This is done with the method as described in Section 3.3.3 under the "numerical method". The results that are obtained using these calculations are stated in Table 3.3. It is found that for geometries with a relatively high r_{τ_s}, the analytically obtained values differ the most from the FE values. Important to note is that these values do not contain local notch information since the weld is not modelled in a shell model. Therefore, although the values are numerically obtained, the C_{bw} parametric function obtained with the analytical method (no local information included in the far field information) should be used. Since the weld is not modelled in a shell model, the linear ratio seems to be less. This could be attributed to the linear stress effect due to the torsional loading is not fully effective which leads to a lower value. This will also be discussed in the next paragraph.

The distribution that can be made with this result are shown in Figure 3.14. The C_{bw} is obtained with Equation (3.28). This is the parametric function where the local notch information is incorporated in the C_{bw} value. It can be clearly seen that even the results for $R_t = 50$ and $t_b = 24$ are following the trend which is obtained with the FE solid model. It could even be argued that the results with the shell model are better than the ones obtained with the analytical input parameters for geometries with a relatively high structural linear stress ratio. Furthermore, the trends are more accurate, though less conservative, in the notch affected region. This could be due to the fact that the analytically obtained linear term is not fully effective. Since the values for r_{τ_s} are smaller compared to the analytical values as can be seen in Table 3.3 this could lead to a more realistic value or representation of the linear stress term but it is hard to conclude since in the basis it are all approximations.

3.4.3. Weld Load Carrying Stress Coefficient

The weld load carrying stress coefficient depends on the geometry and since a fit is found a correlation is expected. These trends of the weld load carrying stress coefficient are discussed in this section.

In Figure 3.18a and 3.18b, the trend of C_{bw} is plotted over the cross plate thickness for two different base plate thicknesses and several weld dimensions ($W = 1$). The dimensions of the weld are highly correlated

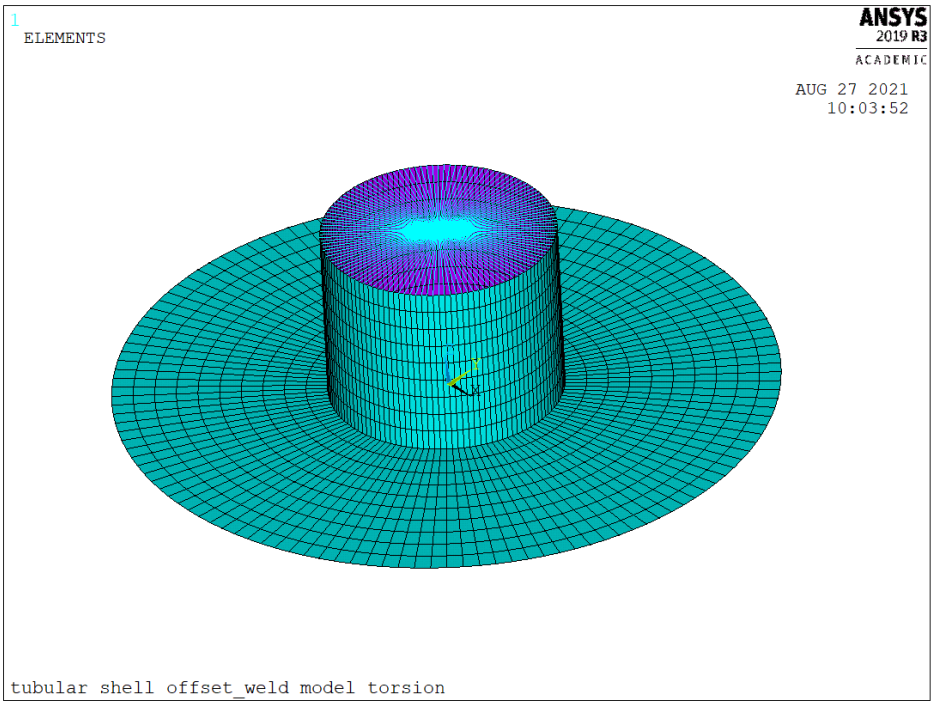

Figure 3.12: The shell model of the tubular welded joint

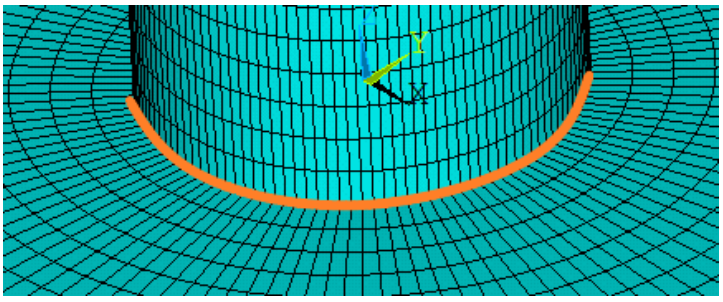

Figure 3.13: The virtual weld seam in the shell model used to obtain nodal forces.

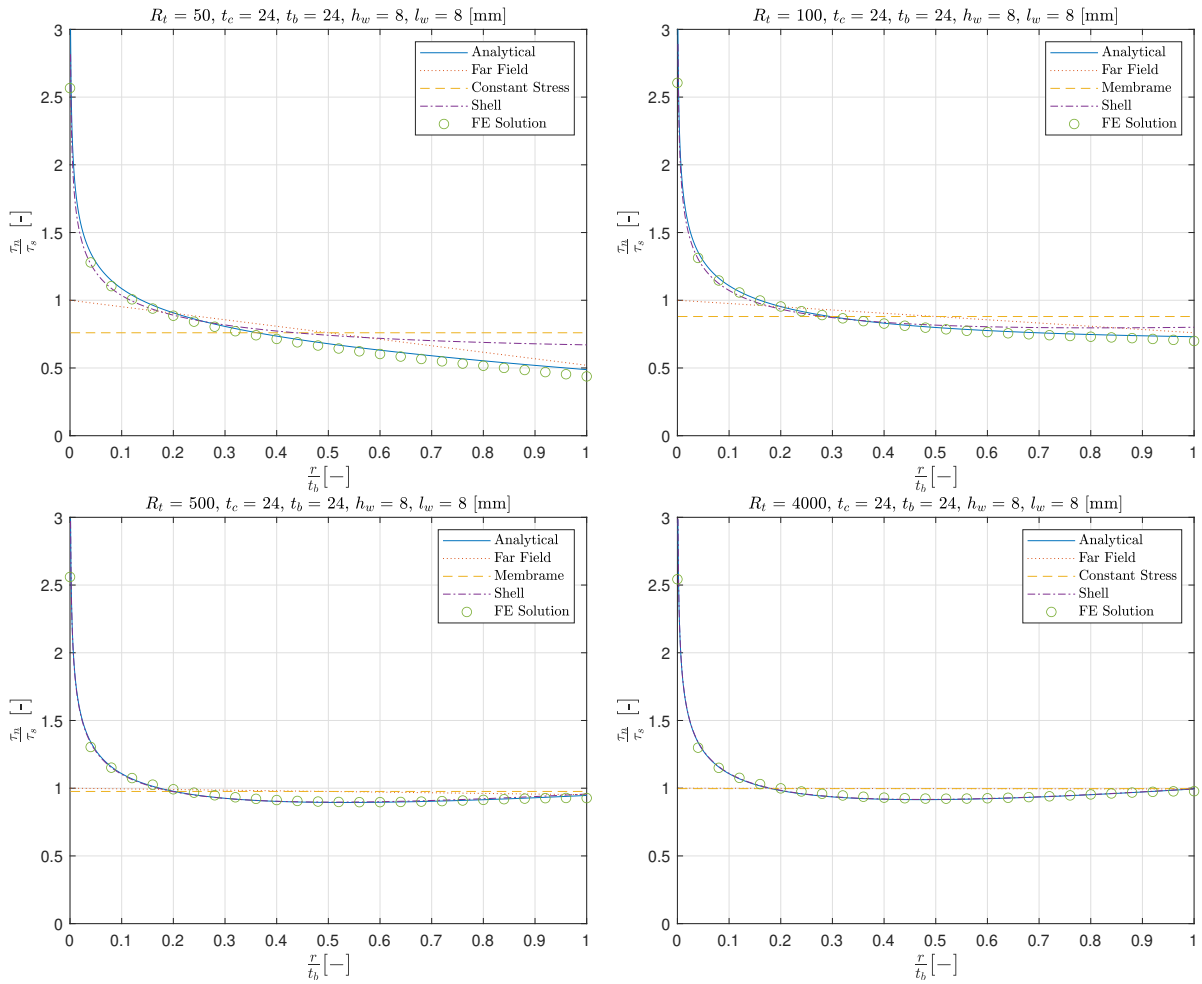

Figure 3.14: Stress distributions of the compared parameters shown in Table 3.3

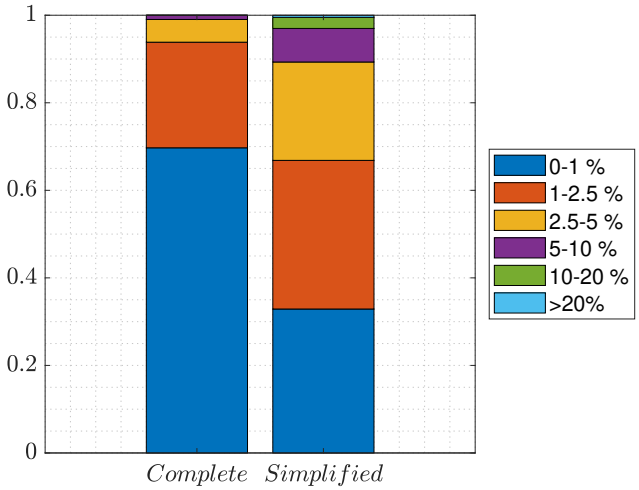

Figure 3.15: Global error estimate for complete and simplified C_{bw} function compared to the linear fitted one, Equation (3.38).

with the height of C_{bw} which can be seen for a large and small r_{τ_s} in respectively Figure 3.18a to 3.18d. The larger the weld, the more load carrying the weld becomes.

This trend becomes more clear if the weld height and weld length are varied. The weld length does not affect the change in C_{bw} significantly as can be seen in Figure 3.18e compared to Figure 3.18f. Varying the weld height shows a significant change, an increase in h_w causes an increase of C_{bw} since this follows from an increase in the relative weld and cross plate load path stiffness. It could also be explained as a small weld height leads to a more blunt notch which leads to a lower stress concentration at the notch due to a softer disturbance.

In Figure 3.18a and 3.18b, it can be noted that increasing the thickness of the base plate decreases C_{bw} since the relative stiffness contribution of the weld and the cross plate load path decreases which means that the weld is less load carrying. It can also be explained that due to the smaller thickness the weld is more load carrying which leads to a higher stress concentration at the notch. This causes a higher C_{bw} for a thinner base plate. Furthermore, can be seen that the weld is less load carrying for a smaller cross plate thickness. This effect is not seen for the cases with a small linear stress ratio as in Figure 3.18c and 3.18d. So it seems that the cross plate is more load carrying compared to the weld if the linear stress is relatively large.

The trends of C_{bw} for Mode-I are analysed by Qin et al. [34]. The trends correspond with the trends seen for Mode-III which is a pleasant finding. This could make it easier to combine the two in a multiaxial concept when the behaviour at the notch is comparable.

The variation of the base plate thickness is hard to visualise. The C_{bw} value has four parameters which leads to a 4D problem. Since t_b is involved in 3 of the 4 ratios it is hardly impossible to show the trend with t_b on the x-axis with a constant r_{τ_s} value. This can be attributed to the choice of the radii of the specimens which could be incorporated in a future study.

$$\eta_4 = \frac{C_{bw,fit} - C_{bw,function}}{C_{bw,function}} \tag{3.38}$$

In Figure 3.16 and 3.17, the linear fitted C_{bw} values and the ones obtained with the empirical fitted function are plotted for the complete and simplified function. It is clear that the blue dots (parametric function) follow the trend of the red dots (linearly fitted). In the bar plots in Figure 3.15, η_4 shows the error for the C_{bw} values. For the complete function more than 99% of the values have an error less than 10% where for the simplified function the error is larger. Although the error for C_{bw} it self is larger, the total error for the stress distribution is slightly smaller compared to the complete function which can be noted in Figure 3.15. Therefore it has been decided to use the simplified function for the analysis.

3.4.4. Weld Load Carrying Stress Fitting Functions

The empirical function as stated in Equation (3.28) is the simplified version. The original function where all the four different ratios are incorporated to the 4^{th} order is stated in Appendix A. That one is significantly more

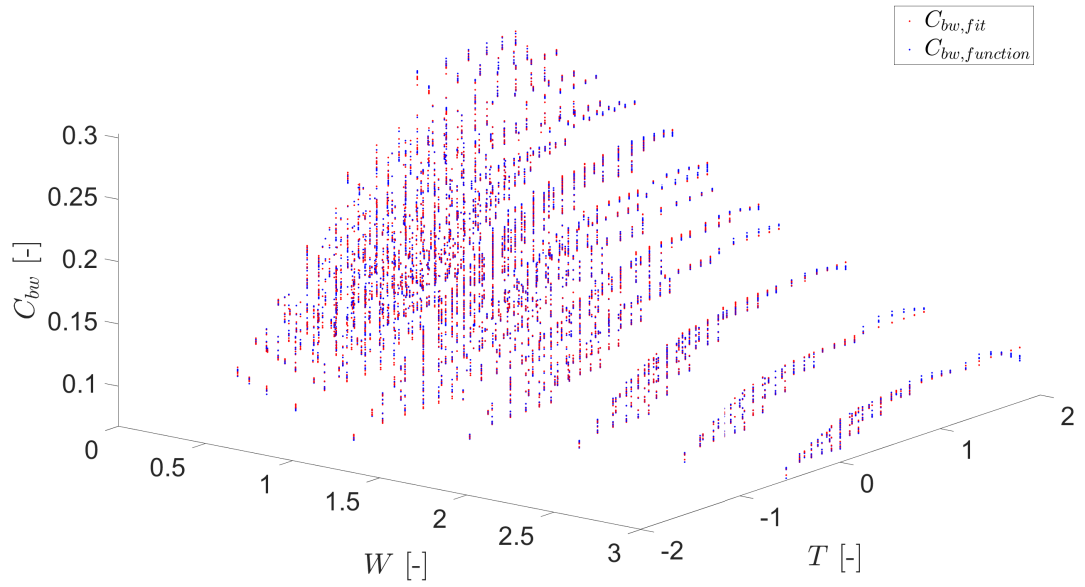

Figure 3.16: All fitted, $C_{bw,fit}$, and complete function $C_{bw,function}$ values for all geometry configurations regarding W and T.

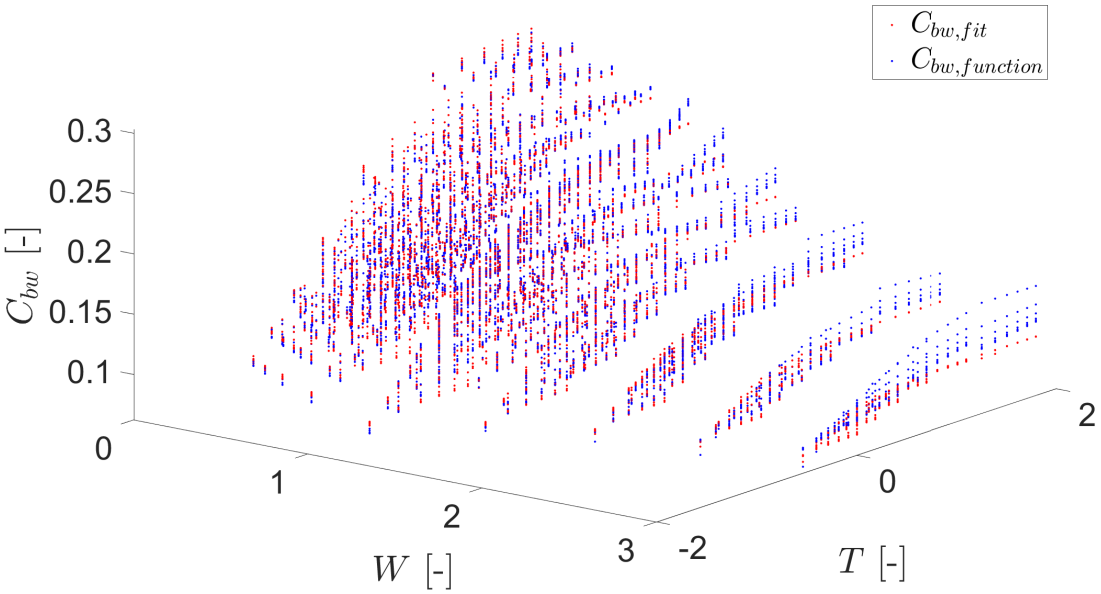

Figure 3.17: All fitted, $C_{bw,fit}$, and simplified function $C_{bw,function}$ values for all geometry configurations regarding W and T.

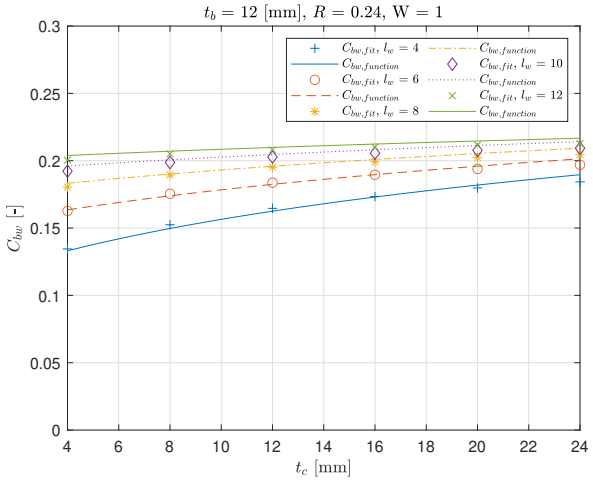

(a) Varying cross plate thickness.

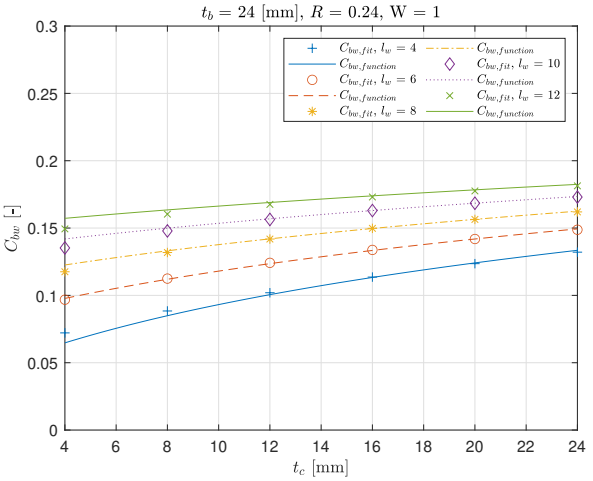

(b) Varying cross plate thickness.

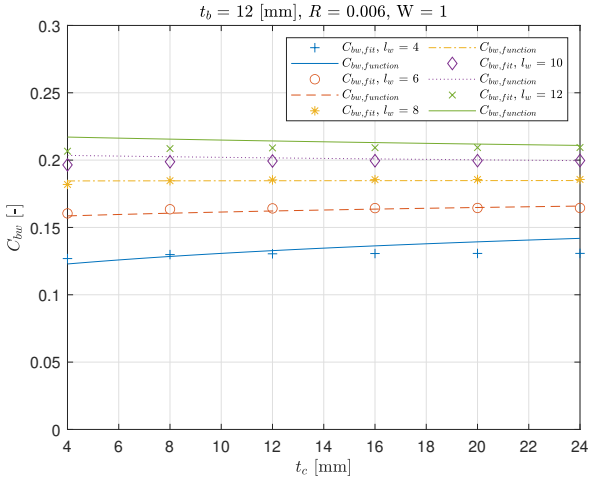

(c) Varying cross plate thickness for $r_{\tau_s} = 0.003$ with $t_b = 12$.

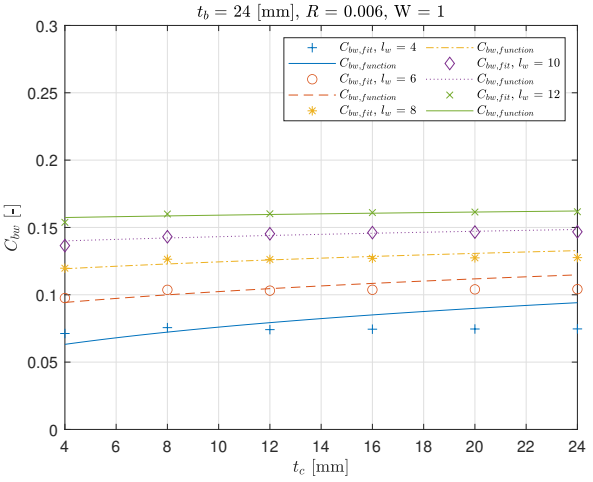

(d) Varying cross plate thickness for $r_{\tau_s} = 0.003$ with $t_b = 24$.

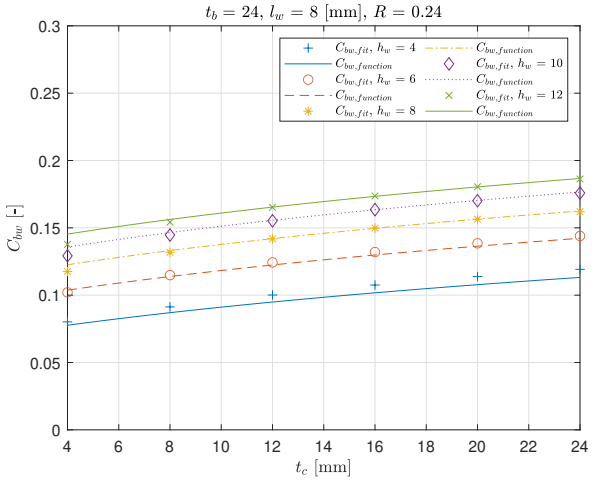

(e) Constant weld length with varying weld height.

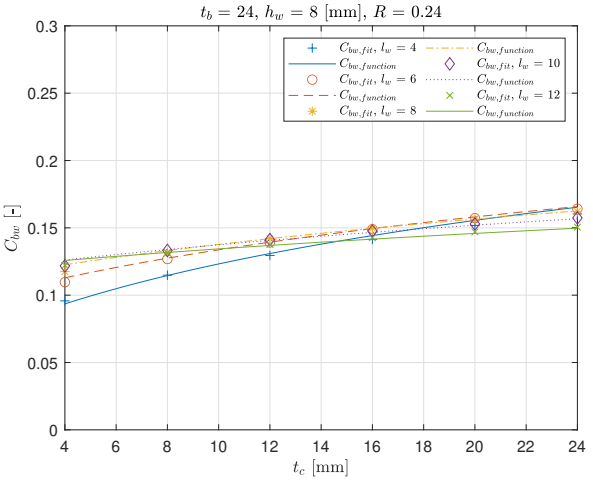

(f) Constant weld height with varying weld length.

Figure 3.18: Trends of C_{bw} for varying dimensions.

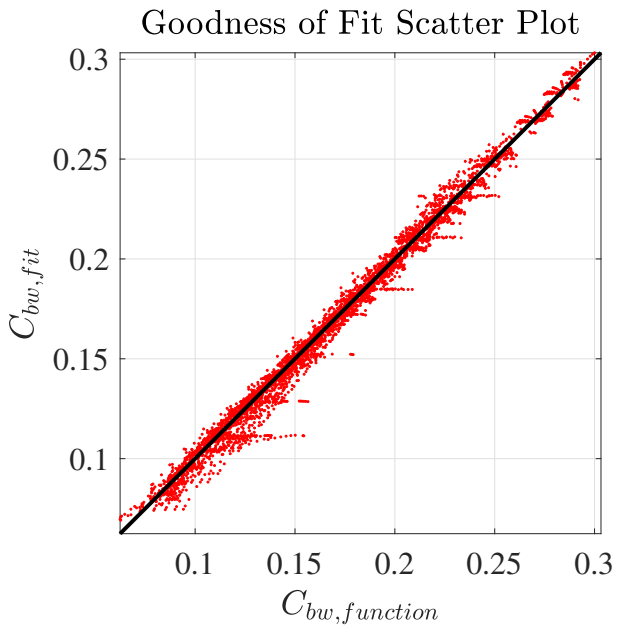

R^2	0.9881
MAE	0.0240
MAESTD	0.0270

Figure 3.19: Goodness of fit plot and fitting parameters of Equation (A.1)

complex and therefore the estimation of C_{bw} is better but it has not a significant influence on the accuracy of the stress distributions and gives even a slightly worse result as can be seen in Figure 3.8. The complete function can be used for research purposes or when the accuracy of C_{bw} is more important than the accuracy of the stress distribution. For engineering purposes the simplified function is easier to use since it is more simple to implement and as already said, slightly more accurate on the stress distribution for the tested geometries.

The fitting parameters and the goodness of fit plot of the simplified function are stated in Figure 3.19. The coefficient of estimation, R^2, for the simplified function is 0.9881. This value should be as close to 1 and therefore this function gives a good approximation of C_{bw}. The original function as stated in Equation (A.1) has a R^2 value of 0.9984 which shows the higher accuracy of using all the terms.

For Equation (A.1), (A.2) and (A.3) a leave one out cross validation is performed. The results of this validation are stated in Appendix A and show that the performance of the fits are good in that sense since the results are almost identical to the original fitting parameters. For Equation (3.28) this is not the case since this function is manually adjusted, this is done since it was requested to have a formulation as simple as possible.

The formulation for C_{bw} regarding the numerically obtained far field information is also stated in Appendix A, Equation (A.3). This formulation can be used when a solid model is present and it is hard to determine the far field loading that is applied on the structure to obtain the analytical far field values. It should not be used in combination with shell models since then local notch information is not taken into account in the numerical far field information nor in the weld load carrying stress estimate. It is furthermore a less accurate fit then the ones for which the local notch information is incorporated. This could be attributed to the fact that the values are quite small, which makes the fit error sensitive. Since the effect of the numerically obtained C_{bw} is small in general this is not per se a problem since it does not really effect the stress distribution outcomes.

3.4.5. Road map Semi-Analytical Formulation

In this section, a road map is presented on how to use the semi-analytical formulation. There are three scenarios namely "No FE model", "Shell model" and "Solid model". For every scenario it is briefly described which Equations to use for obtaining the correct far field information and which functions should be used to grasp the correct C_{bw}.

$$\tau_n\left(\frac{r}{t_b}\right) = \tau_s\left[C_m\left(\frac{r}{t_b}\right)^{\lambda-1} - (C_b + C_{bw})\left\{2\cdot\left(\frac{r}{t_b}\right) - 1\right\} - 2\cdot r_{\tau_s}\cdot\left(\frac{r}{t_b}\right)\right] \tag{3.39}$$

$$C_m = \lambda \tag{3.40}$$

$$C_b = \frac{3(\lambda-1)}{\lambda+1} \tag{3.41}$$

$$\lambda = \frac{\pi}{2\alpha} \tag{3.42}$$

Scenario	**No FE Model**	**Shell Model**	**Solid Model**
Type of structures	Only simple structural assembly, axisymmetric structures	Every simple or complex structural assembly	Every simple or complex structural assembly
τ_s and r_{τ_s}	Analytically obtained using Equations (3.9) - (3.14)	Numerically obtained using nodal forces along the seam where the weld would be with Equations (3.15) - (3.19)	Numerically obtained using nodal forces along the weld toe seam where mode-III loading & response is noted with Equations (3.15) - (3.19)
C_{bw} Formulation	Local notch information incorporated in formulation Equation (3.28).	Local notch information is **not** incorporated in the far field information and is therefore incorporated in the C_{bw} value, therefore use Equations (3.28).	Local notch information is incorporated in the far field information since the weld is modelled, therefore use Equation (A.3).

Table 3.4: Road map: How to use the semi analytical formulation, Equation (3.39) in different situations.

3.4.6. Conclusion

The goal of this part was to establish a semi-analytical formulation for weld notch shear stress distribution which can be used for the effective notch stress concept. This is achieved and stated in Equation 3.20. The formulation for the weld load carrying stress coefficient is accurate enough to obtain distributions that follow the FE solution trend. The weld notch stress distributions are more conservative at the notch than the FE solutions but this is not seen as a problem. It is found that the far field information can be obtained using FE shell models which makes the formulation useful for engineering practices. It can even be concluded that the far field information obtained with shell models gives a better representation of the stress distribution in the notch affected zone compared to the analytically obtained far field information.

4

Material Characteristic Length ρ^*

In Section 2.3.5 it is shown that the material characteristic length ρ^* is the length over which the stress distribution is integrated in the effective notch stress concept to obtain the effective notch stress. In literature, no specific value is found for this length in relation to mode III loading & response conditions. Therefore, this value needs to be obtained. The procedure of doing this will be discussed in this Chapter. The developed weld notch shear distribution from the previous chapter is used in this chapter to obtain the effective notch stress. Experimental fatigue test data necessary for the analysis will be discussed. The regression analysis that is used to find a value for the material characteristic length is elaborate on and an evaluation regarding the results is given.

4.1. Experimental Fatigue Test Data

Experimental fatigue test data is used to estimate the material characteristic length, the estimation process is discussed in Section 4.2. Therefore, the found data will be discussed. For test specimens, the shear stress distribution is calculated by using the formulation which is described in Chapter 3. The geometry dimensions needed as input for the semi-analytical formulation are found in papers. The different data sets which are found will be discussed below. The dimensions of the several specimens are stated in Table 4.1. If detailed Figures are presented they are added to Appendix C

Source	t_b	t_c	l_w	h_w	R_t [mm]	r_l
Sonsino [48]	10	25	9	9	44.45	-1
Seeger [42]	8	20	6.3	6.3	54	-1
Yousefi [59]	8	25	10	10	42.45	0/-1
Siljander [43]	9.525	9.525	8	8	25.4	0/-1
Amstutz [3]	7.7	25	9	9	42.15	0/-1
Razmjoo [37]	3.2	12	11	11	24.3	0
Yung [61]	7.95	8	7.7	7.7	23.8	-1

Table 4.1: Dimensions of the used experimental fatigue test data.

4.1.1. The Experimental Data Sets

Sonsino

Sonsino et al. [48] performed fatigue tests for a tube-flange connection. The geometry is stated in Figure 4.1. The weld notch has a radius of 0.45 [mm] which means there is no fully effective singularity. This could have an effect on the effective notch stress calculation for sharp notches. Still the data is used since there is already few data and the expectation is that the effect is small.

Seeger

Seeger et al. [42] performed fatigue tests for a flange-tube-flange connection. The geometry is stated in Figure 4.1 The data is used by Sonsino [46] and Hu [21] but together with the original paper [42] the dimensions for the welds are not clear. The data is used as presented by Hu but with adjusted radius of the tube since this can be clearly extracted from the original paper. The recommendation is to pay extra attention to this in future research since Seeger performed even more tests for which the dimensions are not fully clear but it could be useful data.

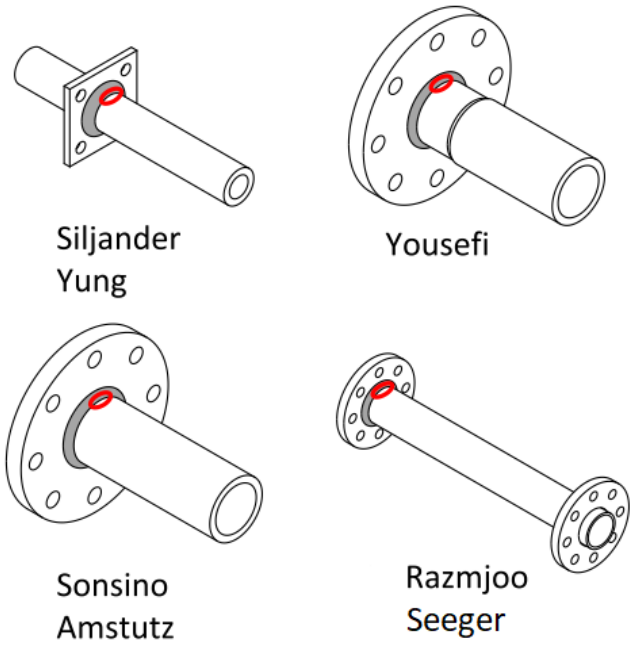

Figure 4.1: The geometries of the experimental data [31].

Yousefi
Yousefi et al. [59] performed fatigue tests for a tube-flange connection. It is not exactly clear how they calculated the torsion moment. They say they use Equation (4.1). But the length in this equation conform Figure C.5 does not really make sense for the torsion moment. Therefore, in this research, it is assumed that the torsion moment is applied as it is applied in the FE models used in this research. The geometry can be seen in Figure 4.1.

$$M_t = F_t \cdot l \tag{4.1}$$

Siljander
Siljander et al. [43] performed fatigue tests for a tube-flange connection where the geometry can be seen in Figure 4.1. The nominal torsion stress is taken as the maximum applied torsional stress, T_{xz}^{max}. In the nomenclature, $\Delta\tau_{max}$ can be find as the maximum local shear stress. It is not fully clear which can be taken as the structural stress at the outer radius of the tube. Furthermore, the geometry is double sided as can be seen in Figure 4.1. This is not an issue for now, but could be taken into account in future research when double sided flange structures are used to validate the stress distribution.

Amstutz
Amstutz et al. [3] performed fatigue tests for a tube-flange connection. The geometry is stated in Figure 4.1. There tests are straight forward and therefore useful for this research. No specialities are noted.

Razmjoo
Razmjoo [37] performed fatigue tests for a flange-tube-flange connection. The geometry can be seen in Figure 4.1. The base plate thickness of Razmjoo is only 3.2 mm. This could be seen as an outlier. The weld size is 11 mm. This can be seen as really large compared to the thickness of the base plate which makes the data exceptional.

Yung
Yung et al. [61] performed fatigue tests for a tube-flange connection. The geometry is double sided as can be seen in Figure 4.1. This is not an issue for now, but could be taken into account in future research when double sided flange structures are used to validate the stress distribution.

Conclusion Regarding Data Sets
It is clear that limited data is available. The data which is available is mostly comparable. The data sets lack variability, mainly in the base plate thickness which is important for this research. Therefore, it will be a hard task to gain confidence for the material characteristic length. For future research, more experimental data is needed, but it is not only about the quantity. The variety in geometry and response ratios should also be taken into account.

4.1.2. Walker Mean Stress Correction

Two loading ratios, r_l, can be observed in Table 4.1. These load ratios effect the fatigue life time. In order to improve the life time estimates, exponential mean stress models have been developed to incorporate the difference in loading ratio. This is mainly important for relatively low stress range and high mean stress. Walker's mean stress model [9] can be used to take the effects into account by using the stress range, Equation (4.2) and loading ratio, Equation (4.3), as the characteristics of the loading & response cycle in space. The formulation is stated in Equation (4.4).

This correction makes it possible to compare and use the experiments with different loading ratios. Furthermore, the loading ratio can be studied since the effect can be of importance for fatigue analysis of particular structures. Thereby, the load ratio coefficient γ is one of the maximum log likelihood estimates (MLE). This means the value will be varied to find an optimum, together with the other MLEs. This will be explained in the next section. Last but not least, the results will be evaluated and a conclusion will be drawn.

$$\Delta\tau = (\tau_{\max} - \tau_{\min}) \tag{4.2}$$

$$r_{lr} = \frac{\tau_{s_{min}}}{\tau_{s_{max}}} \tag{4.3}$$

$$S_{e,eff} = \Delta\tau_{e,eff} = \frac{\Delta\tau_e}{(1 - r_{lr})^{1-\gamma}} \tag{4.4}$$

Where:

r_{lr} = Load ratio [-]
γ = Load ratio coefficient [-]

4.2. Regression Analysis

Regression analysis can be used to determine the several parameters needed for a SN-curve which is used to determine the fatigue resistance. In case of the effective notch stress concept, the SN-curve is also depending on ρ^* since this influences the value of the effective notch stress. First, the theory behind the maximum likelihood regression analysis will be discussed. Thereafter, the profile log likelihood plots which show the uncertainty of the values and shows if the values are stable enough to use in practice will be shown. Lastly, a Monte Carlo type of approach is discussed where after the method using the AIC criterion is set out.

4.2.1. Maximum Likelihood Regression

The regression analysis, the maximum likelihood regression, tries to find the optimum values that are most likely to give a stable solution for the problem. The values are called the maximum log likelihood estimates. In the case of this study there are 5 estimated values: $\{\log(C), m, \sigma, \rho^*, \gamma\}$. The optimisation is executed by the Matlab function *fmincon*. This function is trying to find the optimum of the 5 parameters. For every parameter ranges are defined where the value should be in to constrain the problem and to secure a reasonable outcome. The log likelihood function is defined in Equation (4.5).

$$\mathscr{L}(\boldsymbol{\theta}; N \mid S) = \sum_{j=1}^{n} \delta_j \log\{f\left(N_j \mid S_j; \boldsymbol{\theta}\right)\} + \left(1 - \delta_j\right) \log\{1 - F\left(N_j \mid S_j; \boldsymbol{\theta}\right)\} \tag{4.5}$$

$$\boldsymbol{\theta} = \{\log(C), m, \sigma, \rho^*, \gamma\} \tag{4.6}$$

Where:

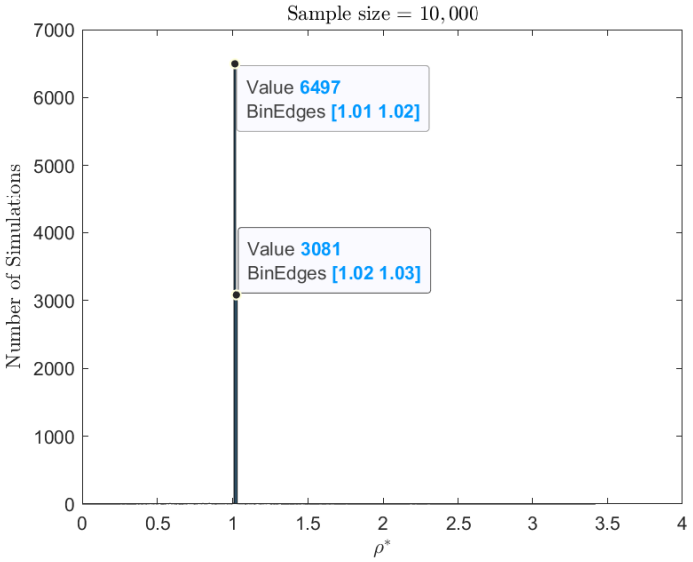

Figure 4.2: Results of a Monte Carlo simulation to obtain ρ^*.

δ = Data type {complete = 1, censored = 0} [-]
σ = Standard deviation [-]
C = Fatigue resistance constant [N/mm^2]
f = Probability density function [-]
F = Cumulative distribution function [-]
m = Fatigue resistance slope [-]
N = Total number of cycles until failure [-]
S = Stress range [N/mm^2]

4.2.2. Maximum Likelihood Regression Using Profile Likelihood Plots

Figure 4.5 shows the results of the profile log likelihood regression and it can be seen that the value found for ρ^* gives low confidence. Although the analysis gives an optimal value of 1.01 the results do not get significantly worse when a value between 0.01 and 9 is used. These are the values corresponding with the 75% confidence level which is visualised in Figure 4.5d. The value for log(C) is also not clear. This can be related to the fact that ρ^* could go up to close to zero which leads to close to an infinite effective notch stress which gives a highly unstable log(C). In cases of a high log(C) this leads to a rather conservative fatigue resistance curve in relation to the experimental data.

4.2.3. Maximum Likelihood Regression Using Monte Carlo

The maximum likelihood regression is also used with Monte Carlo simulation based initial parameter estimates. Like the single peak value in a parameter profile likelihood plot, the same MLEs for a range of Monte Carlo simulation based initial parameter estimates, provides a qualitative type of confidence that the set of MLEs reflect the global optimum in the design space. $\{\log(C), m, \sigma, \rho^*, \gamma\}$, are the randomly chosen input parameters out of uniform distributions to obtain results for the MLEs. The boundaries for the parameters are chosen such that reasonable output is guaranteed. The results for ρ^* are shown in Figure 4.2. 65% of the 10,000 taken samples give a value between 1.01 and 1.02, where 95% give a value between 1.01 and 1.03.

The result is reasonable and corresponds to the result that is obtained with the profile log likelihood plots. It gives extra confidence that the ρ^* value of 1.01 [mm] is in the right direction. Still the amount of experimental data and the lack of variation in base plate thickness makes it hard to proof that this result is the right result.

4.2.4. Akaike Information Criterion

The Akaike information criterion (AIC) [2] is a method to obtain the most likely parameter considering the number of parameters. The lowest AIC for a certain data set is taken as the most likely value by using the max-

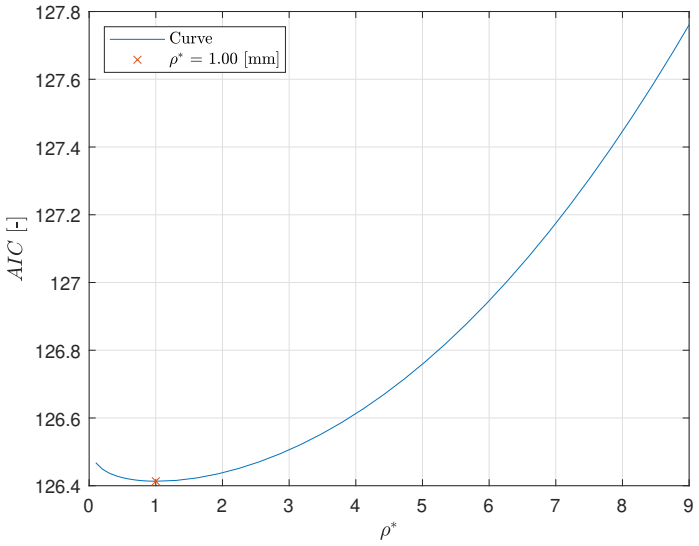

Figure 4.3: Akaike information criterion for varying ρ^*.

imum likelihood value, $\max\{\mathscr{L}(\boldsymbol{\theta}; N \mid S)\}$, subtracting the amount of parameters, k. This result is multiplied by a factor 2 coming from the χ^2 distribution. The formulation is stated in Equation 4.7. Executing this for ρ^* leads to a value of 1.00 [mm] as can be seen in Figure 4.3.

$$\text{AIC} = -2[\max\{\mathscr{L}(\boldsymbol{\theta}; N \mid S)\} - k] \tag{4.7}$$

4.3. Evaluation and Conclusion

The final ρ^* that is obtained from the analysis is 1.01 [mm]. The effective notch stress is obtained by integrating over this value. This leads to a SN-curve of which the MLEs are on top of Figure 4.5. Although it visually all looks pretty good, the confidence regarding the results is low as is most clearly described by the relative parameter profile likelihood plots mainly of $log(C)$ and ρ^* in Figure 4.5a and 4.5d.

The ρ^* of approximately 1 [mm] is the same as the material characteristic length that is obtained by using a support factor of 1 and a reference radius, ρ_f, of 1 [mm] as described in Section 2.3.5. The typical obtained value for mode-I found in literature is 0.4 [mm] but Qin et al. [35] found a value for mode-I which is also approximately 1 [mm]. The term "approximate" is an important one, since for both mode-I and mode-III it seems clear that a range of ρ^* values around the approximated ones give results that make give reasonable answers as well.

The values for the load ratio coefficient, γ, are 0.87 for mode-I [34] and 0.97 for mode-III obtained in this research. The difference could be declared to the fact that compressive stress has less influence on the fatigue lifetime then tensile strength. Negative stress in case of mode-I is compressive, while negative stress for mode-III is not. Therefore, it could be said that the influence of the mean stress correction is larger for mode-I. It should me noted that also for the load ratio coefficient the confidence levels are rather high.

The differences regarding the tested specimens can also be evaluated. Although it is very subjective due to the low amount of variation. In Figure 4.4 a difference between a load ratio of -1 and 0 can still be noted besides the fact the mean walker correction is already applied. Though it is hard to define the reason since large differences for the same loading condition are also present.

In Figure 4.6, five SN-curves are plotted where distinguishes are made clear between the specimens. Figure 4.6b shows the differences for the type of weld treatment. Only four specimens are as welded which also all have a relatively high stress range. This makes it hard to draw conclusions from this.

Figure 4.6c shows the difference in base plate thickness. It can be noted that the specimens of Seeger and Yousefi are both 8 [mm] and somehow are in line with each other. Amstutz has base plate thickness 7.7 [mm]. One should expect this also around Seeger and Yousefi, on the contrary this is not the case. Therefore, also the base plate thickness is a hard parameter to distinguish the different effects.

Figure 4.6d shows the differences in weld size. A spread is seen for various weld sizes. Actually the same

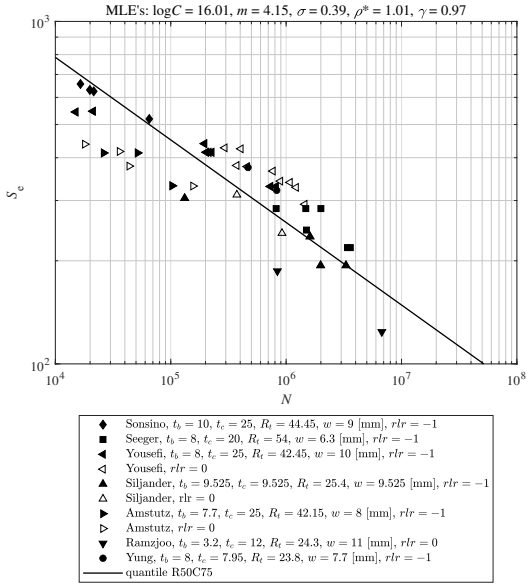

Figure 4.4: SN-curve showing the research project and load ratio in one.

conclusion can be drawn as for the base plate thickness, it is hard to find a pattern. A note can be made by the specimen of Razmjoo, these have a weld size of 11 [mm] but a thickness of 3.2 [mm]. This is ratio is an outlier. When more data is available, the data of Razmjoo should be evaluated if the set makes sense. Figure 4.6a and 4.6e can be also distinguished from Figure 4.4 and are already discussed before.

The final conclusion that can be drawn is that to obtain a profound solution for ρ^*, more experimental data is needed that represent a wider variety of specimen geometries. Now all almost all data sets have approximately the same plate thickness, radius and loading conditions. These data sets could help to gain more confidence over the obtained ρ^*. This could be done by using notch specimen data for which a material characteristic parameter should be present as well. The difference in type of notch can be covered by the stress angle β. Potential differences in material could be obviated by using a strain model.

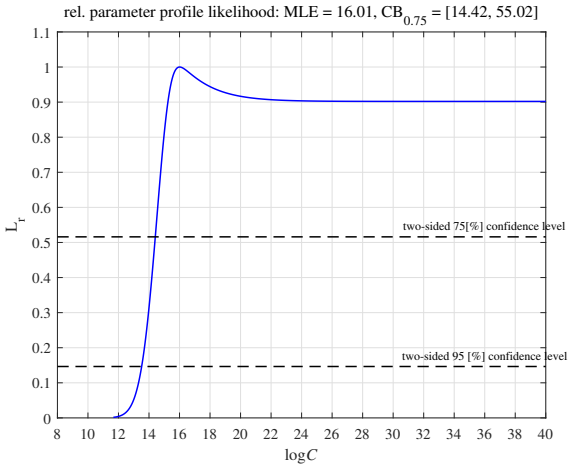

(a) The profile log likelihood of $\log C$.

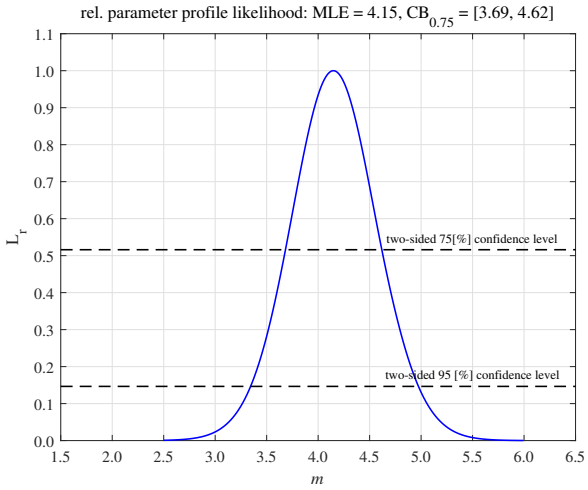

(b) The profile log likelihood of slope m.

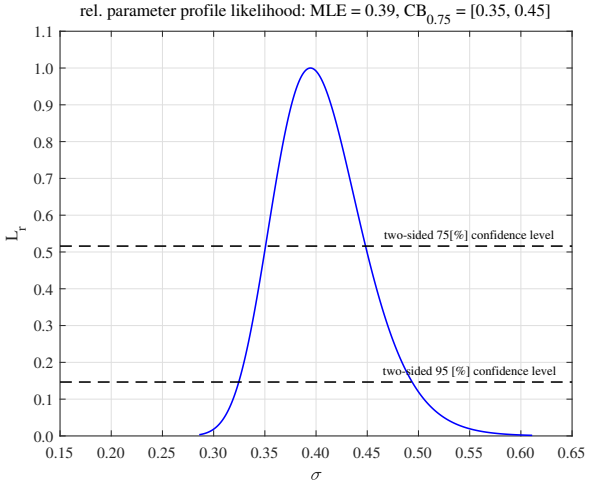

(c) The profile log likelihood of σ.

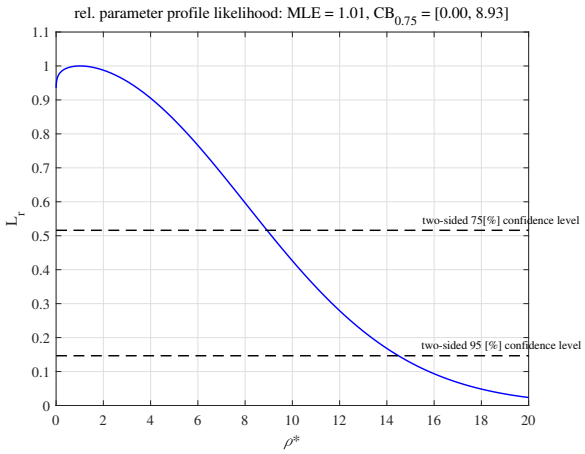

(d) The profile log likelihood of ρ^*.

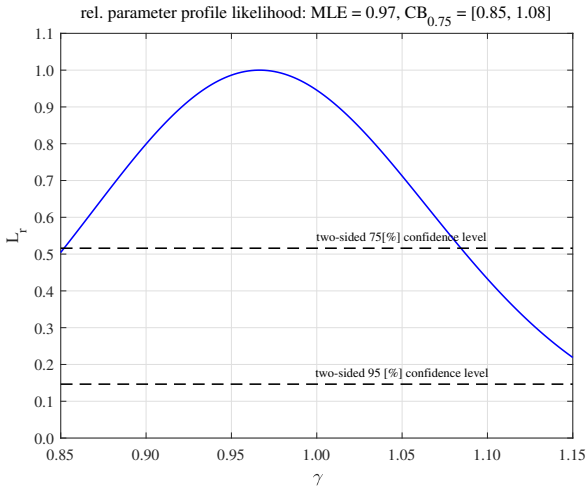

(e) The profile log likelihood of γ.

Figure 4.5: Profile log likelihood plots of the parameters to obtain a fatigue resistance curve for the effective notch stress concept SN-curve.

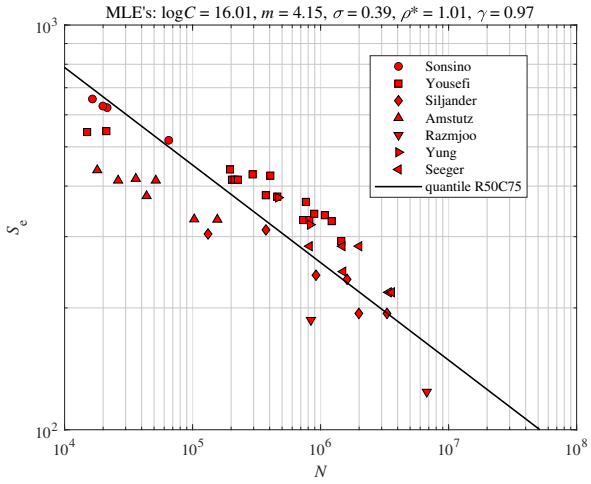

(a) Specimens divided based on the research projects.

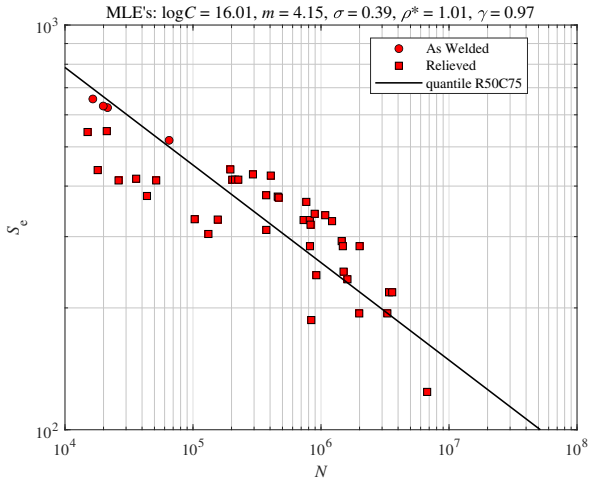

(b) Specimens divided based on the threatment of the weld.

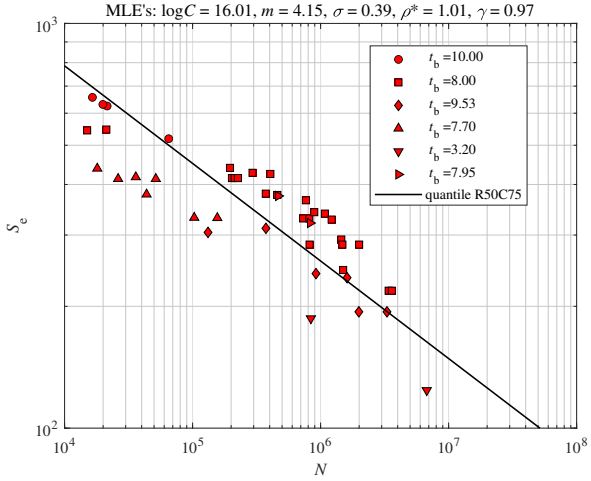

(c) Specimens divided based on the plate thickness.

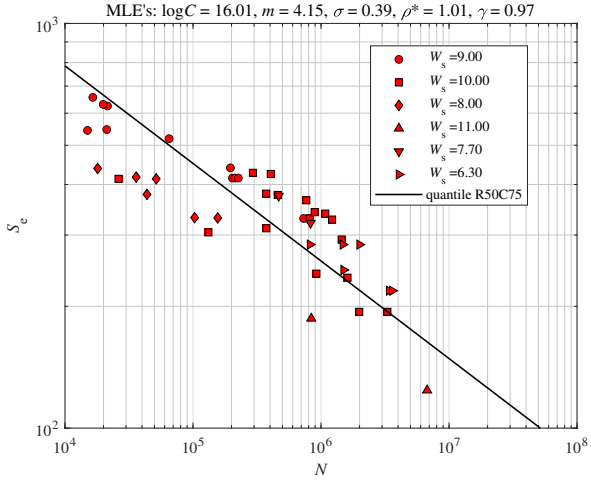

(d) Specimens divided based on the weld size.

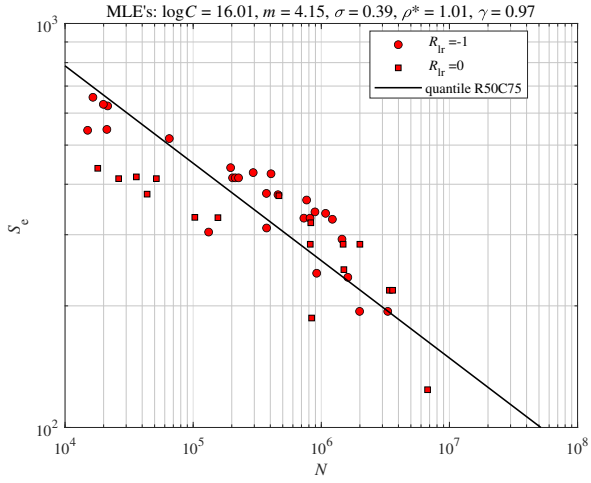

(e) Specimens divided based on the loading ratio.

Figure 4.6: SN-curves showing the trends of differences between the specimens.

5

Conclusion and Discussion

In this chapter, the research question will be answered and with that the conclusion of this research is stated. Thereafter, several results will be briefly discussed and a recap of the mentioned recommendations is given.

5.1. Research Questions

In this section, first the sub-questions will be answered where after a conclusion can be drawn regarding the main research question.

5.1.1. Sub-Questions

In which way is it possible to find a semi-analytical formulation for the through thickness weld notch shear stress distribution that can be used for the effective notch stress concept?

A semi-analytical formulation is obtained by using a notch stress, far field stress and weld load carrying stress component. These three are combined to a semi-analytical function that can describe the weld notch shear stress distribution. Accurate results are obtained and therefore the formulation can be used as input for the effective notch stress concept. The weld load carrying stress component uses a weld load carrying stress estimate to obtain good results for the distribution near the notch. This estimate is based on a polynomial function that uses the geometry dimensions of the structure.

Can the obtained semi-analytical formulation be used for practical engineering applications? In other words, is it possible to obtain information about the through thickens weld notch shear stress distribution from a coarse FE shell model without including local details (i.e. welds)?

The semi-analytical formulation that is obtained can be used with far field information extracted from a shell model. The obtained results for the stress distributions are in line with the FE trends. This means that if a shell model of a structure is present, engineers can use nodal forces to obtain the far field information and use the formulation to obtain the weld notch shear stress distribution of specific notches in a structure.

What is the effective notch stress related material-characteristic microstructural length parameter for mode-III loading?

The material characteristic microstructural length parameter for mode-III loading that is found in this research is 1 [mm]. This meets the expectation but the basis on which this is calculated is weak. The experimental data set is small which leads to uncertainties and large confidence bounds. More research, and mainly more experimental fatigue test data, in quantity and in variety, is necessary to obtain confidence over the results.

5.1.2. Main Research Question

How can the effective notch stress concept be used to investigate welded joints subjected to mode-III loading & response conditions and contribute to multiaxial fatigue assessment of welded joints in marine structures?

The effective notch stress concept can be used to investigate mode-III loading & response conditions. However, more confidence need to be gained on the material characteristic microstructural length to make it fully suitable for application. After this, a study can start on the application for multiaxial applications. In

this research, while searching for only torsion data, quite some multiaxial fatigue test data is found. This can be used to obtain a SN-curve where the effective notch stress is calculated both for mode-I with the method of Qin et al. [35] and the method for mode-III obtained in this research.

5.2. Recommendations

First of all, more experimental fatigue test data is needed in quatinty and variety. This is an outcome of many fatigue research project but not less important. Hopefully, the offshore wind turbine industry will keep investing in doing tests to make fatigue life time estimates more accurate.

Secondly, all FEA is done for a one sided tubular joint. Qin et al. [35] made up two formulations. One for a T-joint and one for a cruciform joint. The potential effects of the weld on the other side of the cross plate could be investigated in future research since it could be that the semi-analytical formulation developed in this research is applicable for that type of geometries.

When more certainty about the material characteristic length is obtained, the comparison could be made between the structural hot spot stress and the effective notch stress concept. This could gain insides on which method is most conservative after all. Furthermore, this is a good proof of concept on marine structures modelled in FE shell models.

In a validation study of the semi-analytical formula, the ratio between the radius and the base plate thickness could be chosen so that analysis on the trend of the weld load carrying stress coefficient is more practical. This can be done by varying the base plate thickness for constant ratios instead of fixed radii.

A method to obtain the "far" far field information as input for the "analytical method" could be studied. For example, what are the results if one take the stress from a distance from the notch where the load is linear but as close as possible to the notch.

A

Polynomial Functions for the Weld Load Carrying Stress Estimate, C_{bw}

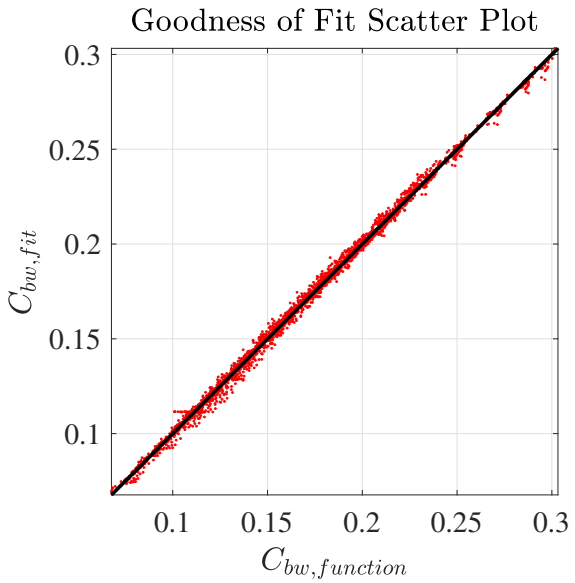

R^2	0.9984
MAE	0.0090
MAESTD	0.0100
CVRSquare	0.9983
CVMAE	0.0091
CVMAESTD	0.0102

Figure A.1: Goodness of fit plot and fitting parameters of Equation (A.1)

Function for C_{bw} with all the terms and correlations incorporated to the 4$^{\text{th}}$ order where r_s and τ_s are obtained analytically for the volume model:

$$
\begin{aligned}
C_{bw} = {} & -0.006203T^4 + 0.004146T^3W + 0.0372T^3S - 0.05115T^3R - 0.01099T^3 - 0.001147T^2W^2 \\
& - 0.0192T^2WS + 0.0007596T^2WR + 0.009642T^2W - 0.04274T^2S^2 + 0.07698T^2SR - 0.001759T^2S \\
& - 0.1907T^2R^2 - 0.07464T^2R + 0.01148T^2 - 0.001243TW^3 - 0.0007054TW^2S - 0.0007774TW^2R \\
& + 0.005868TW^2 + 0.009705TWS^2 - 0.01973TWSR + 0.02265TWS + 0.09198TWR^2 - 0.02886TWR \\
& - 0.02558TW + 0.005575TS^3 - 0.04881TS^2R + 0.07756TS^2 + 0.3065TSR^2 + 0.02561TSR \\
& - 0.1268TS - 0.2422TR^3 - 0.5451TR^2 + 0.2999TR + 0.05296T + 0.0008737W^4 + 0.001324W^3S \\
& + 0.003067W^3R - 0.01241W^3 - 0.003314W^2S^2 - 0.005437W^2SR + 0.01018W^2S \\
& - 0.03186W^2R^2 - 0.009344W^2R + 0.05654W^2 - 0.005961WS^3 + 0.005739WS^2R + 0.0331WS^2 \\
& + 0.0268WSR^2 + 0.05858WSR - 0.1058WS + 0.04575WR^3 + 0.1487WR^2 - 0.03219WR - 0.1217W \\
& - 0.008007S^4 - 0.05913S^3R + 0.06573S^3 + 0.1198S^2R^2 + 0.4048S^2R - 0.2779S^2 \\
& + 0.9186SR^3 - 0.3514SR^2 - 0.9149SR + 0.4721S + 0.3047R^4 - 1.026R^3 - 0.05018R^2 + 0.5067R + 0.1038
\end{aligned}
\tag{A.1}
$$

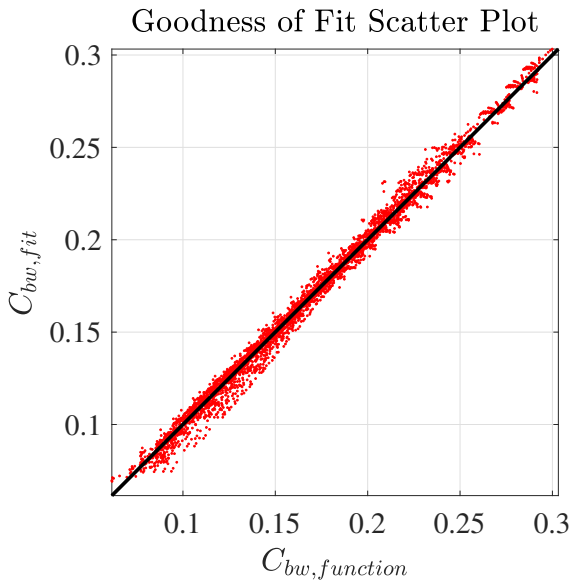

R^2	0.9925
MAE	0.0204
MAESTD	0.0223
CVR^2	0.9924
CVMAE	0.0206
CVMAESTD	0.0225

Figure A.2: Goodness of fit plot and fitting parameters of Equation (A.2)

Function of C_{bw} with T to the 1st, W and S to the 2nd and R to the 4th order where r_s and τ_s are obtained analytically for the volume model:

$$
\begin{aligned}
C_{bw} &= 0.04918T - 0.06191W + 0.3476S + 0.3817R - 0.01052W^2S^2 - 0.05106W^2R^2 \\
&+ 0.1372S^2R^2 + 0.001179TW - 0.1022TS + 0.1981TR - 0.1503WS - 0.101WR - 0.5244SR \\
&- 0.004839TW^2 + 0.05057TS^2 - 0.07678TR^2 + 0.07238WS^2 + 0.01302W^2S - 0.2183TR^3 + 0.2089WR^2 \\
&+ 0.008514W^2R + 0.01449WR^3 - 0.966SR^2 + 0.1021S^2R + 0.8919SR^3 + 0.017W^2 - 0.1256S^2 \\
&+ 0.257R^2 - 1.204R^3 + 0.5704R^4 - 0.01868TWS^2 + 0.0135TW^2S + 0.04942TWR^2 - 0.002805TW^2R \\
&+ 0.04197TSR^2 - 0.01334TS^2R + 0.1069WSR^2 - 0.00158WS^2R - 0.01625W^2SR - 0.001091TWS \\
&- 0.01327TWR + 0.02516TSR + 0.1468WSR - 0.03644TWSR + 0.1172
\end{aligned}
\tag{A.2}
$$

R^2	0.9807
MAE	0.2182
MAESTD	4.6836
R^2_{CV}	0.9804
CVMAE	0.2243
CVMAESTD	4.8505

Figure A.3: Goodness of fit plot and fitting parameters of Equation (A.3)

Function of C_{bw} with all the terms and correlations incorporated to 4^{th} order where r_s and τ_s are obtained numerically from the volume model:

$$
\begin{aligned}
C_{bw} &= 0.1723R^4 + 0.05414R^3S + 0.1042R^3T + 0.045R^3W - 0.2693R^3 - 0.02734R^2S^2 + 0.04444R^2ST \\
&+ 0.04868R^2SW - 0.06108R^2S - 0.002548R^2T^2 + 0.006188R^2TW - 0.1093R^2T - 0.009589R^2W^2 \\
&- 0.01432R^2W + 0.1004R^2 - 0.001341RS^3 - 0.01107RS^2T + 0.003866RS^2W + 0.01557RS^2 \\
&+ 0.007883RST^2 - 0.002697RSTW + 0.01398RST - 0.0009021RSW^2 - 0.01009RSW \\
&- 0.008668RS - 0.002748RT^3 + 0.001869RT^2W - 0.01296RT^2 - 0.001003RTW^2 + 0.00225RTW \\
&+ 0.009376RT + 0.00129RW^3 - 0.004492RW^2 + 0.01229RW - 0.01292R - 0.0001756S^4 \\
&+ 0.001894S^3T - 0.000334S^3W - 0.0002405S^3 - 0.008462S^2T^2 + 0.001904S^2TW + 0.006134S^2T \\
&- 0.0006556S^2W^2 - 0.0005258S^2W - 0.001282S^2 + 0.008079ST^3 - 0.004406ST^2W + 0.01098ST^2 \\
&- 0.0002464STW^2 + 0.0114STW - 0.03535ST + 0.0002512SW^3 + 0.002775SW^2 - 0.01179SW \\
&+ 0.01836S - 0.002457T^4 + 0.0004025T^3W - 0.0058T^3 - 0.0003663T^2W^2 - 0.0002073T^2W \\
&+ 0.005545T^2 - 0.0004382TW^3 + 0.001269TW^2 - 0.006309TW + 0.01554T + 0.001329W^4 \\
&- 0.01229W^3 + 0.04047W^2 - 0.05955W + 0.03364
\end{aligned}
\tag{A.3}
$$

B

Trends C_{bw} for the Simplified Function.

In this Appendix, Figures are stated that show the accuracy of the polynominal function for C_{bw} for all different combinations for the x and y-axis.

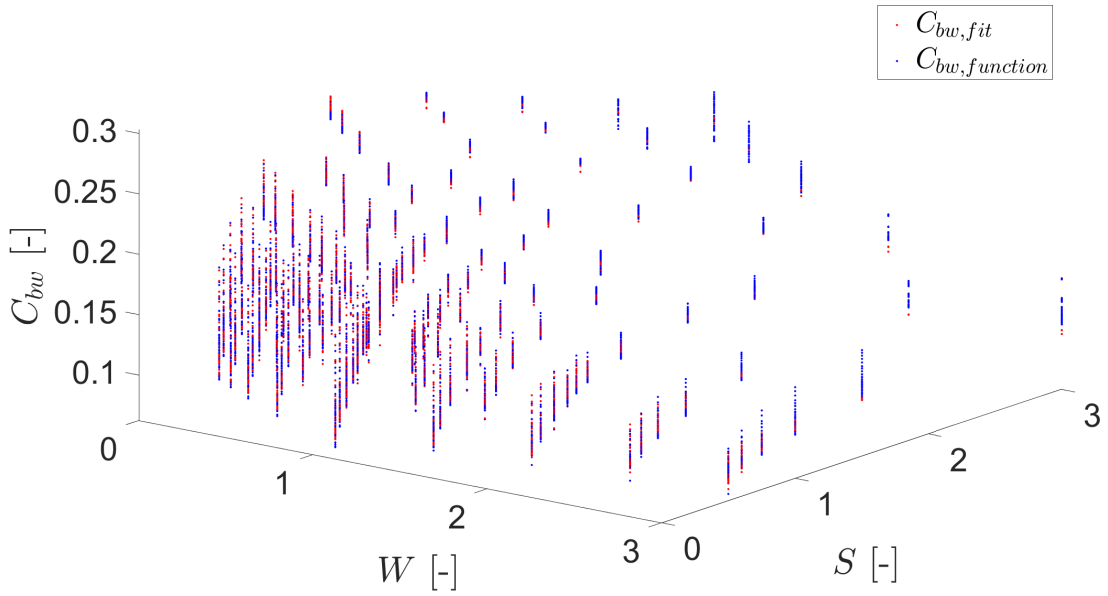

Figure B.1: All fitted and simplified function C_{bw} values for all geometry configurations regarding W and S.

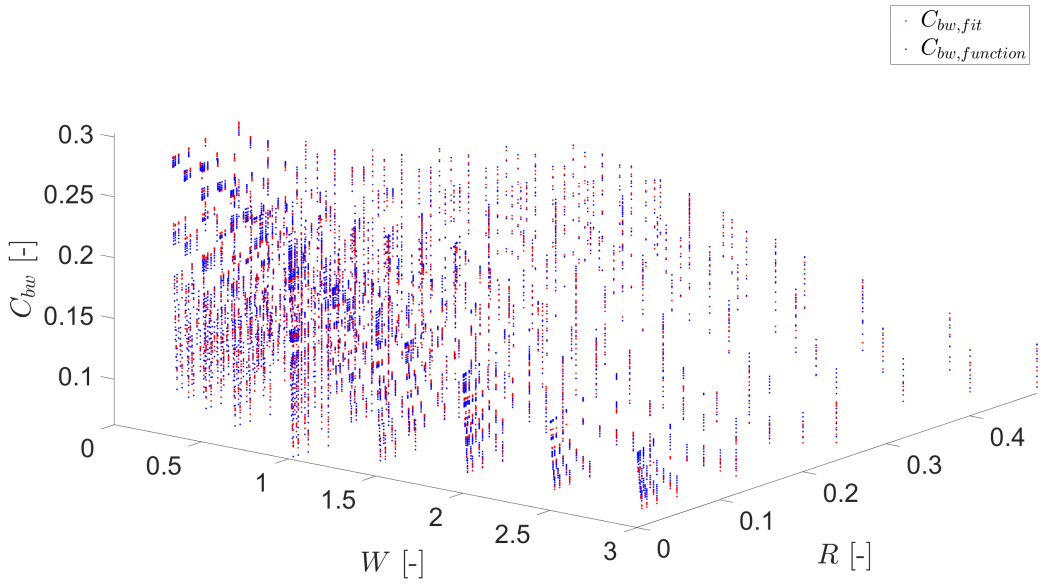

Figure B.2: All fitted and simplified function C_{bw} values for all geometry configurations regarding W and R.

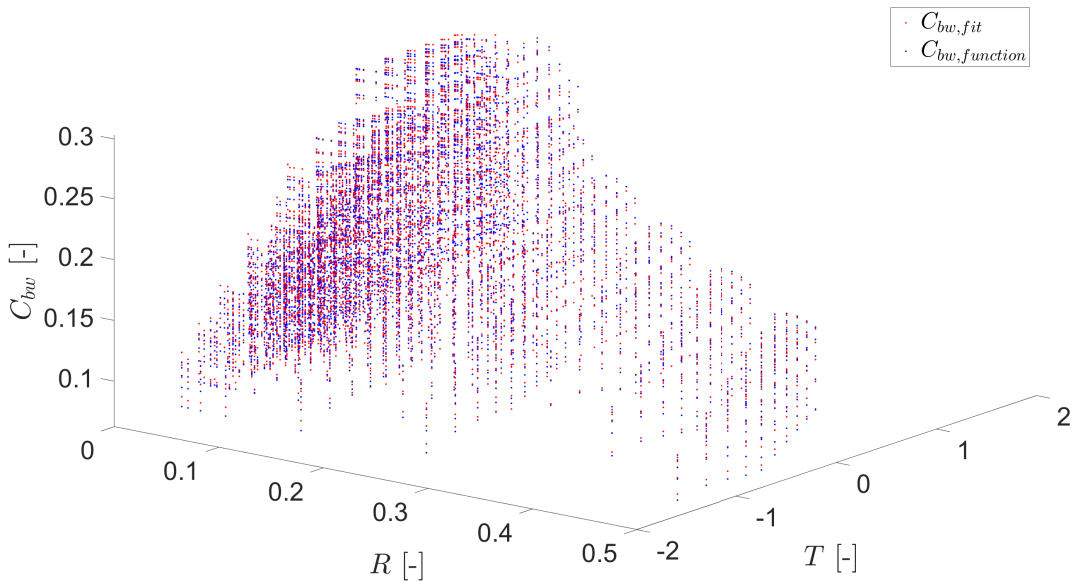

Figure B.3: All fitted and simplified function C_{bw} values for all geometry configurations regarding R and T.

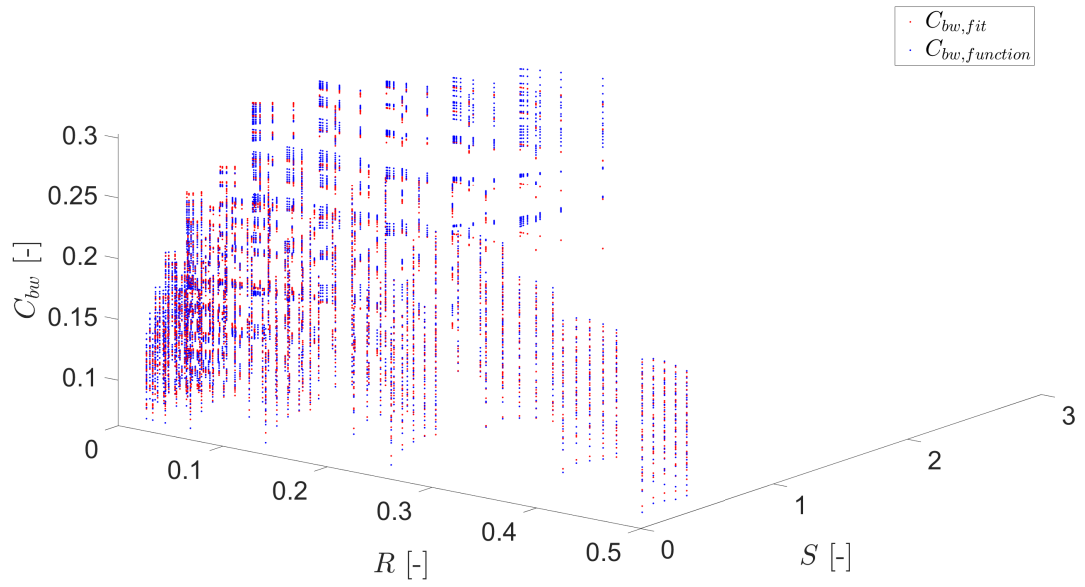

Figure B.4: All fitted and simplified function C_{bw} values for all geometry configurations regarding R and S.

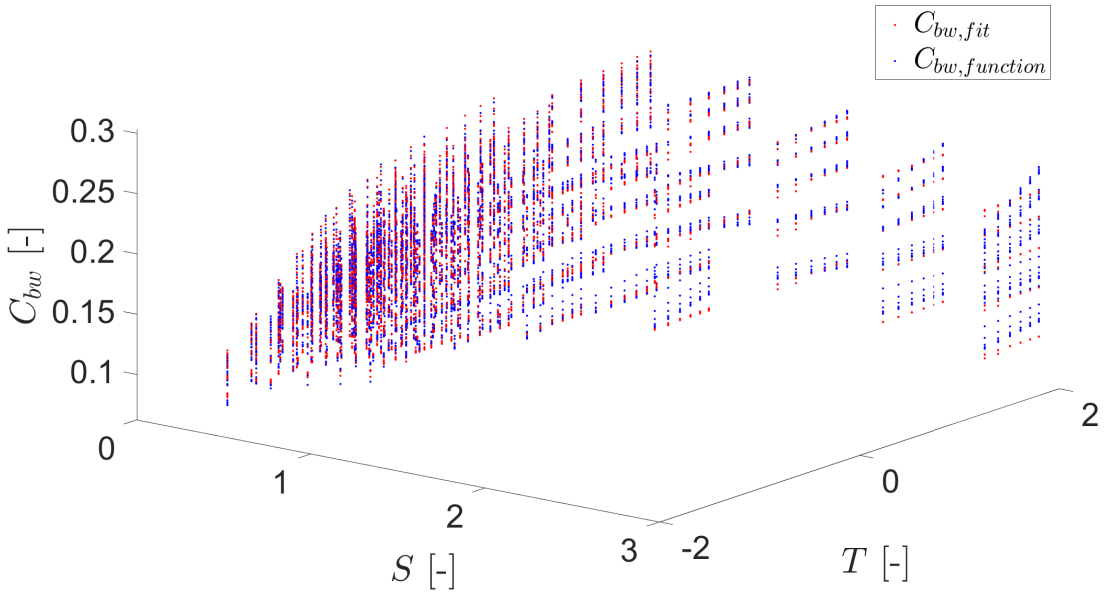

Figure B.5: All fitted and simplified function C_{bw} values for all geometry configurations regarding S and T.

C

Detailed Figures of Specimens

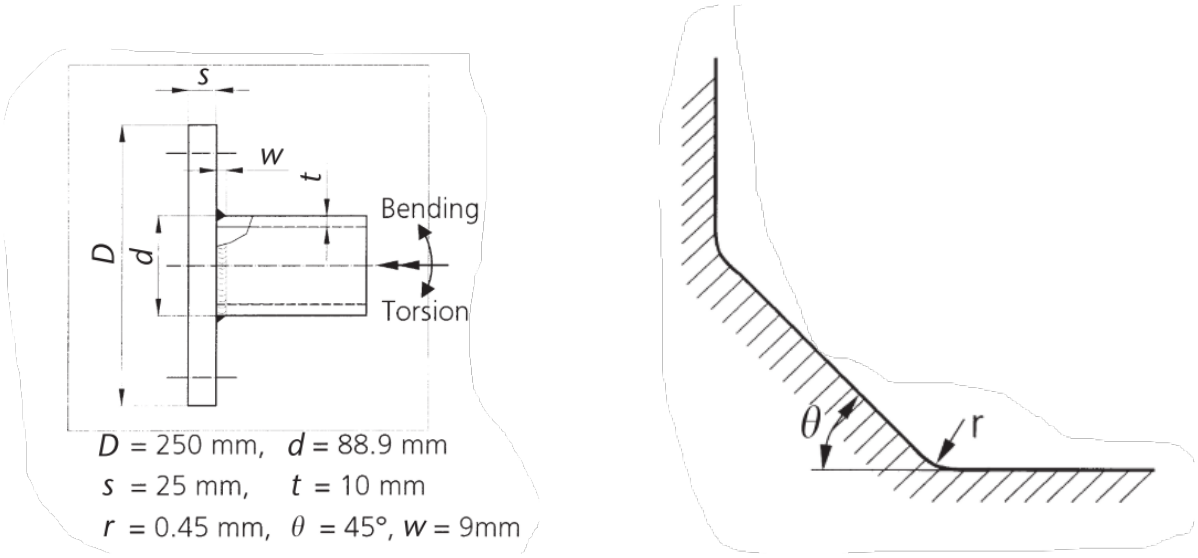

(a) Dimensions of the specimen.

(b) The weld-seam in detail.

Figure C.1: Tube–flange connection investigated by Sonsino et al. [48].

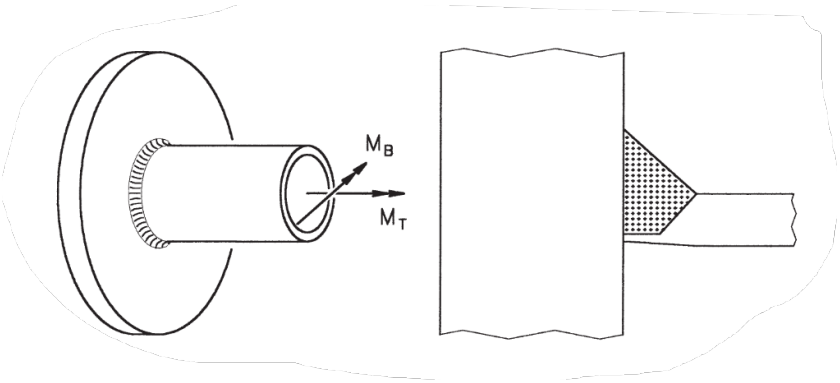

Figure C.2: Tube–flange connection investigated and seam geometry by Amstutz et al. [3].

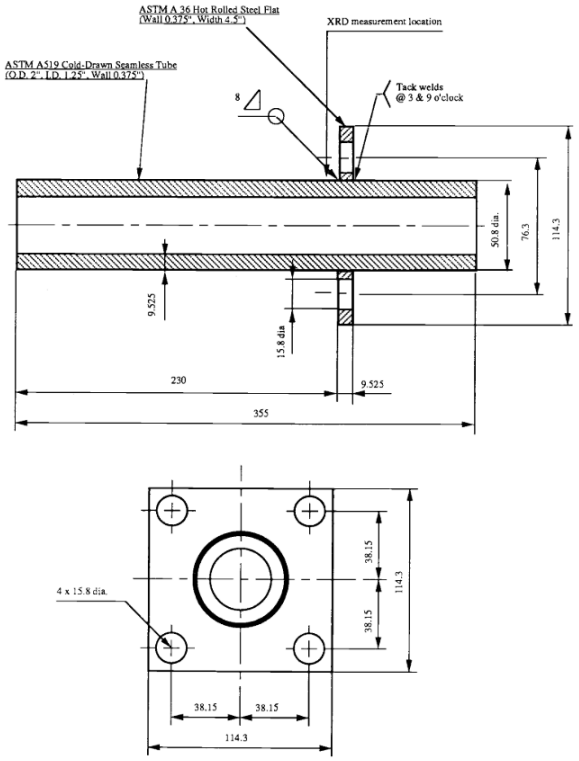

Figure C.3: Geometry of specimen investigated by Siljander et al. [43]

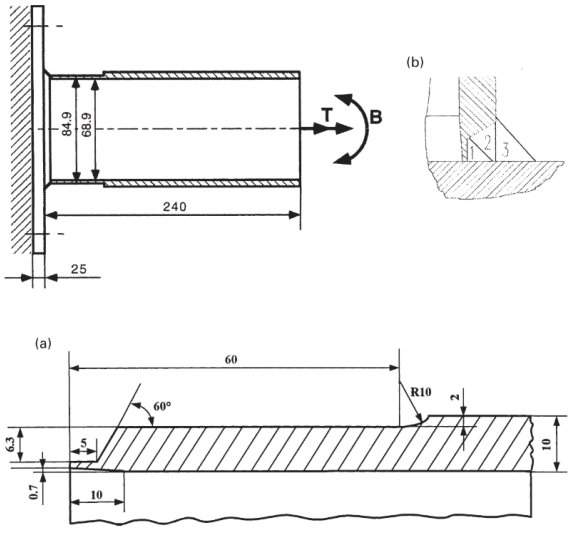

Figure C.4: Geometry of the specimen of Yousefi et al. [59]. (a) Detail of the seam preparation. (b) Detail of the seam.

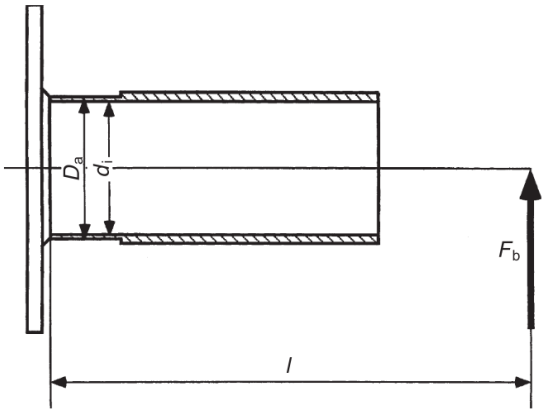

Figure C.5: Geometric data for calculating the nominal stress [59]

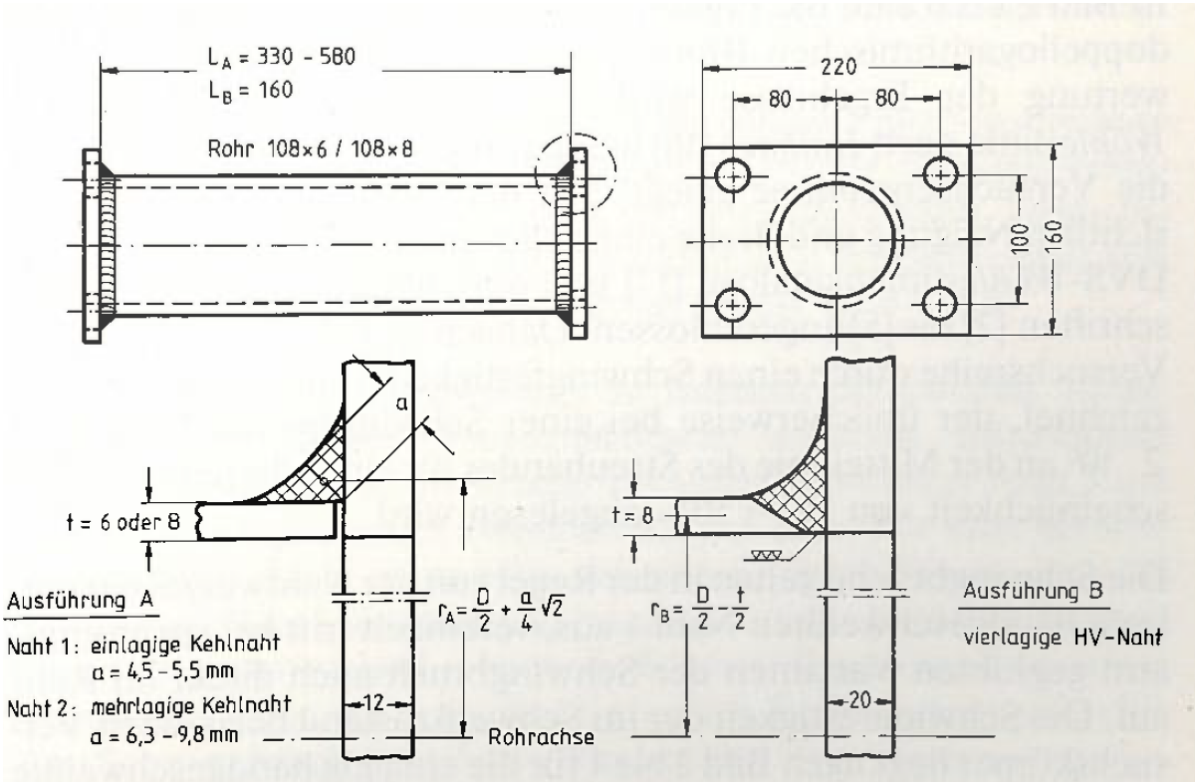

Figure C.6: Geometry of the specimen of Seeger et al. [42]. This research is using option B.

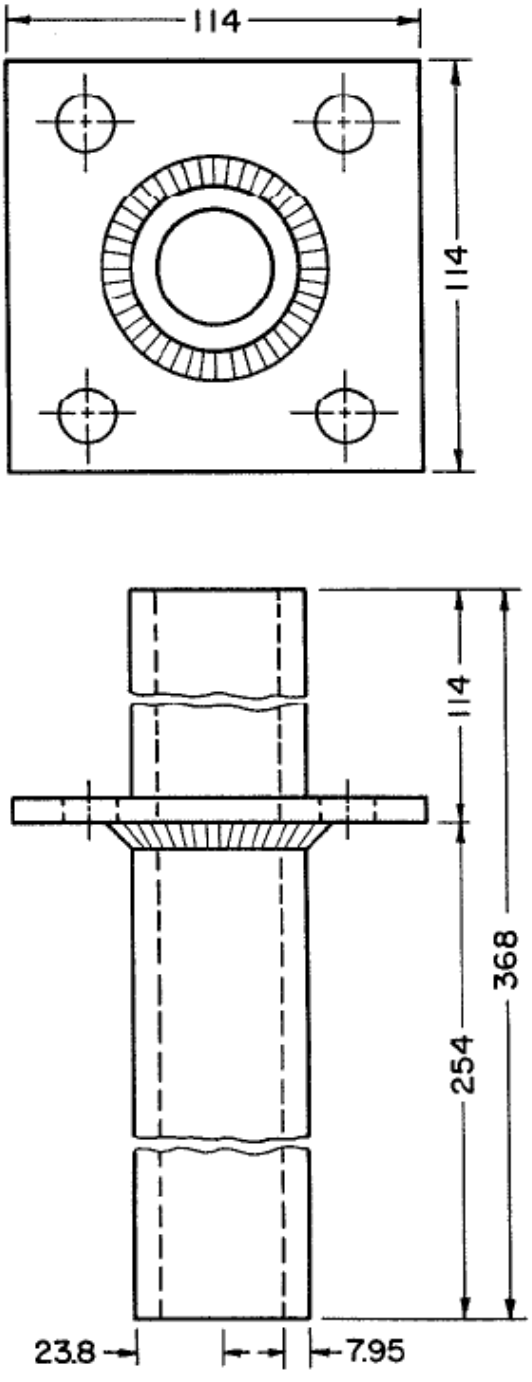

Figure C.7: Geometry of the specimen of Yung et al. [61]

References

[1] A. Hobbacher. “IIW document IIW-1823-07 FATIGUE DESIGN OF WELDED”. In: (2008).

[2] Hirotogu Akaike. “Information theory and an extension of the maximum likelihood principle”. In: *Selected papers of hirotugu akaike*. Springer, 1998, pp. 199–213.

[3] H. Amstutz, K. Störzel, and T. Seeger. “Fatigue crack growth of a welded tube-flange connection under bending and torsional loading”. In: *Fatigue and Fracture of Engineering Materials and Structures* 24.5 (2001), pp. 357–368. ISSN: 8756758X. DOI: 10.1046/j.1460-2695.2001.00408.x.

[4] Mika Bäckström. *Multiaxial fatigue life assessment of welds based on nominal and hot spot stresses at 12 o'clock noon*. Tech. rep. 2003. URL: http://www.vtt.fi/inf/pdf/.

[5] J. Baumgartner et al. “Fatigue assessment of welded joints using stress averaging and critical distance approaches”. In: *Welding in the World* 59.5 (2015), pp. 731–742. ISSN: 00432288. DOI: 10.1007/s40194-015-0248-x.

[6] D. Benasciutti, D. Zanellati, and A. Cristofori. “The “projection-by-projection” (PbP) criterion for multiaxial random fatigue loadings: Guidelines to practical implementation”. In: *Frattura ed Integrita Strutturale* 13.47 (Jan. 2019), pp. 348–366. DOI: 10.3221/IGF-ESIS.47.26.

[7] F. Berto, P. Lazzarin, and D. Radaj. “Fictitious notch rounding concept applied to sharp V-notches: Evaluation of the microstructural support factor for different failure hypotheses. Part I: Basic stress equations”. In: *Engineering Fracture Mechanics* 75.10 (July 2008), pp. 3060–3072. ISSN: 00137944. DOI: 10.1016/j.engfracmech.2007.12.011.

[8] Henk den Besten. “Fatigue damage criteria classification, modelling developments and trends for welded joints in marine structures”. In: *Ships and Offshore Structures* 13.8 (2018), pp. 787–808. ISSN: 17445302. DOI: 10.1080/17445302.2018.1463609.

[9] J.H. den Besten. *A total stress concept*. 2015, pp. 1–396. ISBN: 9789462330405.

[10] D. J. Burns and J. S. C. Parry. “Effect of Large Hydrostatic Pressures on the Torsional Fatigue Strength of two Steels”. In: *Journal of Mechanical Engineering Science* 6.3 (Sept. 1964), pp. 293–310. ISSN: 0022-2542. URL: http://journals.sagepub.com/doi/10.1243/JMES_JOUR_1964_006_042_02.

[11] Andrea Carpinteri, Andrea Spagnoli, and Sabrina Vantadori. “Multiaxial fatigue life estimation in welded joints using the critical plane approach”. In: *International Journal of Fatigue* 31.1 (Jan. 2009), pp. 188–196. ISSN: 01421123. DOI: 10.1016/j.ijfatigue.2008.03.024.

[12] Henk Den Besten. *Lecture Slides OE44085*. 2020. URL: https://brightspace.tudelft.nl.

[13] Pingsha Dong, Zhigang Wei, and Jeong K. Hong. “A path-dependent cycle counting method for variable-amplitude multi-axial loading”. In: *International Journal of Fatigue* 32.4 (Apr. 2010), pp. 720–734. ISSN: 0142-1123. DOI: 10.1016/J.IJFATIGUE.2009.10.010.

[14] C. Erny et al. “Experimental and Numerical Analyses of Fatigue Behavior of Welded Cruciform Joints”. In: *Fatigue and Fracture Mechanics: 9th International Volume, 37th National Volume* (May 2011), pp. 466–466. DOI: 10.1520/STP49301S. URL: http://www.astm.org/DIGITAL_LIBRARY/STP/PAGES/STP49301S.htm.

[15] S. Filippi, P. Lazzarin, and R. Tovo. “Developments of some explicit formulas useful to describe elastic stress fields ahead of notches in plates”. In: *International Journal of Solids and Structures* 39.17 (Aug. 2002), pp. 4543–4565. ISSN: 00207683. DOI: 10.1016/S0020-7683(02)00342-6.

[16] W. N. Findley. “A Theory for the Effect of Mean Stress on Fatigue of Metals Under Combined Torsion and Axial Load or Bending”. In: *Journal of Engineering for Industry* 81.4 (1959), pp. 301–305. ISSN: 0022-0817. DOI: 10.1115/1.4008327.

[17] W. Fricke. *IIW Recommendations for the fatigue assessment of welded structures by notch stress analysis*. Vol. 53. 9. 2013, pp. 1689–1699. ISBN: 9788578110796.

[18] A F Hobbacher. *Recommendations for Fatigue Design of Welded Joints and Components*. IIW Collection. Cham: Springer International Publishing, 2016. ISBN: 978-3-319-23756-5. DOI: 10.1007/978-3-319-23757-2. URL: http://www.springer.com/series/13906%20http://link.springer.com/10.1007/978-3-319-23757-2.

[19] A. F. Hobbacher. *Erratum to: Recommendations for Fatigue Design of Welded Joints and Components*. 2019, E3–E3. ISBN: 9781855733152. DOI: 10.1007/978-3-319-23757-2{_}8.

[20] B. Hu, P. Stumpf, and W. van der Deijl. "Offshore Wind Access 2019". In: *Offfshore Wind Acces Report* January (2019), pp. 1–40. URL: https://repository.tno.nl/islandora/object/uuid:e8f05155-aa5a-4aad-a7ba-8bed2e9b08fe.

[21] Yaoyu Hu et al. "Notch stress analysis and fatigue strength assessment of tube-flange welded joints under torsion loading". In: *Ocean Engineering* 186.March (2019), p. 106074. ISSN: 00298018. DOI: 10.1016/j.oceaneng.2019.05.056. URL: https://doi.org/10.1016/j.oceaneng.2019.05.056.

[22] M Janssen, J Zuidema, and RJH Wanhill. *Fracture Mechanics: Second edition*. 2017, pp. 1–418. ISBN: 9783319249995. DOI: 10.1007/978-3-319-24999-5.

[23] N. LAUTROU, D. THEVENET, and J.-Y. COGNARD. "Fatigue crack initiation life estimation in a steel welded joint by the use of a two-scale damage model". In: *Fatigue & Fracture of Engineering Materials & Structures* 32.5 (May 2009), pp. 403–417. ISSN: 1460-2695. DOI: 10.1111/J.1460-2695.2009.01344.X.

[24] J. Lemaitre, J.P. Sermage, and R. Desmorat. "A two scale damage concept applied to fatigue". In: *International Journal of Fracture 1999 97:1* 97.1 (1999), pp. 67–81. ISSN: 1573-2673. DOI: 10.1023/A:1018641414428.

[25] Jean Lemaitre. *A course on damage mechanics*. Springer Science & Business Media, 2012.

[26] SJ Maddox and GR Razmjoo. "Interim fatigue design recommendations for fillet welded joints under complex loading". In: *Fatigue & Fracture of Engineering Materials & Structures* 24.5 (2001), pp. 329–337.

[27] Mina Nacheva et al. *SPE-198600-MS Setting the Standard for Safety in the Offshore Access Industry*. Tech. rep. 2019.

[28] H. Neuber. *Kerbspannungslehre (4. Aufl.)* 1937, 1958, 1985, 2001. ISBN: 3-540-67657-0.

[29] A Pålmgren. "The fatigue life of ball-bearings". In: *Zeitung Verein deutscher Ingeneure ZVDI* 68 (1924), pp. 339–441.

[30] Jan Papuga and Milan Růžička. "Two new multiaxial criteria for high cycle fatigue computation". In: *International Journal of Fatigue* 30.1 (Jan. 2008), pp. 58–66. ISSN: 01421123. DOI: 10.1016/j.ijfatigue.2007.02.015.

[31] M. M. Pedersen. "Multiaxial fatigue assessment of welded joints using the notch stress approach". In: *International Journal of Fatigue* 83 (Feb. 2016), pp. 269–279. ISSN: 01421123. DOI: 10.1016/j.ijfatigue.2015.10.021.

[32] RE Peterson. "Notch-sensitivity". In: *Metal fatigue*. Ed. by Waisman JL Sines G. McGraw Hill, 1959, pp. 293–306.

[33] Jun Qian and Norio Hasebe. "Property of eigenvalues and eigenfunctions for an interface V-notch in antiplane elasticity". In: *Engineering Fracture Mechanics* 56.6 (1997), pp. 729–734. ISSN: 00137944. DOI: 10.1016/s0013-7944(97)00004-0.

[34] Yanxin Qin et al. "Fatigue design of welded double-sided T-joints and double-sided cruciform joints in steel marine structures: A total stress concept". In: *Fatigue and Fracture of Engineering Materials and Structures* 42.12 (2019), pp. 2674–2693. ISSN: 14602695. DOI: 10.1111/ffe.13089.

[35] Yanxin Qin et al. "Mid- and High-Cycle Fatigue of Welded Joints in Steel Marine Structures: Effective Notch Stress and Total Stress Concept Evaluations". In: *International Journal of Fatigue* 142.April 2020 (2021), p. 105822. ISSN: 01421123. DOI: 10.1016/j.ijfatigue.2020.105822.

[36] Dieter Radaj and Michael Vormwald. *Advanced methods of fatigue assessment*. Vol. 9783642307. 2013, pp. 1–490. ISBN: 9783642307409. DOI: 10.1007/978-3-642-30740-9.

[37] GR Razmjoo. "Fatigue of load-carrying fillet welded joints under multiaxial loading". In: *5 th International Conference on Biaxial/Multiaxial Fatigue & Fracture*. 1997, pp. 53–70.

[38] Klemens Rother and Wolfgang Fricke. “Effective notch stress approach for welds having low stress concentration”. In: *International Journal of Pressure Vessels and Piping* 147 (Nov. 2016), pp. 12–20. ISSN: 03080161. DOI: 10.1016/j.ijpvp.2016.09.008.

[39] Nicolas Saintier et al. “Non-local energy based fatigue life calculation method under multiaxial variable amplitude loadings”. In: *International Journal of Fatigue* 54 (Sept. 2013), pp. 68–83. ISSN: 0142-1123. DOI: 10.1016/J.IJFATIGUE.2012.12.013.

[40] Jaap (Delft University of Technology) Schijve. *Fatigue of Structures and Materials*. 2008, pp. 373–394. ISBN: 9781402068072. DOI: 10.1007/978-1-4020-6808-9{_}12.

[41] Walter Schütz. “A history of fatigue”. In: *Engineering Fracture Mechanics* 54.2 (May 1996), pp. 263–300. ISSN: 00137944. DOI: 10.1016/0013-7944(95)00178-6.

[42] T Seeger and R Olivier. “Ertragbare und zulässige Schubspannungen schwingbeanspruchter Schweißverbindungen”. In: *STAHLBAU, DER* 56.8 (1987).

[43] Aslak Siljander, Peter Kurath, and Frederick V. Lawrence. “Nonproportional fatigue of welded structures”. In: *ASTM Special Technical Publication* 1122 (1992), pp. 319–338. ISSN: 00660558. DOI: 10.1520/stp24166s.

[44] Olli Aslak Siljander. “Nonproportional biaxial fatigue of welded joints”. PhD thesis. University of Illinois at Urbana-Champaign, 1991.

[45] G. Sines. “Behaviour of metals under complex stresses”. In: *Metal fatigue*. Ed. by Waisman JL Sines G. McGraw Hill, 1959, pp. 145–169.

[46] C. M Sonsino et al. *Fatigue behaviour of welded high-strength components under combined multiaxial variable amplitude loading: final report*. 2001, p. 111. ISBN: 9289420677. URL: https://op.europa.eu/nl/publication-detail/-/publication/0b94f2d4-91ec-4520-9664-de7b6e4234a9%20http://hdl.handle.net/10068/269973.

[47] C. M. Sonsino. “Multiaxial fatigue assessment of welded joints - Recommendations for design codes”. In: *International Journal of Fatigue* 31.1 (2009), pp. 173–187. ISSN: 01421123. DOI: 10.1016/j.ijfatigue.2008.06.001. URL: http://dx.doi.org/10.1016/j.ijfatigue.2008.06.001.

[48] C. M. Sonsino and M. Kueppers. “Multiaxial fatigue of welded joints under constant and variable amplitude loadings”. In: *Fatigue and Fracture of Engineering Materials and Structures* 24.5 (2001), pp. 309–327. ISSN: 8756758X. DOI: 10.1046/j.1460-2695.2001.00393.x.

[49] C.M. Sonsino, C.M. Sonsino, and S.J. Maddox. *Sixth International Conference on Biaxial/ Multiaxial Fatigue*. 2001, pp. 3–15.

[50] Luca Susmel. “Four stress analysis strategies to use the Modified Wöhler Curve Method to perform the fatigue assessment of weldments subjected to constant and variable amplitude multiaxial fatigue loading”. In: *International Journal of Fatigue* 67 (2014), pp. 38–54.

[51] Luca Susmel. *Multiaxial notch fatigue*. Elsevier, 2009.

[52] Keisuke Tanaka. “Engineering formulae for fatigue strength reduction due to crack-like notches”. In: *International Journal of Fracture* 22.2 (1983), R39–R46.

[53] D. Taylor. “The theory of critical distances”. In: *Engineering Fracture Mechanics* 75.7 (May 2008), pp. 1696–1705. ISSN: 00137944. DOI: 10.1016/j.engfracmech.2007.04.007.

[54] David Taylor. “Geometrical effects in fatigue: a unifying theoretical model”. In: *International Journal of Fatigue* 21.5 (1999), pp. 413–420.

[55] David THEVENET et al. “Modélisation du comportement en fatigue d’assemblages soudés de type naval”. In: *Congrés français de mécanique* (2009). ISSN: 2491-715X. URL: http://documents.irevues.inist.fr/handle/2042/37133.

[56] P. S. Van Lieshout, J. H. Den Besten, and M. L. Kaminski. “Multiaxial fatigue assessment of welded joints in marine Structures: Literature overview of progress in academia and engineering practice”. In: *International Shipbuilding Progress* 65.1 (2018), pp. 29–71. ISSN: 15662829. DOI: 10.3233/ISP-170141.

[57] J. M. Whitney and R. J. Nuismer. “Stress Fracture Criteria for Laminated Composites Containing Stress Concentrations”. In: *Journal of Composite Materials* 8.3 (1974), pp. 253–265. DOI: 10.1177/002199837400800303.

[58] M L Williams and Calif Pasadena. *Stress Singularities Resulting Frolll Vari-ous Boundary Conditions in Angular Corners of Plates in Extension*. Tech. rep. 1952.

[59] Mario Witt, Farhad Yousefi, and Harold Zenner. "Fatigue strength of welded joints under multiaxial loading: Comparison between experiments and calculations". In: *ASTM Special Technical Publication* 1387 (2000), pp. 191–210. ISSN: 00660558. DOI: 10.1520/stp13505s.

[60] August Wöhler. "Versuche zur Ermittlung der auf die Eisenbahnwagenachsen einwirkenden Kräfte und die Widerstandsfähigkeit der Wagen-Achsen". In: *Zeitschrift für Bauwesen* 10.1860 (1860), pp. 583–614.

[61] J-Y Yung and FV Lawrence Jr. "Predicting the fatigue life of welds under combined bending and torsion". In: *Mechanical Engineering Publications, Biaxial and Multiaxial Fatigue,* (1989), pp. 53–69.